The Importance of Material and Irradiation Parameters on Void Growth in Metals - Part I: The Effect of Displacement Rate and Cascade Efficiency

N. Ghoniem and G.L. Kulcinski

April 1977

UWFDM-203

FUSION TECHNOLOGY INSTITUTE

UNIVERSITY OF WISCONSIN

MADISON WISCONSIN

The Importance of Material and Irradiation Parameters on Void Growth in Metals - Part I: The Effect of Displacement Rate and Cascade Efficiency

N. Ghoniem and G.L. Kulcinski

Fusion Technology Institute
University of Wisconsin
1500 Engineering Drive
Madison, WI 53706

http://fti.neep.wisc.edu

April 1977

UWFDM-203

Legal Notice

"This report was prepared by the University of Wisconsin as an account of work sponsored by the Electric Power Research Institute, Inc. ("EPRI"). Neither EPRI, members of EPRI, nor the University of Wisconsin, nor any person acting on behalf of either:

"a. Makes any warranty or representation, express or implied, with respect to the accuracy, completeness, or usefulness of the information, apparatus, method, or process disclosed in this report may not infringe privately owned rights; or

"b. Assumes any liabilities with respect to the use of, or for damages resulting from the use of, any information, apparatus, method of process disclosed in this report."

The Importance of Materials and Irradiation Parameters on Void Growth in Metals

Part I. The Effect of Displacement Rate and Cascade Efficiency

N. Ghoniem

G. Kulcinski

April 1977

UWFDM-203

Fusion Technology Program
Nuclear Engineering Department
University of Wisconsin
Madison, Wisconsin 53706

Abstract

A Fully Dynamic Rate Theory (FDRT), based on the Brailsford and Bullough rate theory, is utilized to analyze in detail the dynamics of point defects as well as voids, interstitial loops and vacancy loops. Information on point defects, voids, rate processes and other microstructures are studied as a function of irradiation dose and temperature. The effect of collision cascade collapse and displacement rate on the growth aspect of void swelling in metals is investigated. For 316 SS, cascade collapse efficiencies greater than 7.5% are found to completely inhibit growth of voids at any temperature and dose rate. To relate ion simulation experiments to actual reactor irradiations, appropriate nucleation conditions of the microstructure are found to be important.

TABLE OF CONTENTS

I. Introduction

The phenomenon of void growth in metals is known to be a strong function of both the intrinsic materials properties and the irradiation environment. Two of the most common parameters studied are the temperature and fluence dependence of the swelling. However, there are many more parameters which influence the production, migration and agglomeration of point defects and in the Brailsford and Bullough rate theory model[1] and the Fully Dynamic Rate Theory (FDRT)[2] there are at least 16 materials and 5 irradiation parameters which need to be considered.

The object of this report is to use the FDRT to examine the significance of two of the more important irradiation parameters, the displacement rate and cascade collapse efficiency, on the swelling of 316 stainless steel over a range of temperatures and fluences. Future reports will concentrate on the effect of the different materials parameters.

There is a great deal of experimental evidence on the effect of displacement rate on the swelling in metals[3]. In general, the higher the displacement rate, the higher the supersaturation level of both vacancies and interstitials. These higher defect concentrations can affect both the nucleation (which is assumed to have ceased in the rate theory approach) and the growth of clustered defects. Aside from the obvious interest in void growth it is important to know what effect changing displacement rate has on the other sink removal rates and recombination rates. We will examine displacement rates from 10^{-6} dpa s^{-1} typical of fast reactor conditions to 10^{-3} dpa s^{-1} typical of heavy ion simulation experiments.

The concept of cascade collapse efficiency (ε) was first introduced into the void growth theories by Straalsund[4] and Bullough, Eyre and Krishan[5]. The value of ε is defined as the fraction of vacancies that

are produced directly into vacancy loops. This factor (ε) has two effects on the growth of voids.

1.) A certain fraction of the vacancies is tied up in vacancy loops, thus reducing the total number of vacancies going to voids.

2.) The vacancy loops represent a new sink in the matrix which now must be considered in the dynamics of the point defect behaviour (sink removal and recombination rates).

Qualitatively one expects the value of ε to be zero for electron irradiation and it has been assumed to be $\sim$ 0.044 for heavy ion irradiation of 316 SS.[5] We will investigate values of ε from 0.001 to 0.1 in this study.

The organization of this report is as follows. First a brief description is given about the calculational procedure and assumptions used in this work. The next chapter describes the results of the calculation on a variation of ε from 0.001 to 0.1 at P = 10^{-3}dpa s^{-1} and a variation of P from 10^{-6} to 0.1 dpa s^{-1} at ε = 0.044 (see Figure 1). We have chosen to be very explicit about the data from one calculation, ε = 0.01 and P = 10^{-3} dpa s^{-1} and display the results in great detail. However, only the most interesting points and trends will be quoted from the other ε-P combinations. Following a discussion of the results we make some concluding remarks about this work and suggestions for future work.

II. Calculational Procedure and Assumptions

All calculations were made with the TRANSWELL computer program[6] in conjunction with a recently developed plotting routine, PL3[7]. This latter code allows the information to be plotted in three dimensional form or as contour plots as will be discussed later.

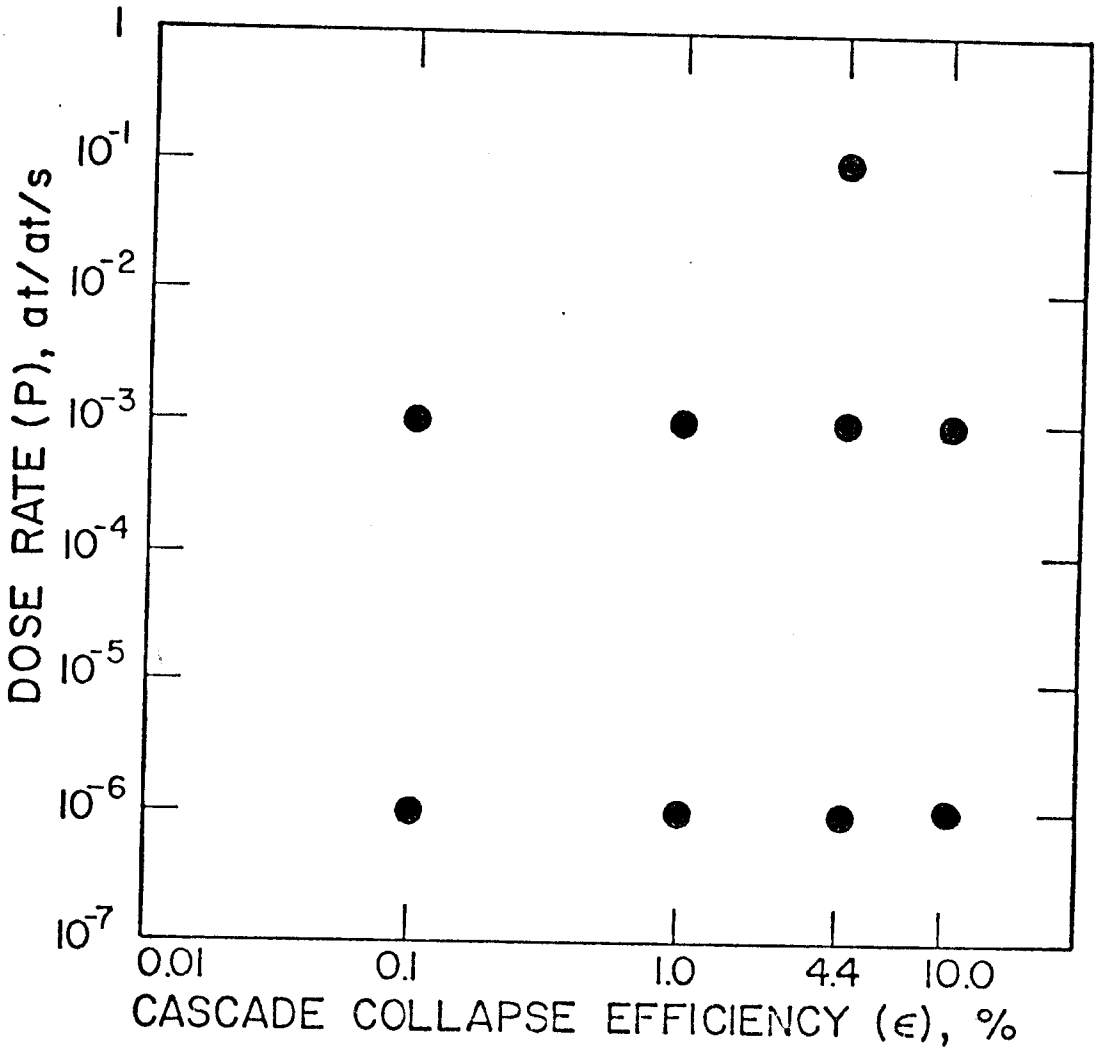

Fig.(1) INVESTIGATED COMBINATIONS OF DOSE RATE AND COLLISION CASCADE COLLAPSE EFFICIENCY FOR 316 SS.

Table 1

Summary of Materials Constants For 316 SS Void Growth Calculations

Surface Energy, γ	$= 1.25 \times 10^{15}$ ev cm^{-2}
Vacancy formation Energy, E_f^v	= 1.6 ev
Vacancy migration Energy, E_m^v	= 1.3 ev
Interstitial formation Energy, E_i^f	= 4.0 ev
Interstitial migration Energy, E_i^m	= 0.2 ev
Vacancy diffusivity, D_v^o	= 0.6 cm^2 s^{-1}
$\frac{\text{recombination coefficient}}{\text{interstitial diffusion coefficient}}$, $\frac{\alpha}{D_i}$	$= 10^{16}$ cm^{-2}
stacking fault energy, γ_{sf}	$= 9.4 \times 10^{12}$ ev cm^{-2}
deformation produced dislocation density, ρ_d^o	$= 10^8$ cm^{-2}
Burgers vector, b	$= 2 \times 10^{-8}$ cm
dislocation bias for vacancies, Z_v	= 1.00
dislocation bias for interstitials, Z_i	= 1.08
Effective modulus, $\mu' = \frac{\mu}{1-\nu}$	$= 4 \times 10^{11}$ dyne cm^{-2}

Following the notations of reference (6), the physical parameters of Table 1 were adopted. Also, the following assumptions were made:

(1) There is only one average void size at a given temperature that starts to grow under irradiation. At high temperatures, nucleated voids must start growing from a bigger size to withstand surface emission of vacancies. In the present computations, we determined the size at which a void could survive at the highest temperature. Also we determined another size at the lowest temperature of interest and linearly interpolated $r_{vo}(T)$ in between.

(2) The initial dislocation density is set at $\rho_d^o = 10^8$ cm/cm^3. This value is not changed with dose and is appropriate for solution treated steels.

(3) No gas generation during irradiation was allowed.

(4) A temperature dependent interstitial loop density as:

$$N_{i\ell} = 1.3 \times 10^{-4} \exp\{2.8 \text{ eV}/kT\}, \text{ cm}^{-3}$$

(5) A temperature dependent void density as:

$$N_c = 3.15 \times 10^{11} \exp\{0.625 \text{ eV}/kT\}, \text{ cm}^{-3}$$

(6) The previous two nucleation functional dependencies, which were determined at $P \simeq 10^{-3}$ dpa s^{-1}, <u>were not changed</u> with dose rate or collapse efficiency to keep the effects of nucleation separate from those of growth.

(7) Finally a total dose of 40 dpa was studied in all cases and represents the total dose beyond the end of the nucleation phase.

Cases studied in this paper may be conveniently divided into two broad categories:

(A) Reactor conditions in which the production rate of point defects is 10^{-6} dpa/sec.

(B) Simulation conditions (accelerator or HVEM) in which the production rate of point defects is in the range 10^{-3} to 10^{-1} dpa/sec.

Studies of the phenomenon of vacancy condensation in vacancy loops are developed in each category. Stainless steel rate theory-defined metallurgical processes are presented both in 3-dimensional plots and as contour plots.

A combination of the two Computer Codes TRANSWELL and PL3 is capable of presenting the following information in both 3-dimensional and contour plot forms: (any one of the following parameters can be plotted in the z direction as a function of two independent variables in the x and y directions).

1. Average void radius, cm.
2. Average non-aligned interstitial loop radius, cm.
3. Number density of non-aligned vacancy loops, cm^{-3}.
4. Fraction of vacancies in non-aligned vacancy loops, at./at.
5. Vacancy concentration, at./at. (space averaged).
6. Interstitial concentration, at./at. (space averaged).
7. Average aligned interstitial loop radius, cm.
8. Number density of aligned vacancy loops, cm^{-3}.
9. Fraction of vacancies in aligned vacancy loops, at./at.
10. Network creep strain, cm/cm.
11. Rate of change of average void radius, cm/sec.
12. Rate of change of average non-aligned interstitial loop radius, cm/sec.
13. Rate of change of the number density of non-aligned vacancy loops, cm^{-3} sec^{-1}.
14. Rate of change of fraction of vacancies in non-aligned vacancy loops, at./at./sec.
15. Rate of change of vacancy concentration, at./at./sec.
16. Rate of change of interstitial concentration, at./at./sec.
17. Rate of change of average aligned interstitial loop radius, cm/sec.

18. Rate of change of number density of aligned vacancy loops, $cm^{-3}sec^{-1}$.

19. Rate of change of fraction of vacancies in aligned vacancy loops, at./at./sec.

20. Network creep strain rate, cm/cm/sec.

21. Total interstitial time constant, sec^{-1}.

22. Total vacancy time constant, sec^{-1}.

23. Total vacancy thermal emission rate from the surfaces of voids and dislocations, at./at./sec.

24. Vacancy flux (D_vC_v), cm^2/sec.

25. Interstitial flux (D_iC_i), cm^2/sec.

26. Line dislocation density of non-aligned dislocation loops, cm/cm^3.

27. Line dislocation density of aligned dislocation loops, cm/cm^3.

28. Line dislocation density of non-aligned vacancy loops, cm/cm^3.

29. Line dislocation density of aligned vacancy loops, cm/cm^3.

30. Total line dislocation density, cm/cm^3.

31. Vacancy thermal emission rate from the surfaces of voids, at./at./sec.

32. Vacancy thermal emission rate from the surfaces of aligned edge dislocations, at./at./sec.

33. Vacancy thermal emission rate from the surfaces of non-aligned edge dislocations, at./at./sec.

34. Vacancy thermal emission rate from the surfaces of all edge dislocations (sum of 32 and 33), at./at./sec.

35. Vacancy thermal emission rate from the surfaces of aligned interstitial loops, at./at./sec.

36. Vacancy of thermal emission rate from the surfaces of non-aligned interstitial loops, at./at./sec.

37. Vacancy thermal emission rate from the surfaces of interstitial loops (sum of 35 and 36), at./at./sec.

38. Vacancy thermal emission rate from the surfaces of aligned vacancy loops, at./at./sec.

39. Vacancy thermal emission rate from the surfaces of non-aligned vacancy loops, at./at./sec.

40. Vacancy thermal emission rate from the surfaces of all vacancy loops, (sum of 38 and 39), at./at./sec.

41. Vacancy time constant due to the presence of voids only, sec^{-1}.

42. Interstitial time constant due to the presence of voids only, sec^{-1}.

43. Vacancy time constant due to the presence of dislocations only, sec^{-1}.

44. Interstitial time constant due to the presence of dislocations only, sec^{-1}.

45. Interstitial total sink removal rate, at./at./sec.

46. Vacancy total sink removal rate, at./at./sec.

47. Point defect recombination rate, at./at./sec.

48. Percent swelling.

49. Change of average void radius, $R_c - R_o$ (for pulsed irradiation), cm.

50. Change of average interstitial loop radius, $R_{i\ell} - R_{i\ell o}$ (for pulsed irradiation), cm.

51. Strain due to interstitial loops, cm/cm.

52. Strain due to vacancy loops, cm/cm.

53. Equivalent void sink density (defined as $4\pi R_c N_c$), cm^{-2}.

Any one of the 53 variables can be plotted in the Z-direction as a function of two independent variables:

a. The x-axis that is chosen from one of the following:

   1. the irradiation dose measured after incubation.

   2. the irradiation time after incubation.

b. The y-axis that is chosen from one of the following:

   1. Temperature, °K

   2. Logarithm to the base 10 of dose rate; dpa/sec.

   3. Logarithm to base 10 of gas generation rate; at./at./sec.

   4. Initial gas content of voids; atoms/void.

   5. Applied stress; psi.

Although the analysis can be extended to most of the 53 variables listed before, we will concentrate only on a few. Interrelationships between different metallurgical processes will be emphasized.

III. Results

III.A. Theory

The basic rate equations used in this computation are given by:

$$\frac{dC_v}{dt} = (1 - \varepsilon)P + P^e - P_{sv} - P_r \qquad (1)$$

$$\frac{dC_i}{dt} = P - P_{si} - P_r \qquad (2)$$

$$\frac{dR_c}{dt} = (D_v C_v - D_i C_i - D_v C_v^e \exp\{(\frac{2\gamma}{R_c} - P_g(R_c, N_g)\frac{\Omega}{kT}\})/R_c \qquad (3)$$

$$\frac{dN_{v\ell}}{dt} = \kappa_1 - \Lambda_1 \tag{4}$$

$$\frac{dq_{v\ell}}{dt} = \kappa_2 - \Lambda_2 \tag{5}$$

$$\frac{dR_{i\ell}}{dt} = [(D_i Z_i C_i - D_v Z_v C_v + D_v Z_v C_v (R_{i\ell})]/b \tag{6}$$

Relations defining different terms in the previous six rate equations are described in reference (6), but a brief description of those terms is given here.

C_v = Average vacancy concentration; at./at.

C_i = Average interstitial concentration; at./at.

ε = Fraction of vacancies produced in vacancy loops (Cascade collapse efficiency).

P = Point defect production rate at./at./sec.

P^e = Total vacancy thermal emission rate; at./at./sec.

P_{sv} = Total vacancy sink removal rate; at./at./sec.

P_r = Point defect recombination rate; at./at./sec.

P_{si} = Total interstitial sink removal rate; at./at./sec.

D_v = Vacancy diffusion coefficient (cm^2/sec)

D_i = Interstitial diffusion coefficient (cm^2/sec)

C_v^e = Thermal equilibrium vacancy concentration; at./at.

R_c = Average void radius; cm.

$R_{i\ell}$ = Average interstitial loop radius; cm.

γ = Void surface energy, eV/cm^2.

P_g = Void internal gas pressure, eV/cm^3.

Ω = Atomic volume, cm^3,

k = Bolzmann's constant; eV/°K

$N_{v\ell}$ = Number density of vacancy loops, cm^{-3}.

$q_{v\ell}$ = Fraction of vacancies tied up in vacancy loops; at./at.

κ_1 = Production rate of vacancy loops; cm^{-3} sec^{-1}.

Λ_1 = Decay rate of vacancy loops; cm^{-3} sec^{-1}.

κ_2 = Production rate of vacancy fraction tied up in vacancy loops; at./at./sec.

Λ_2 = Decay rate of vacancy fraction tied up in vacancy loops; at./at./sec.

$C_v(R_{i\ell})$ = Vacancy concentration at the edge of an average interstitial loop; at./at./sec.

b = Burger's vector, cm.

Z_v = Dislocation-vacancy bias factor.

Z_i = Dislocation-interstitial bias factor.

The set of equations described above (1-6) is nonlinear and simultaneous. There is an interdependence of all the constituents of these equations.

The results presented here are classified into four different groups:

1. Point defect concentrations and fluxes.
2. Resultant average void size and percent swelling.
3. Rate processes:
   a. Vacancy thermal emission rates.
   b. Sink removal rates.
   c. Point defect recombination rate.
4. Microstructural information:
   a. Vacancy loop line dislocation density.
   b. Interstitial loop line dislocation density.
   c. Total dislocation density.
   d. Effective void sink strength ($4\pi R_c N_c$).

III.B. Accelerator Conditions

1. (ε = 0.01 and P = 10^{-3} dpa s^{-1})

a. Point Defect Concentrations and Fluxes

i. Vacancy and Interstitial Concentrations

The vacancy concentration in at/at is shown in Figures (2) and (3). It can be seen that, at any given temperature, the vacancy concentration is decreased as the damage level increases. The reason for this behavior is primarily due to (as we shall see later) the rapid buildup of vacancy loops in the matrix in the first few dpa's (see Fig. 32). This effect is more pronounced at lower temperatures where the vacancy loop lifetime is the longest

The vacancy concentration behavior with respect to temperature is more complex. At any given dose, the vacancy concentration exhibits a peak at the intermediate temperatures. Physically, this behavior is attributed to the following.

1.) The increase in C_v up to ~750°K is due to the drop in the density of both interstitial and vacancy loops which then drastically reduces the loop line density (Figs. 29 and 35). The matrix is then much "cleaner" and both the vacancy and interstitial concentrations can build up to higher values.

2.) The decrease in the point defect concentrations is due to the increased mobility of vacancies above 750°K which in turn promotes more recombination (Figs. 27 and 28) and migration to different sinks.

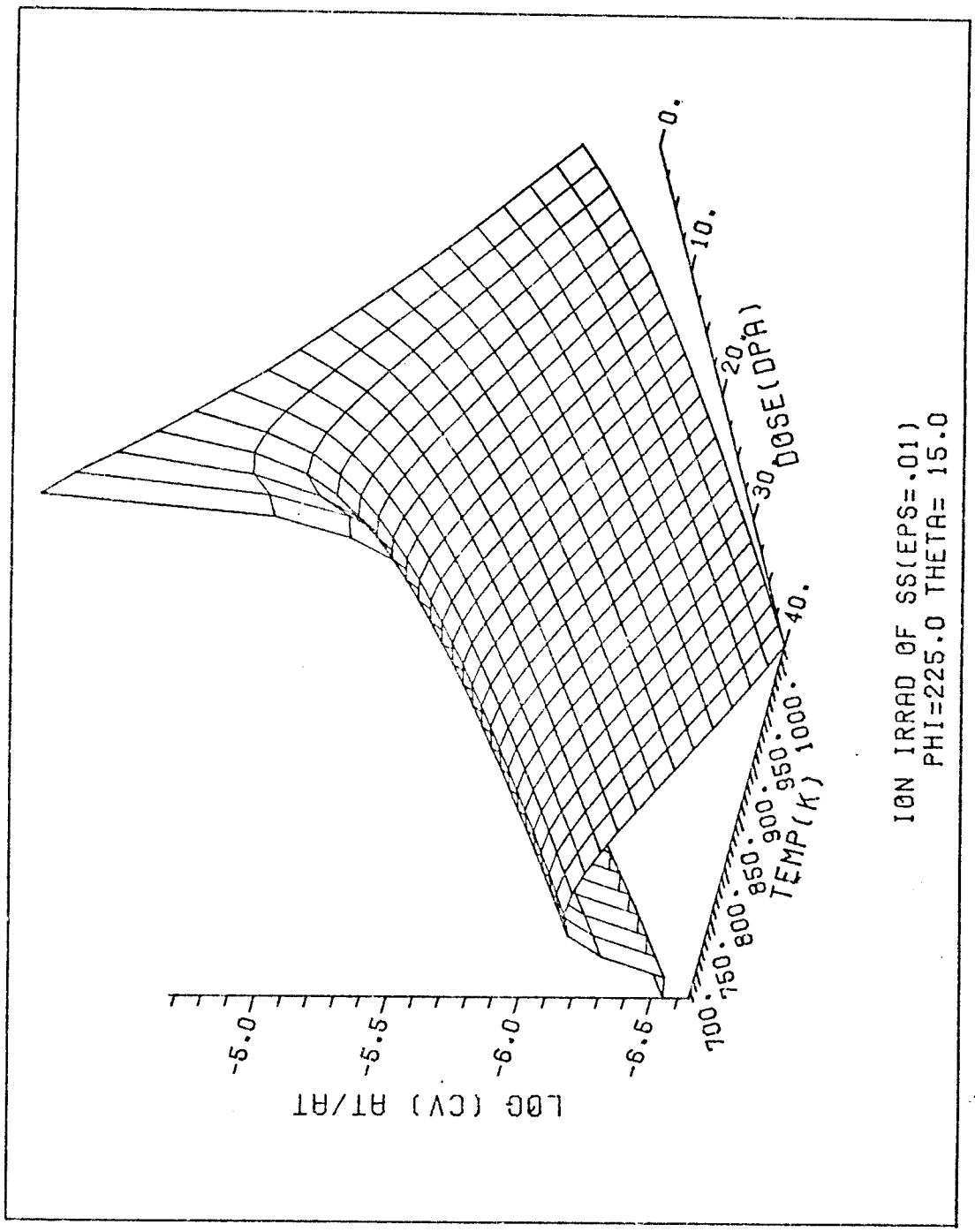

Fig. (2) 3-dimensional plot of vacancy concentration (at./at.) as a function of dose and temperature for ion irradiated ST stainless steel. The dose rate is 10^{-3} dpa/sec and the cascade efficiency is 0.01.

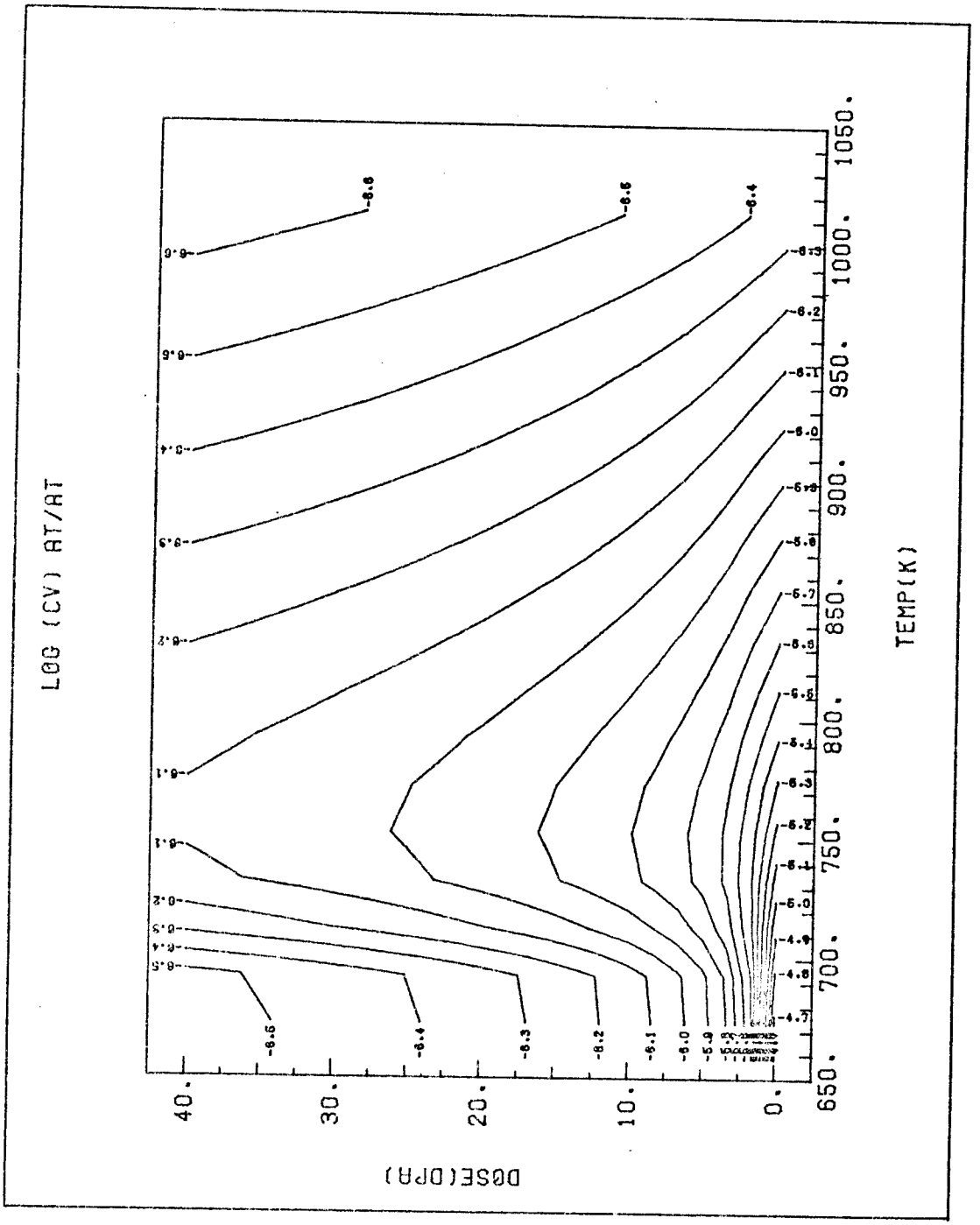

Fig. (3) Contour plot of vacancy concentration (at./at.) as a function of dose and temperature for ion irradiated ST stainless steel. The dose rate is 10^{-3} dpa/sec and the cascade efficiency is 0.01.

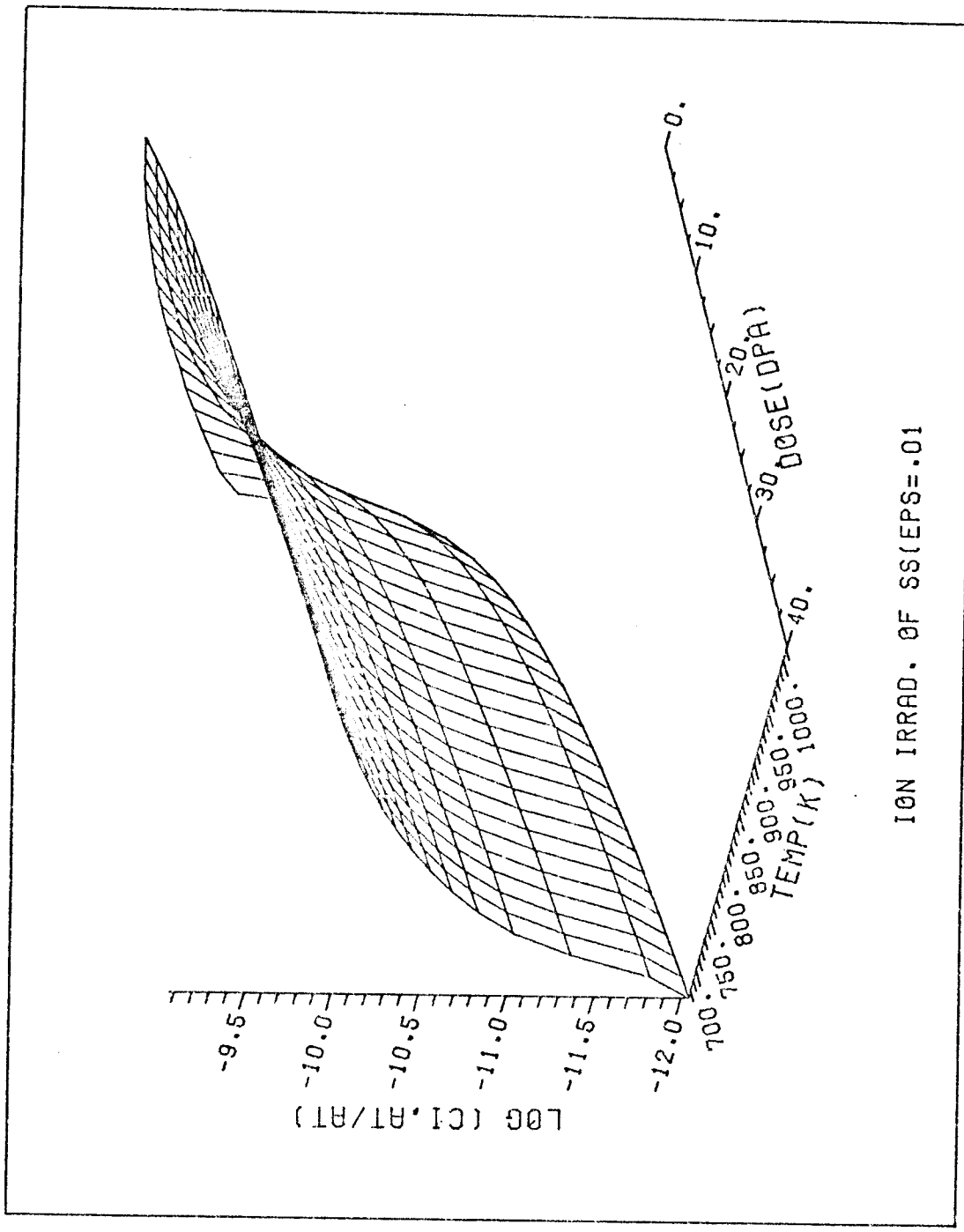

Fig. (4) 3-dimensional plot of interstitial concentration (at./at.) as a function of dose and temperature for ion irradiated ST stainless steel. The dose rate is 10^{-3} dpa/sec and the cascade efficiency is 0.01.

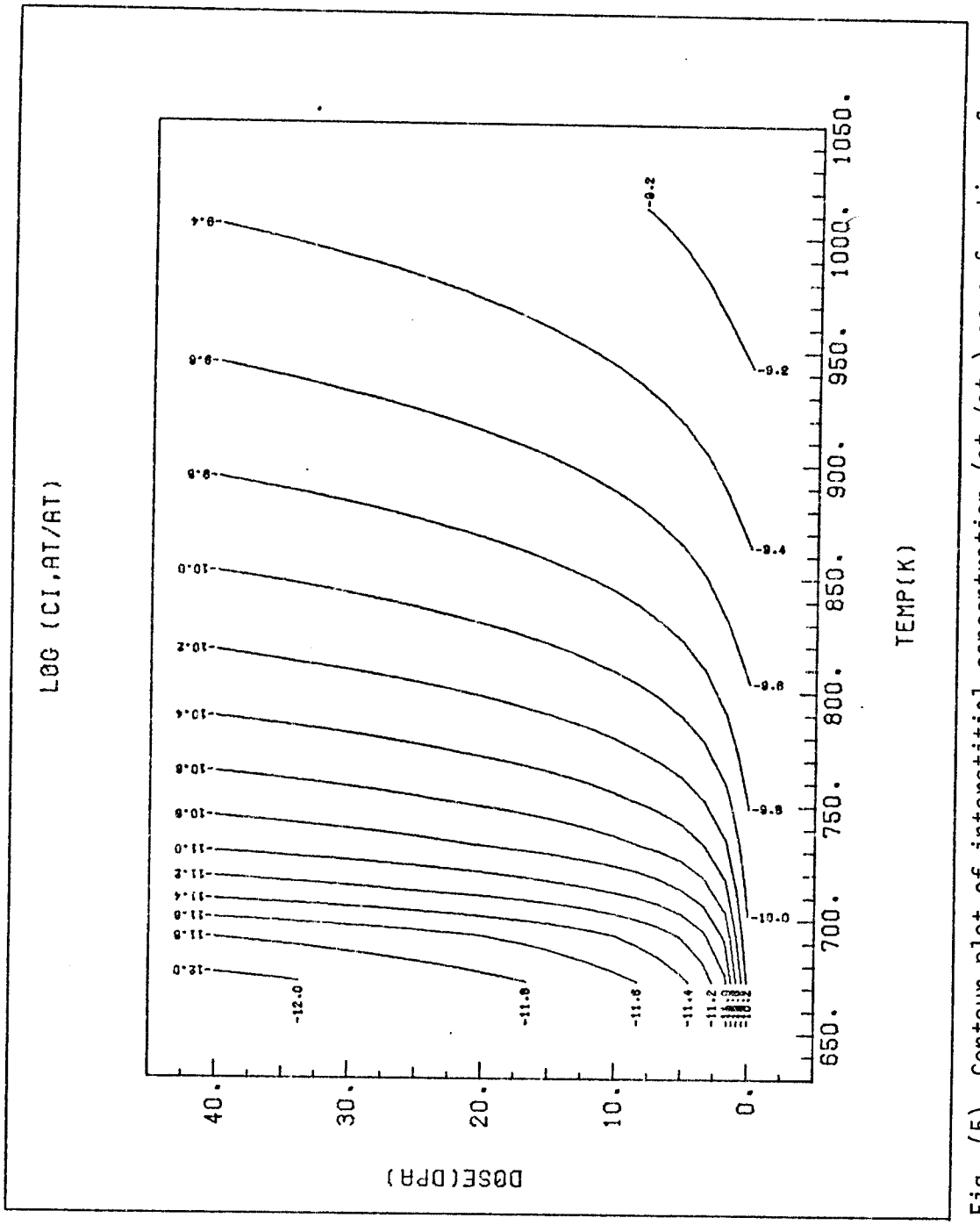

Fig. (5) Contour plot of interstitial concentration (at./at.) as a function of dose and temperature for ion irradiated ST stainless steel. The dose rate is 10^{-3} dpa/sec and the cascade efficiency is 0.01.

The interstitial concentration also decreases with dose at any given temperature because of the buildup in the loop sink density which causes more interstitials to be removed from the matrix. However, in contrast to the vacancy concentration, the interstitial concentration does not reach a maximum with temperature and then decreases. This is due to the low activation energy for migration and the fact that an interstitial is only twice as mobile at $1000^{o}K$ as it is at $750^{o}K$. In contrast, the vacancy at $1000^{o}K$ is over 200 times more mobile than at $750^{o}K$.

ii. Defect Fluxes

Although vacancy concentration is orders of magnitude greater than interstitial concentration, their fluxes arriving at surfaces of voids and dislocations are only slightly different due to the much higher mobility of interstitials. A vacancy flux is defined as $(D_v C_v)$ while an interstitial flux is defined as $(D_i C_i)$. The slightly larger vacancy flux to voids is the driving force causing them to grow.* This small difference in fluxes is also the reason for the sensitivity of the void growth problem to slight changes in material and irradiation variables.

Figures (6) and (7) show the vacancy flux as a function of dose and temperature. As the dose increases, the flux decreases slowly due to a higher probability of vacancy absorption by the sink density which is building up. At higher temperatures, vacancies are more mobile causing the flux to increase with temperature even though the concentration of vacancies is decreasing. In Figures (8) and (9) the same behavior of interstitial flux is displayed and from the values on the contour plots one can see the very small difference from vacancy flux.

Fraction of Vacancies in Loops:

The fraction of vacancies in vacancy loops is shown in Figures (10) and (11) and is a balance between the production rate (which is constant) and the removal rate (which depends on the number and size of loops). This fraction increases slowly with dose but decreases sharply as the temperature is increased. The decrease is due to the emission of vacancies at high temperature. The effect of this fraction of vacancies tied up in vacancy loops is to decrease the free vacancy concentration thus decreasing the vacancy flux.

---

*The reason interstitial loops grow despite the fact that the interstitial flux in the matrix is less than the vacancy flux can be attributed to the bias factor Z_i.

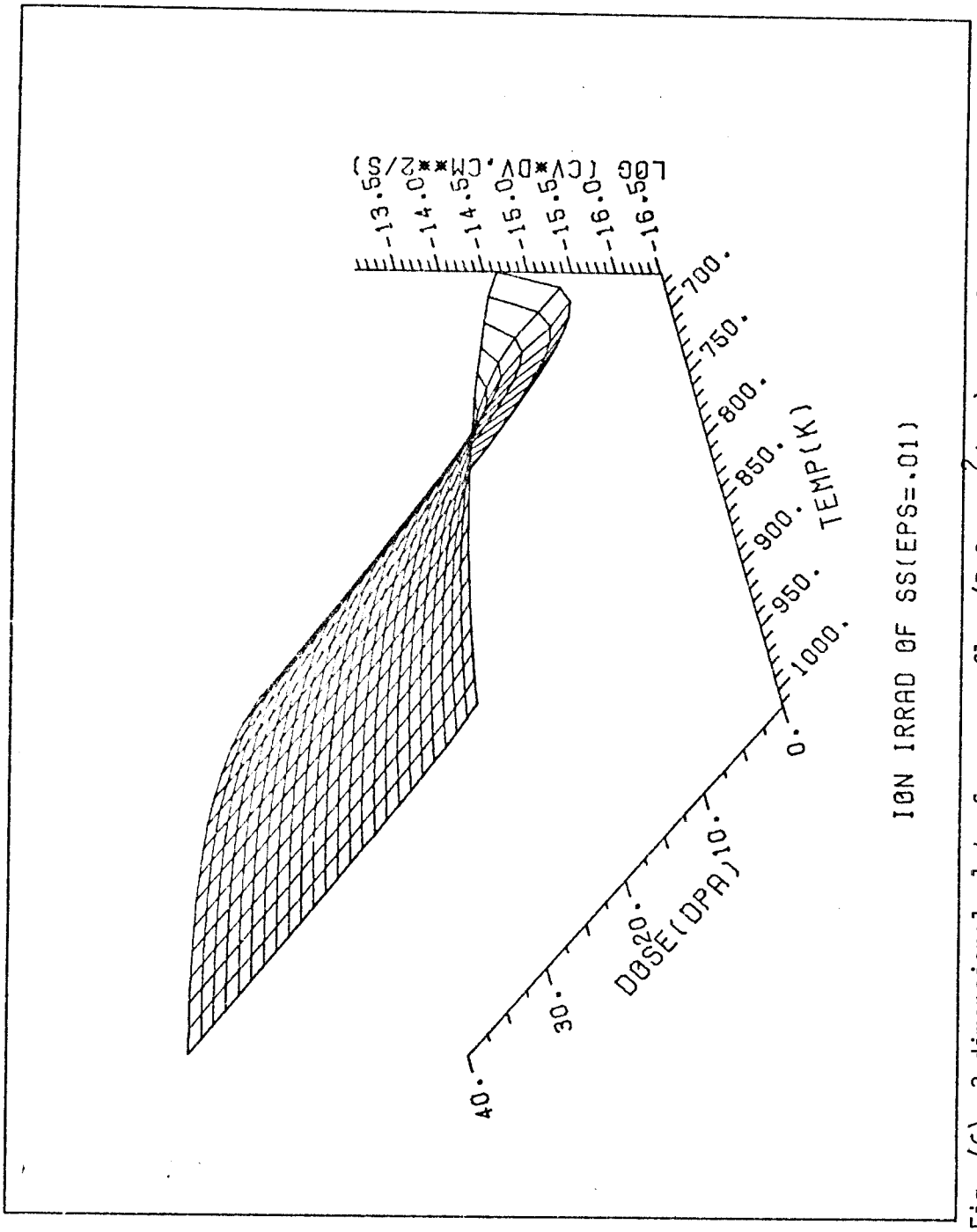

Fig. (6) 3-dimensional plot of vacancy flux ($D_v C_v$, cm^2/sec) as a function of dose and temperature for ion irradiated ST stainless steel. The dose rate is 10^{-3} dpa/sec and the cascade efficiency is 0.01.

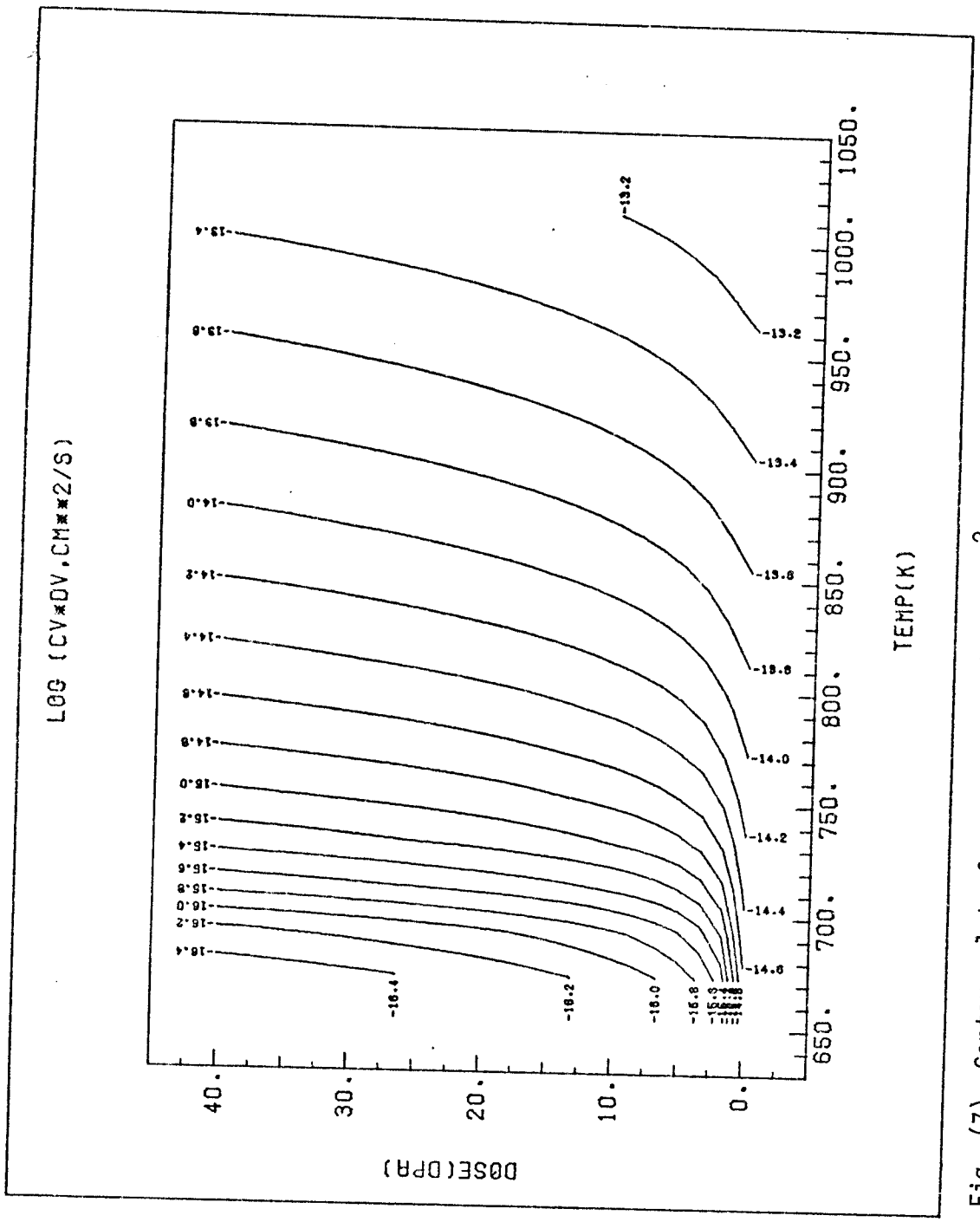

Fig. (7) Contour plot of vacancy flux ($D_v C_v$, cm^2/sec) as a function of dose and temperature for ion irradiated ST stainless steel. The dose rate is 10^{-3} dpa/sec and the cascade efficiency is 0.01.

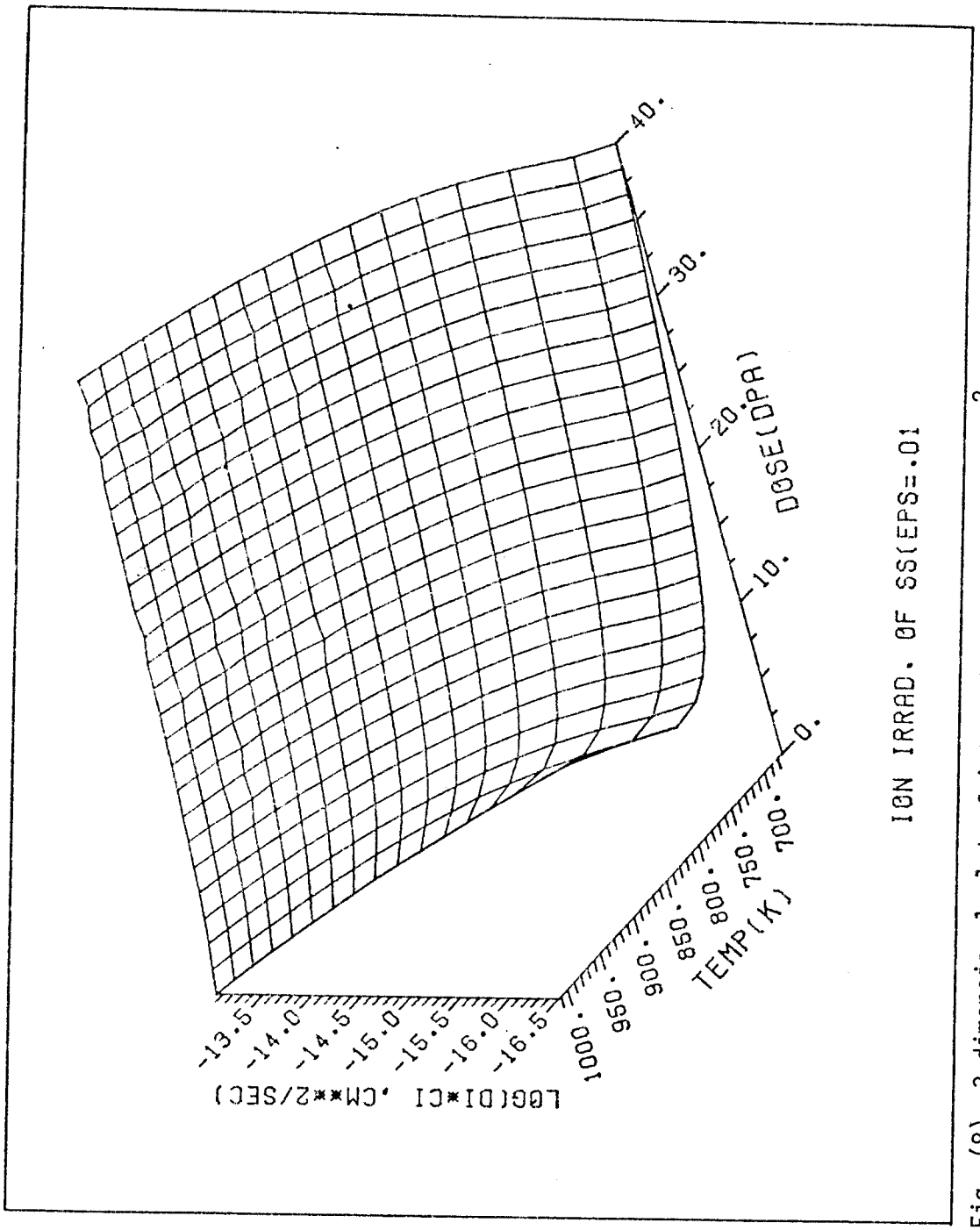

Fig. (8) 3-dimensional plot of interstitial flux (D_iC_i, cm^2/sec) as a function of dose and temperature for ion irradiated ST stainless steel. The dose rate is 10^{-3} dpa/sec and the cascade efficiency is 0.01.

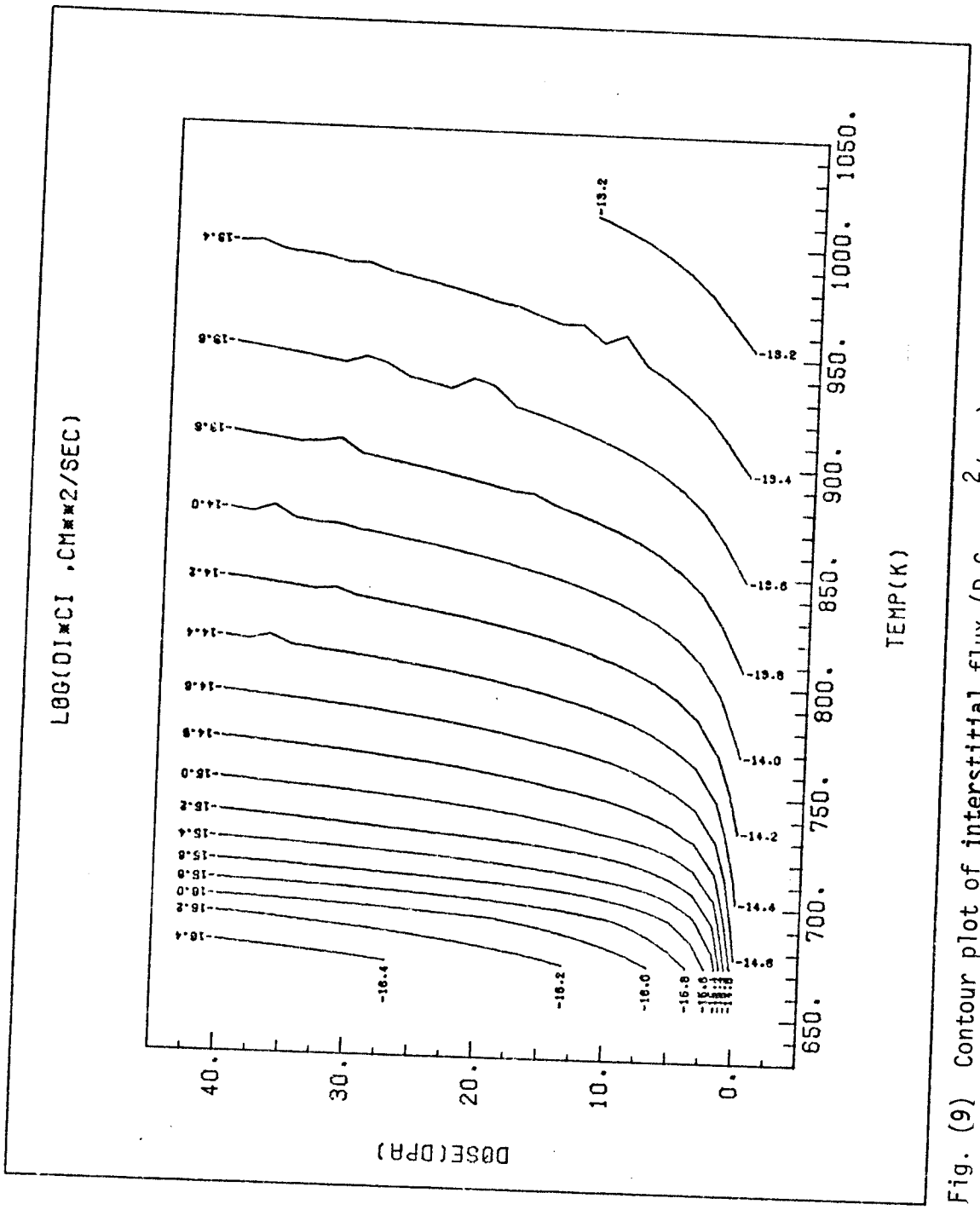

Fig. (9) Contour plot of interstitial flux ($D_i C_i$, cm^2/sec) as a function of dose and temperature for ion irradiated SS stainless steel. The dose rate is 10^{-3} dpa/sec and the cascade efficiency is 0.01.

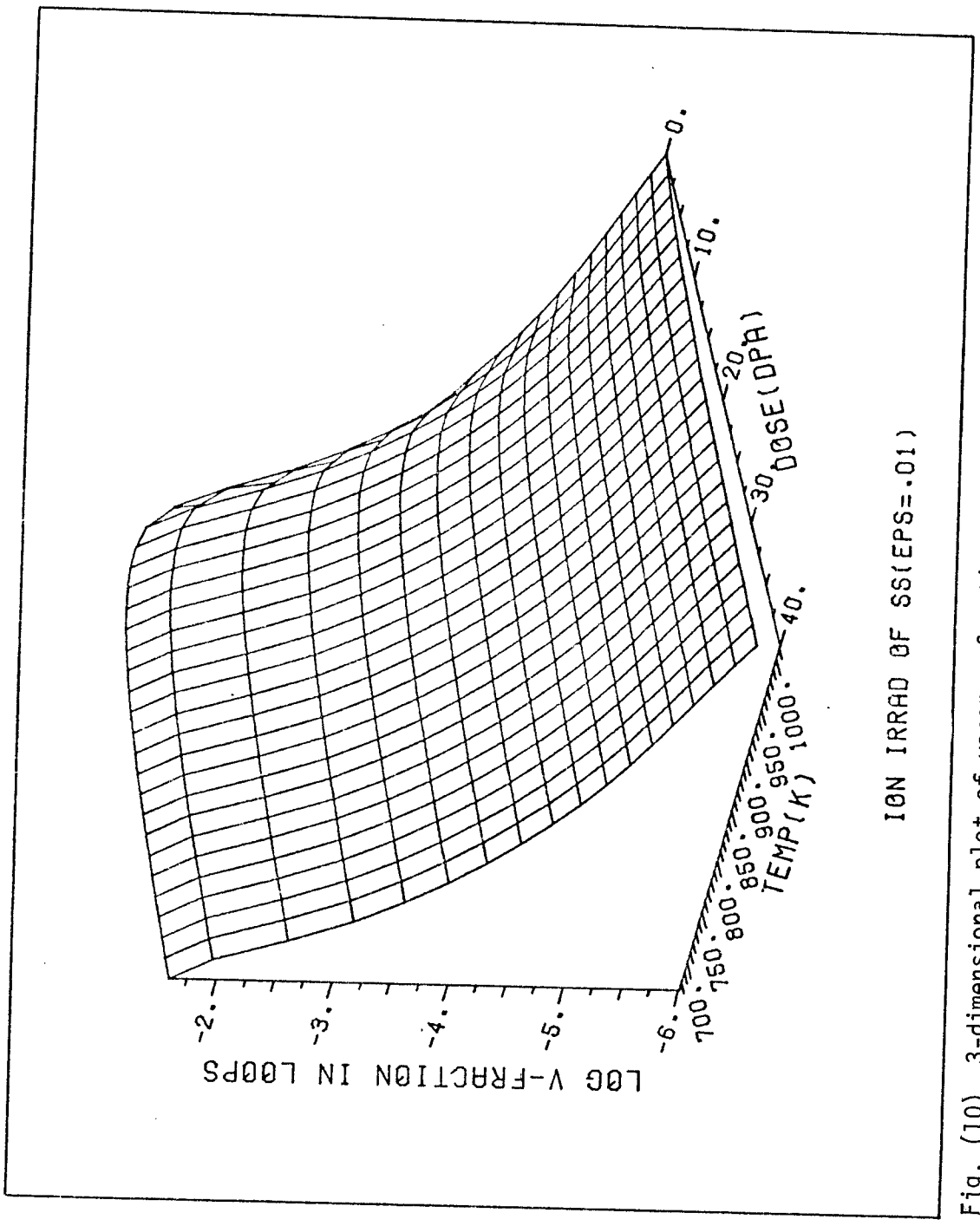

Fig. (10) 3-dimensional plot of vacancy fraction in vacancy loops (at./at.) as a function of dose and temperature for ion irradiated ST stainless steel. The dose rate is 10^{-3} dpa/sec and the cascade efficiency is 0.01.

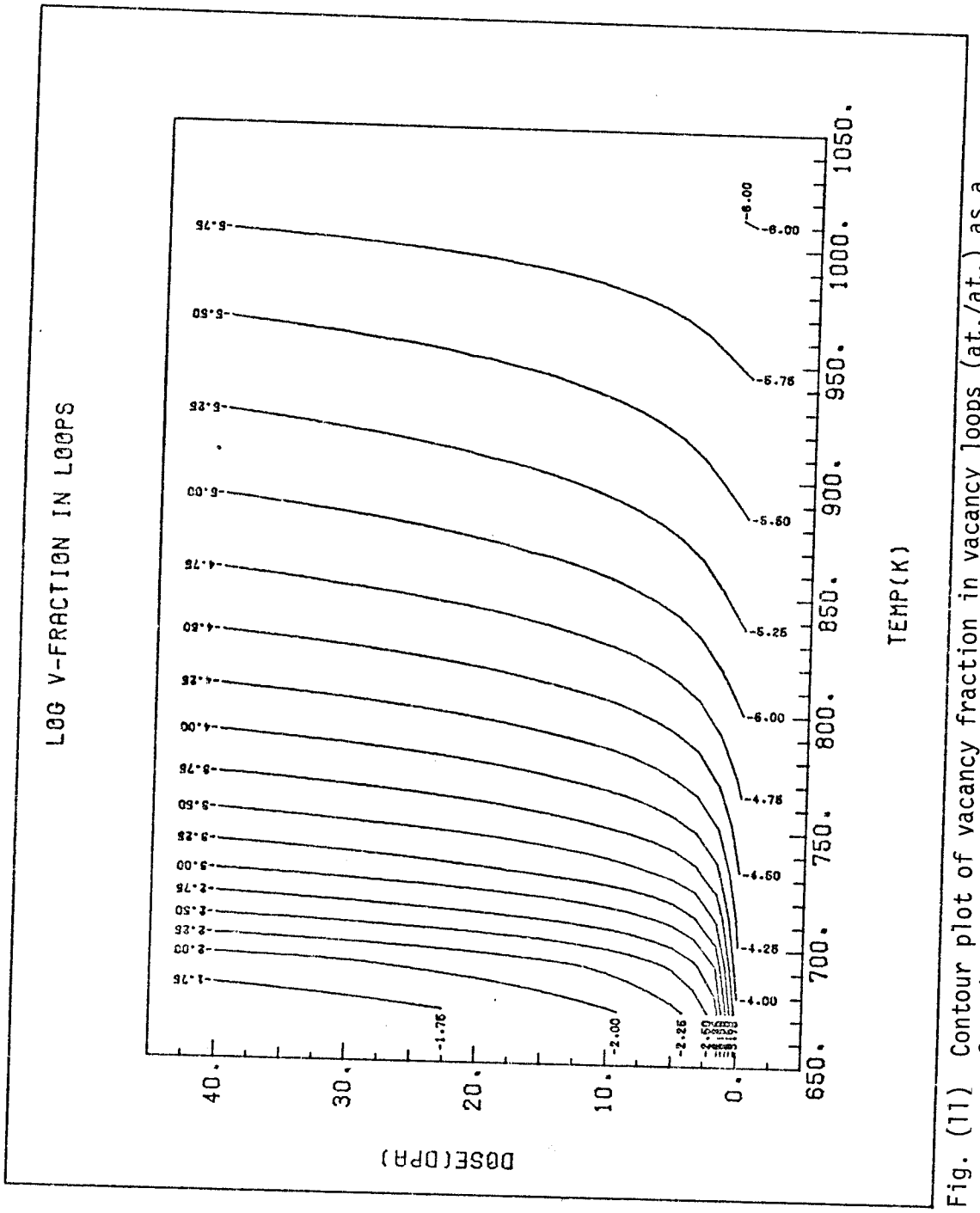

Fig. (11) Contour plot of vacancy fraction in vacancy loops (at./at.) as a function of dose and temperature for ion irradiated ST stainless steel. The dose rate is 10^{-3} dpa/sec and the cascade efficiency is 0.01.

b. Resultant Average Void Size and Percent Swelling

Figure (12) shows the temperature and dose dependence of the average void radius. Due to the excess flux of vacancies arriving at the voids ($D_vC_v > D_iC_i$), they start to grow immediately upon irradiation. Figure (13) shows the contours of constant void radius. At low temperatures the growth rate is not as pronounced as at intermediate temperatures (between 500 and 650°C) due to the lower vacancy flux. At 500 to 650°C the vacancy flux is sufficiently high and the vacancy emission rate sufficiently low that the growth rates are very high. At high temperatures vacancies are more readily emitted from voids (see Figures (19) and (20)), and this has the effect of slowing down the growth of voids since the difference between the vacancy flux (D_vC_v) and the sum of interstitial flux and emitted vacancy flux ($D_iC_i + D_vC_v^e \exp\{(\frac{2\gamma}{R_c} - P_g)\frac{\Omega}{kT}\}$) is very small. At still higher temperatures the vacancy flux falls farther and eventually the vacancy emission rate in conjunction with the interstitial absorption rate exceeds the vacancy flux and the voids will shrink.

The percent swelling is shown in Figures (14) and (15) in a 3-dimensional form while it is displayed as constant swelling contours in Figures (16). It is interesting to note that swelling goes "almost" linear as a function of dose. This is the consequence of a fixed void density and an increasing void size (Figure 13). On the other hand, there is a slightly dose dependent temperature peak for swelling. There are two reasons for this temperature dependence which can be understood by examining the simple swelling expression:

$$S = \frac{4}{3}\pi R_c^3 N_c \quad . \tag{7}$$

i - The void number density goes down exponentially with temperature (nucleation).

ii - The mean void radius goes up with temperature to ~ 800-850°K and then drops very slowly at high temperatures.

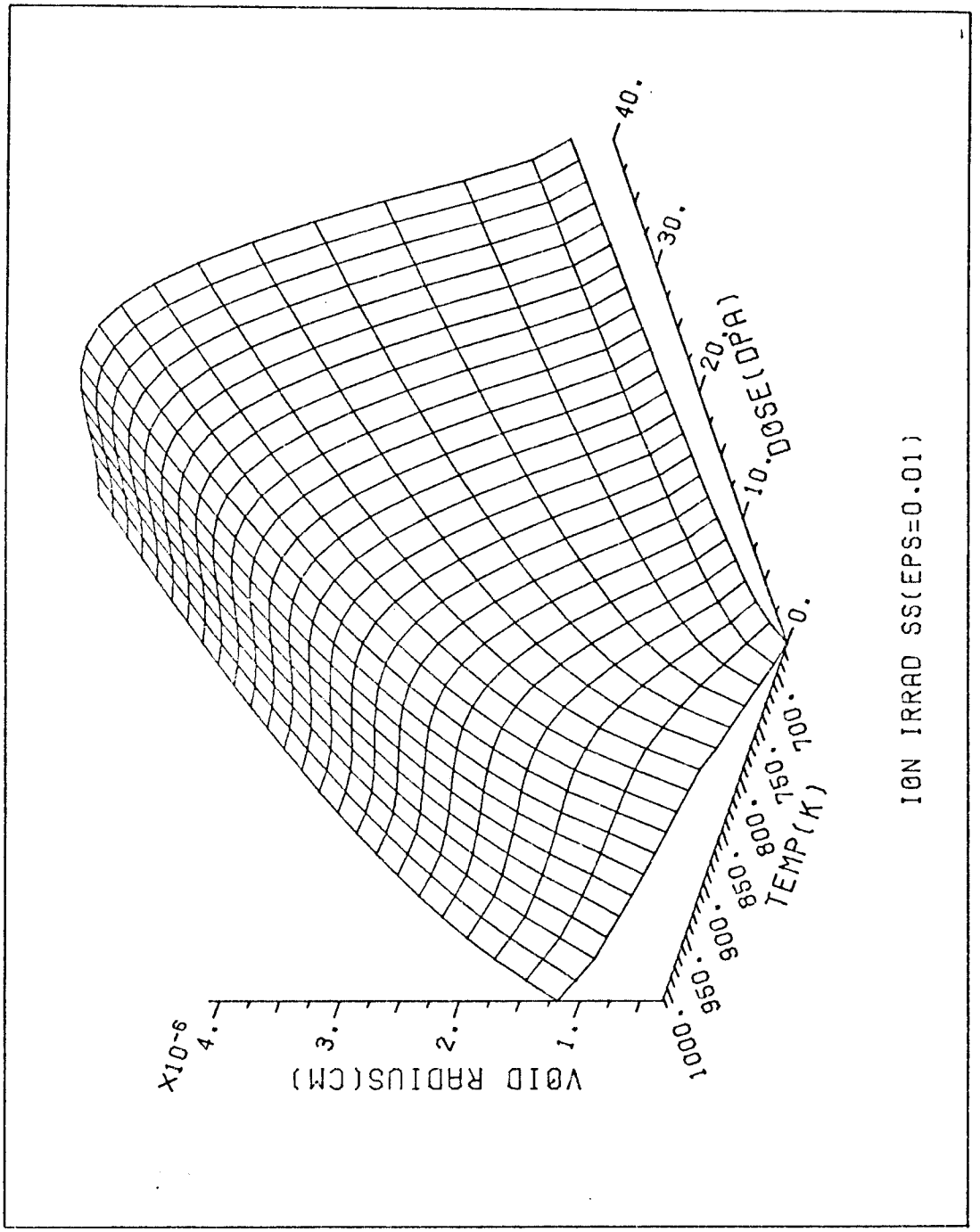

Fig. (12) 3-dimensional plot of mean void radius (cm) as a function of dose and temperature for ion irradiated ST stainless steel. The rate is 10^{-3} dpa/sec and the cascade efficiency is 0.01.

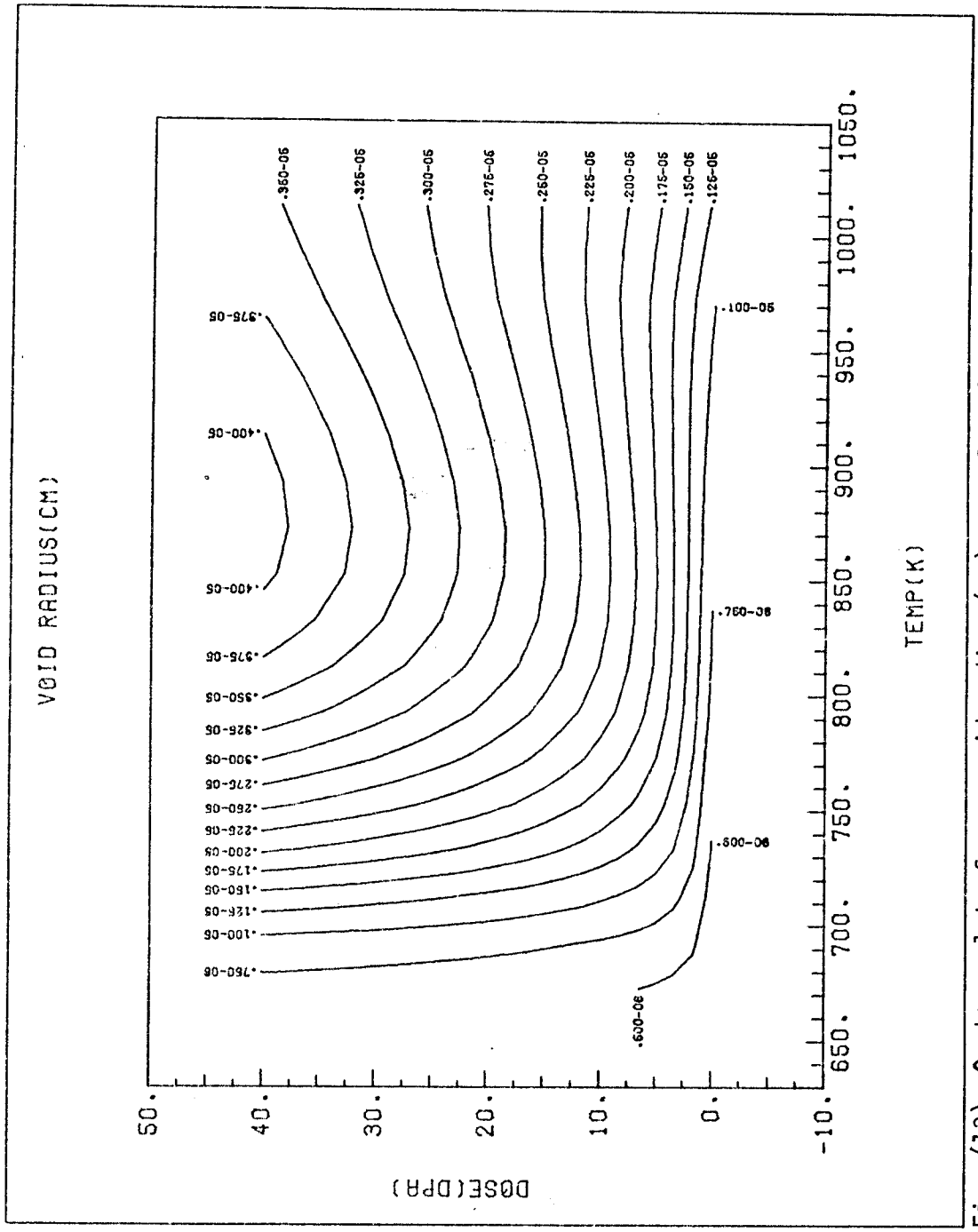

Fig. (13) Contour plot of mean void radius (cm) as a function of dose and temperature for ion irradiated ST stainless steel. The rate is 10-3 dpa/sec and the cascade efficiency is 0.01.

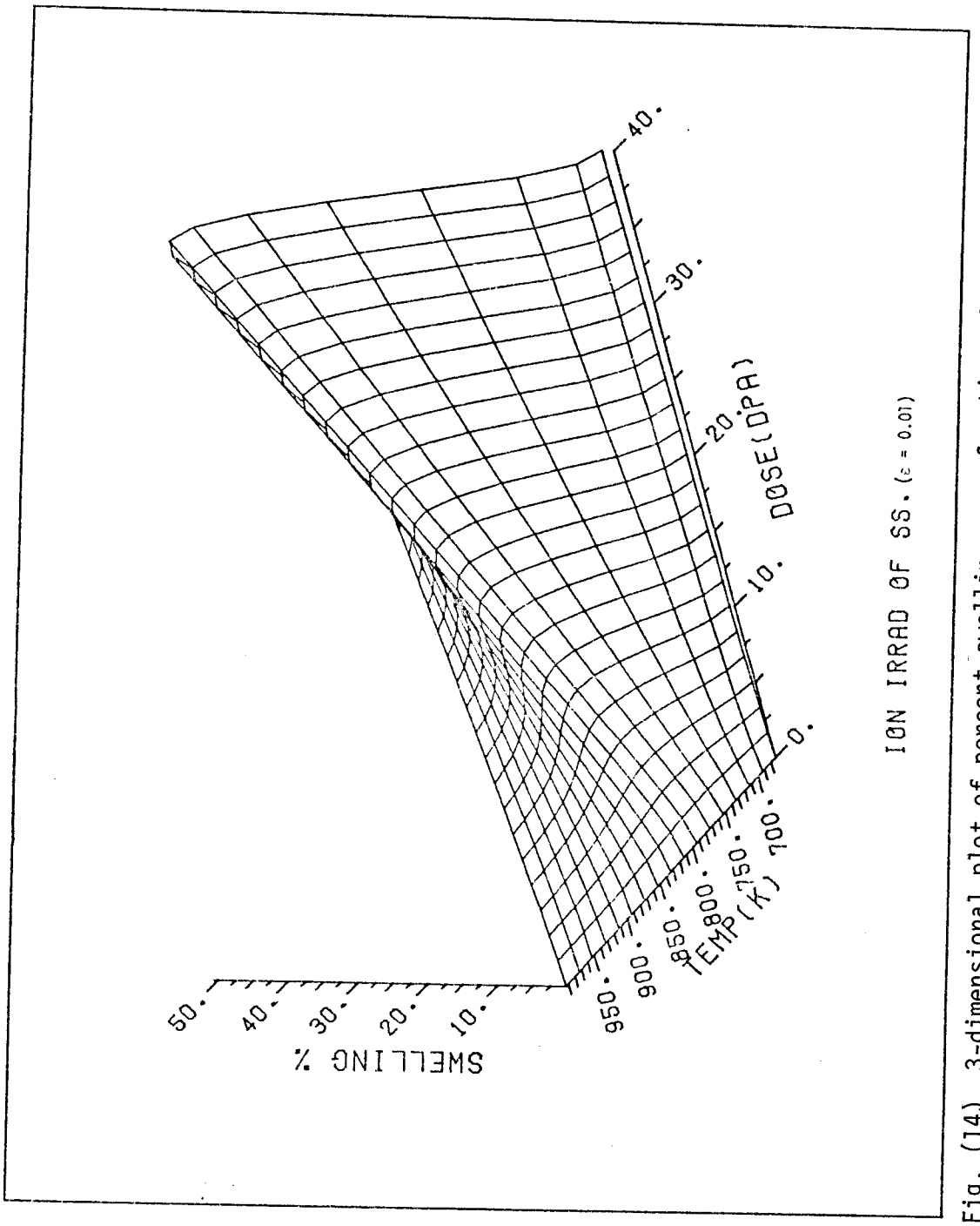

Fig. (14) 3-dimensional plot of percent swelling as a function of dose and temperature for ion irradiated ST stainless steel. The rate is 10^{-3} dpa/sec and the cascade efficiency is 0.01.

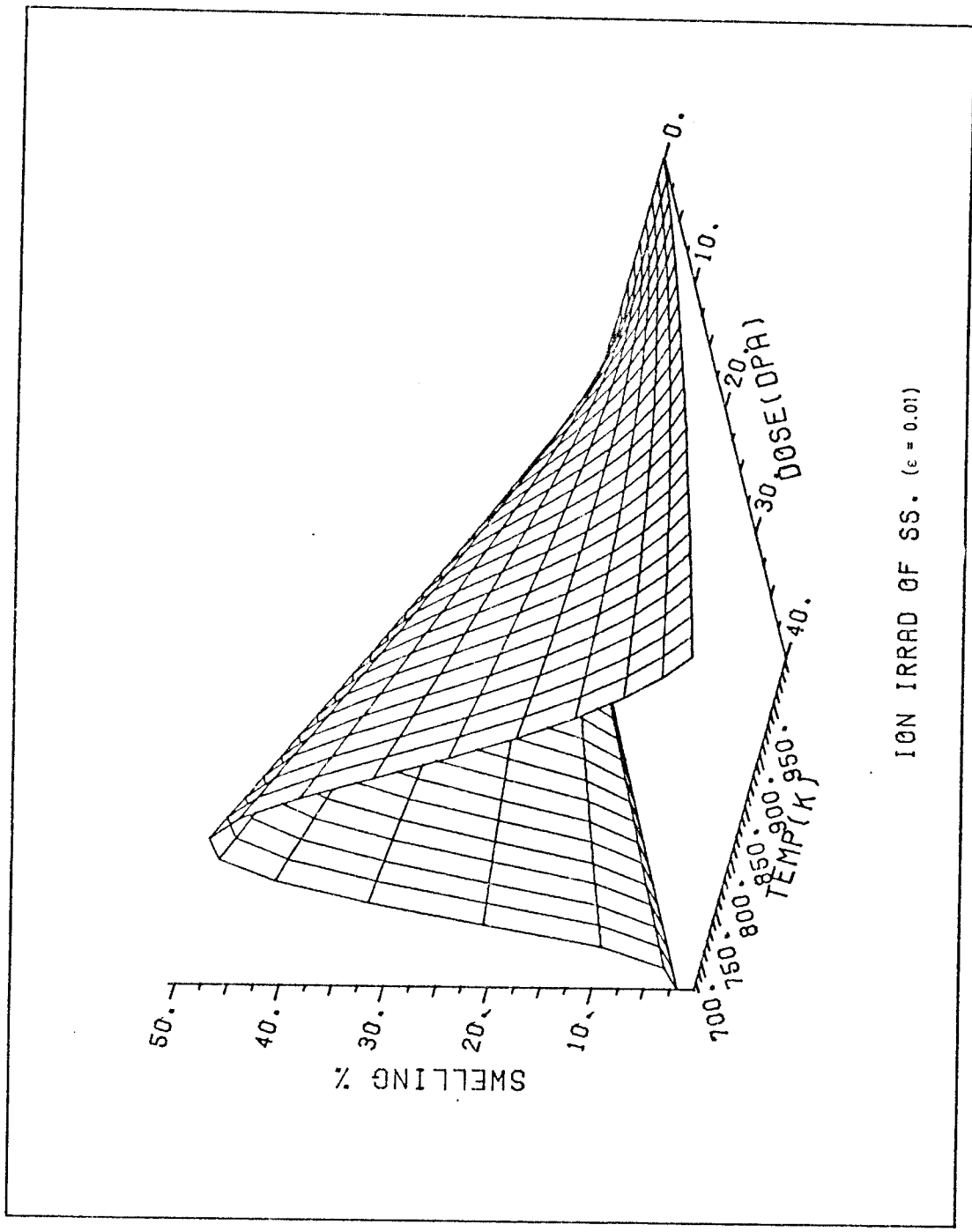

Fig. (15) 3-dimensional plot of percent swelling as a function of dose and temperature for ion irradiated ST stainless steel. The rate is 10^{-3} dpa/sec and the cascade efficiency is 0.01.

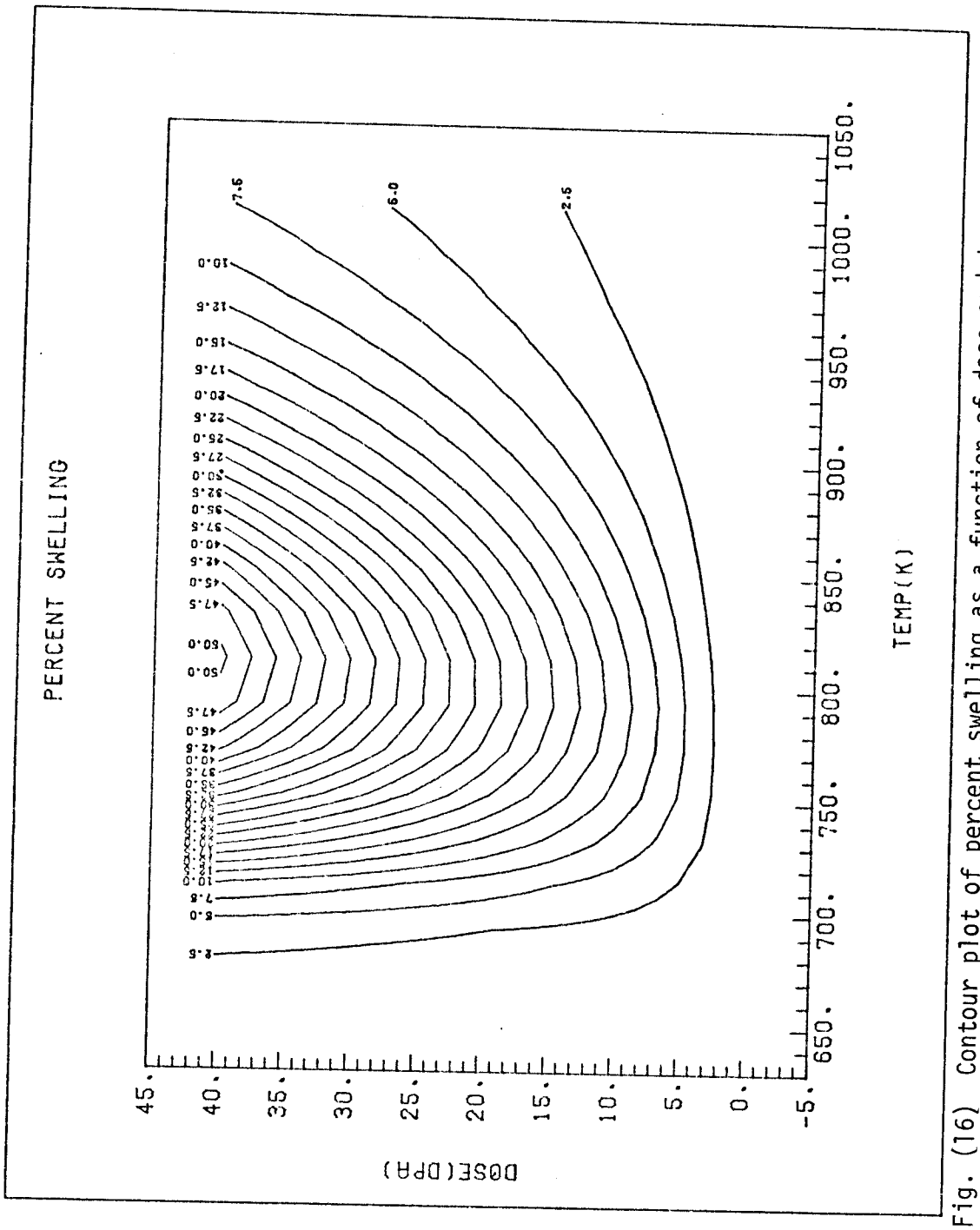

Fig. (16) Contour plot of percent swelling as a function of dose and temperature for ion irradiated ST stainless steel. The rate is 10-3 dpa/sec and the cascade efficiency is 0.01.

The obvious result would be a "bell shaped" swelling curve as frequently observed experimentally.

A large peak swelling value is obtained here ($\sim$ 50% at 40 dpa) compared to the smaller swelling value for the same steel ($\sim$ 12% at 40 dpa) reported in reference (5). The only difference between the two cases is the cascade collapse efficiency (ε) being 1% in this case versus 4.4% in the case studied in reference (5).

c. Rate Processes

i. Vacancy Thermal Emission Rate

Figures (17) and (18) show the thermal vacancy emission from only edge dislocations. It was assumed that the initial deformation produced dislocation density is held at a constant low value ($\sim 10^8$ lines/cm^2) commensurate with solution treated steels. The quantity plotted is equal to ($D_v^s \rho_c^e$) where D_v^s is the self diffusion coefficient of vacancies and ρ_d^e is the deformation produced dislocation density. It is then clear why the temperature dependence of this term is exponential while it is constant as a function of dose.

Figure (17) reveals that thermal emission of vacancies from edge dislocations does not become significant until $\sim 900^oK$ and even then the absolute value of $\sim 10^{-7}$ at/at/sec is much smaller than the production rate of 10^{-3} at/at/sec.

The emission rate of vacancies from the surfaces of voids, that is, $\{D_v^s (4\pi R_c N_c) (\exp [(\frac{2\gamma}{R_c} - P_g) \frac{\Omega}{kT})]\}$, is shown in Figures (19) and (20). As can be seen from the figures, the temperature dependence of this function is mainly controlled by the self diffusion coefficient D_v^s with small contribution from the total void surface and the driving force to emit vacancies.

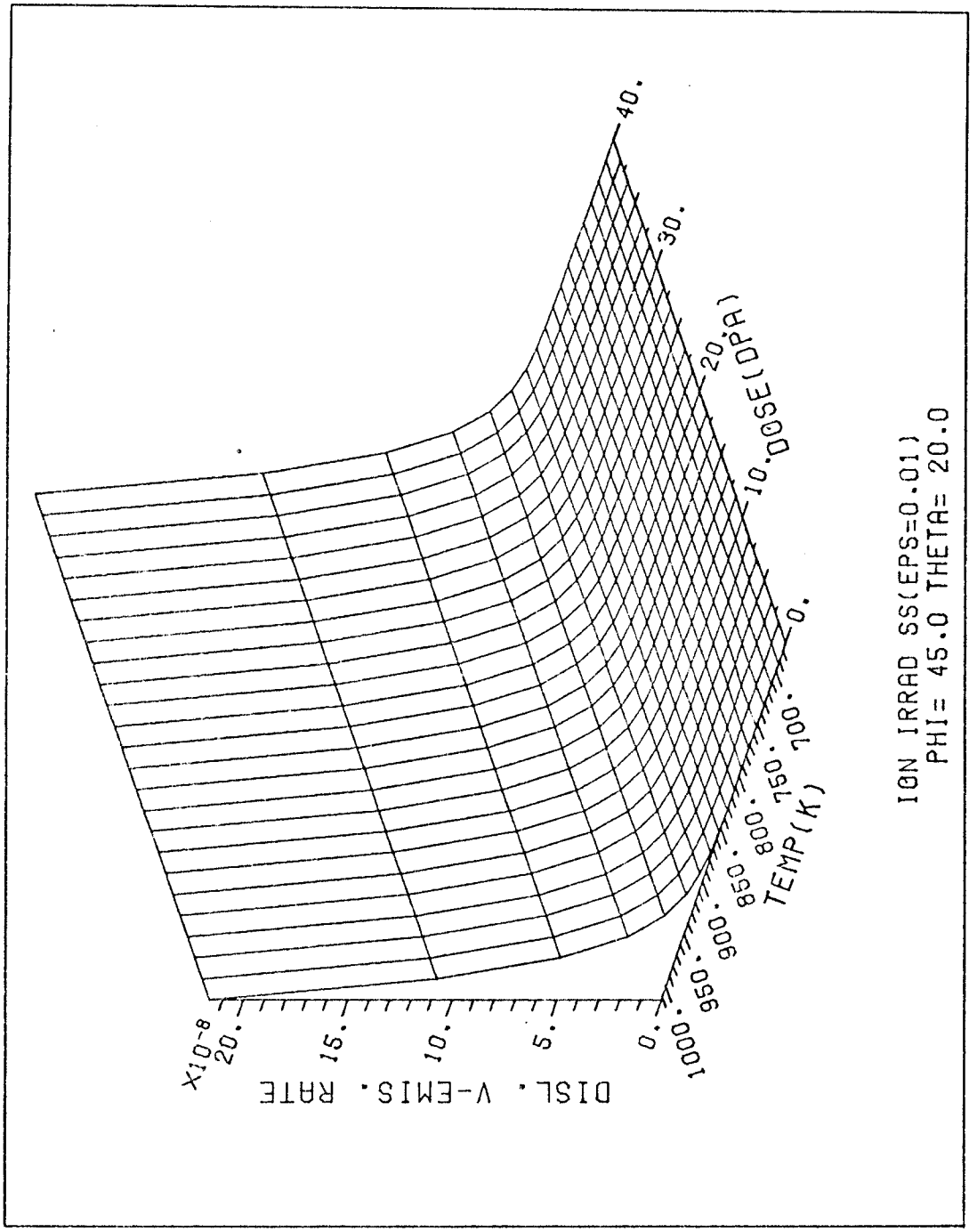

Fig. (17) 3-dimensional plot of vacancy thermal emission rate from edge dislocations (at./at./sec.) as a function of dose and temperature in ST stainless steel. The dose rate is 10^{-3} dpa/sec and the cascade efficiency is 0.01.

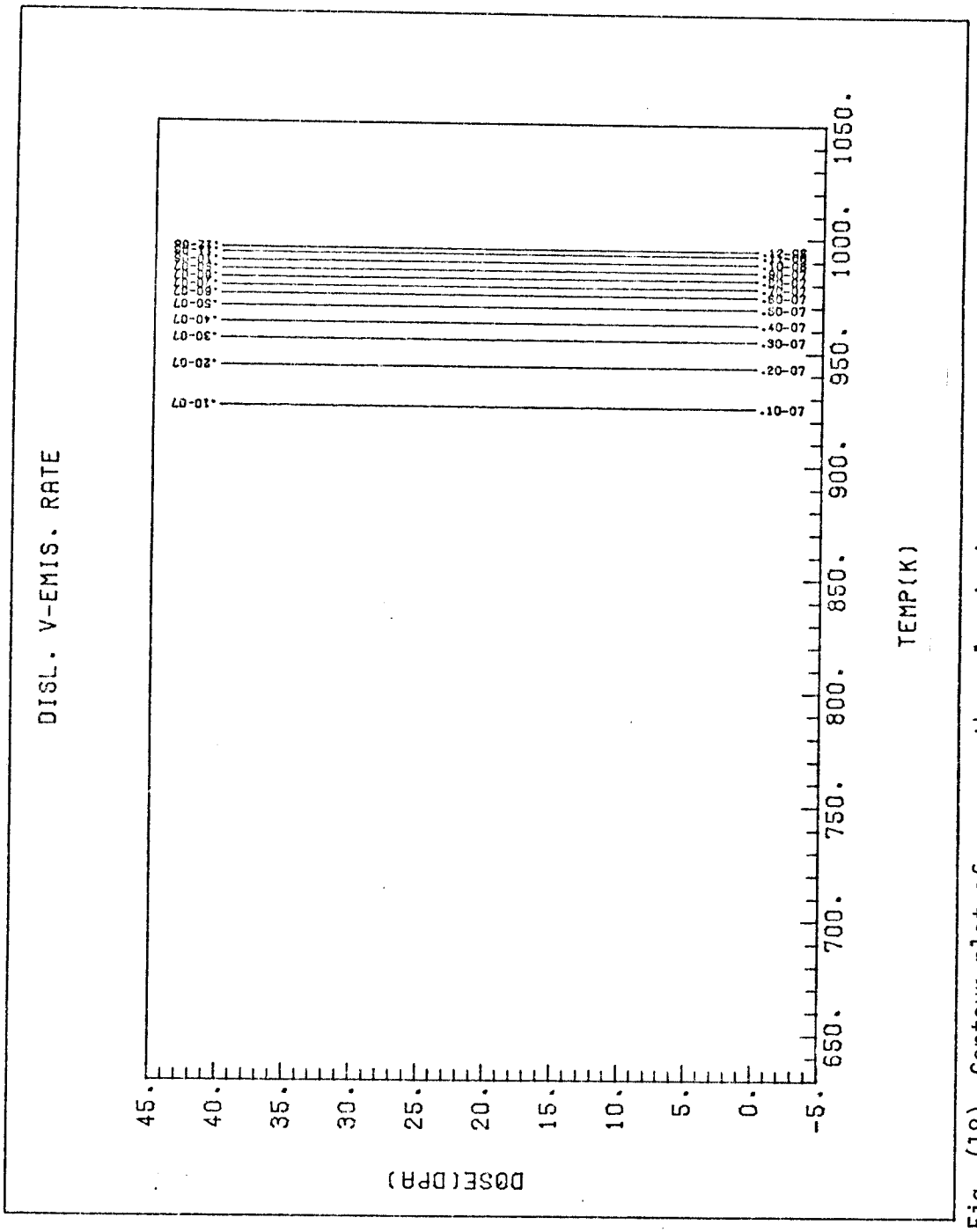

Fig. (18) Contour plot of vacancy thermal emission rate from edge dislocations (at./at./sec.) as a function of dose and temperature in ST stainless steel. The dose rate is 10^{-3} dpa/sec and the cascade efficiency is 0.01.

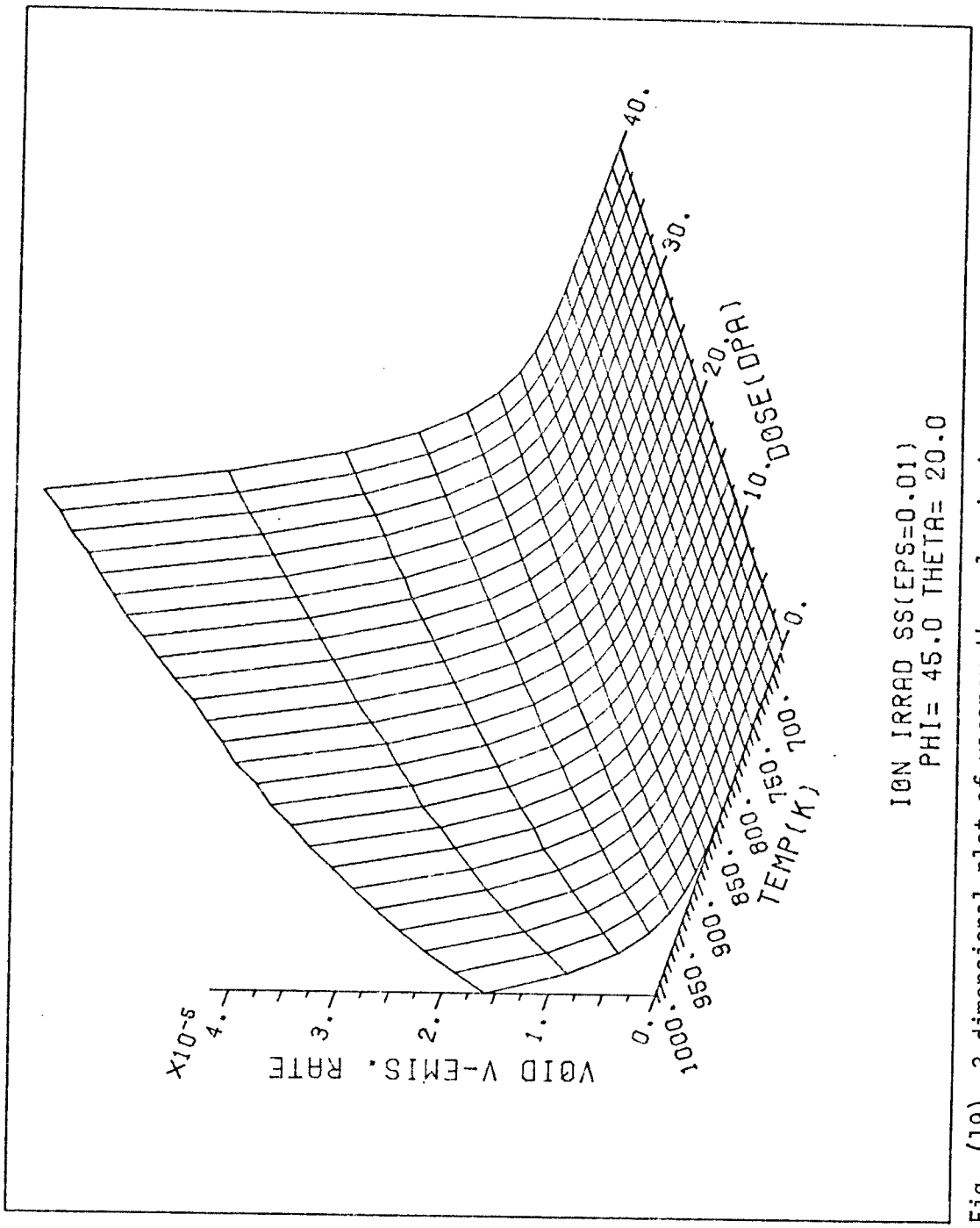

Fig. (19) 3-dimensional plot of vacancy thermal emission rate from voids (at./at./sec.) as a function of dose and temperature in ST stainless steel. The dose rate is 10^{-3} dpa/sec and the cascade efficiency is 0.01.

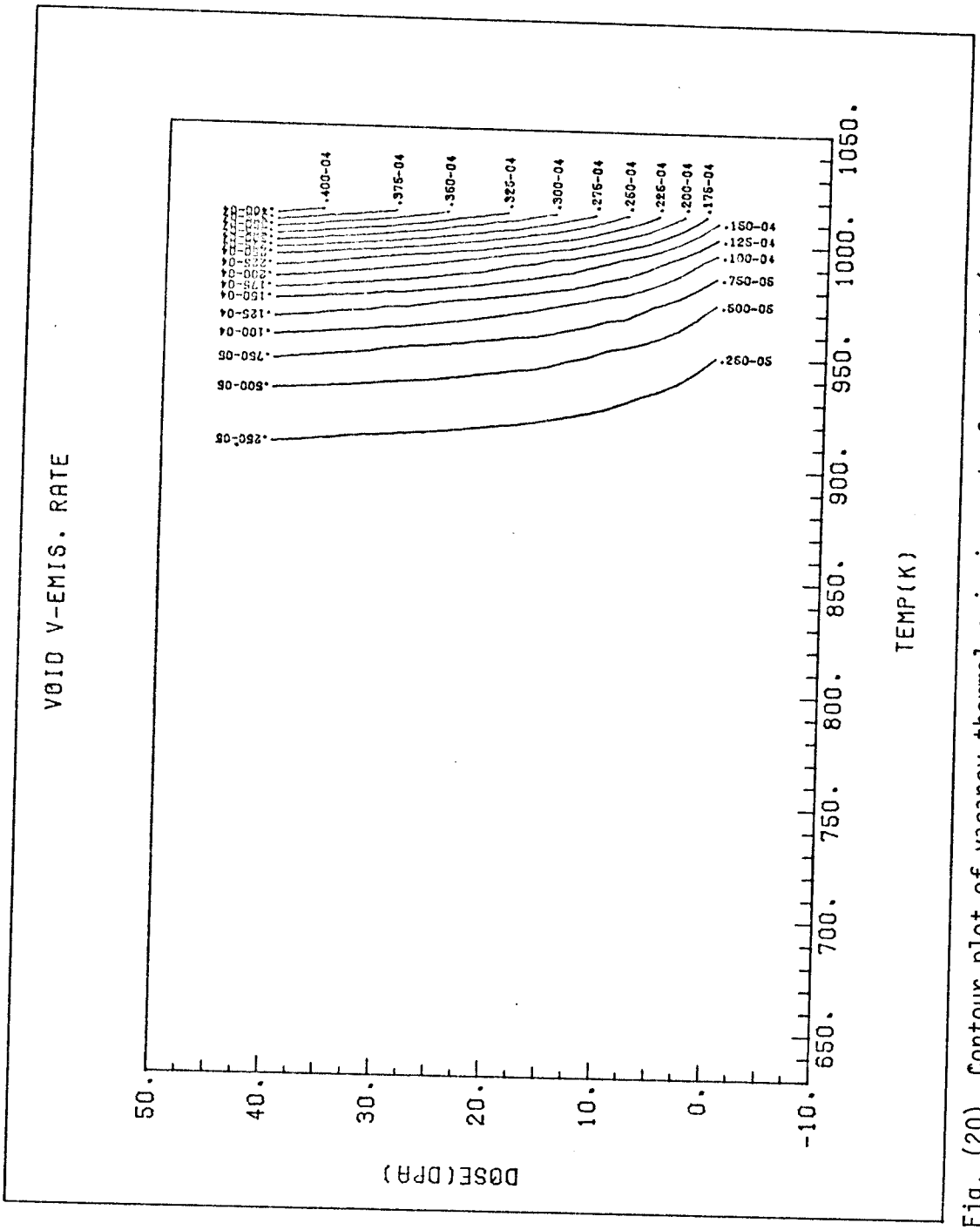

Fig. (20) Contour plot of vacancy thermal emission rate from voids (at./at./sec.) as a function of dose and temperature in ST stainless steel. The dose rate is 10^{-3} dpa/sec and the cascade efficiency is 0.01.

The emission term does not become important until $\sim 900^{o}K$ and it is only slightly dose dependent through the R_c term. Note that the absolute value of a few times 10^{-5} at/at/sec is much larger than the emission from edge dislocations.

The total vacancy emission rate is plotted in Figures (21) and (22). Comparisons with Figures (17), (18), (19) and (20) reveals that vacancy emission in this particular system is mainly controlled by voids alone. The contribution to vacancy emission from voids seems to be roughly 80% and that from the rest of the microstructure (i.e., i-loops, v. loops and edge dislocations) is dominated by the vacancy loops. A final feature of note is that the total vacancy emission rate can approach 5% of the gross production rate.

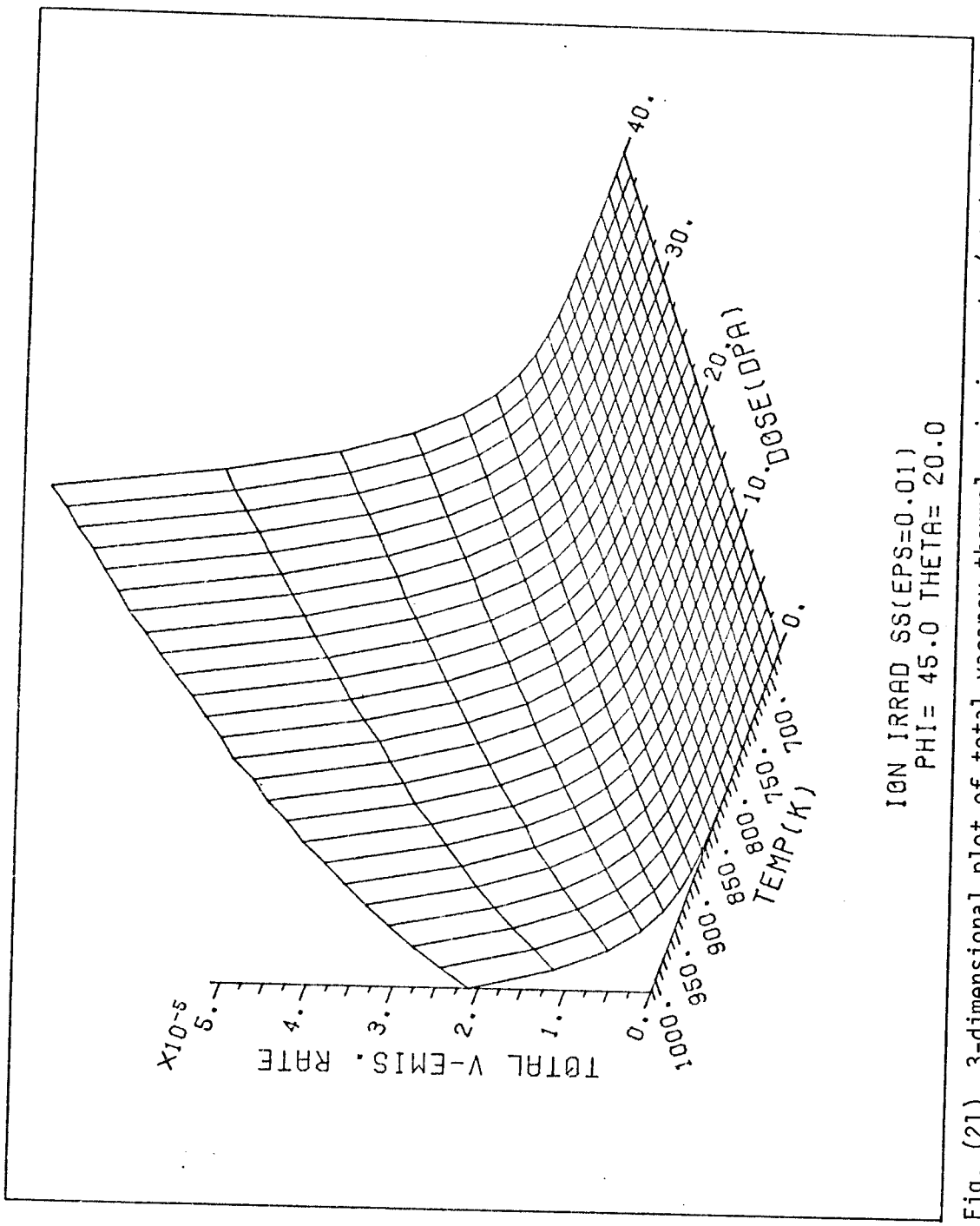

Fig. (21) 3-dimensional plot of total vacancy thermal emission rate (at./at./sec.) as a function of dose and temperature in ST stainless steel. The dose rate is 10^{-3} dpa/sec and the cascade efficiency is 0.01.

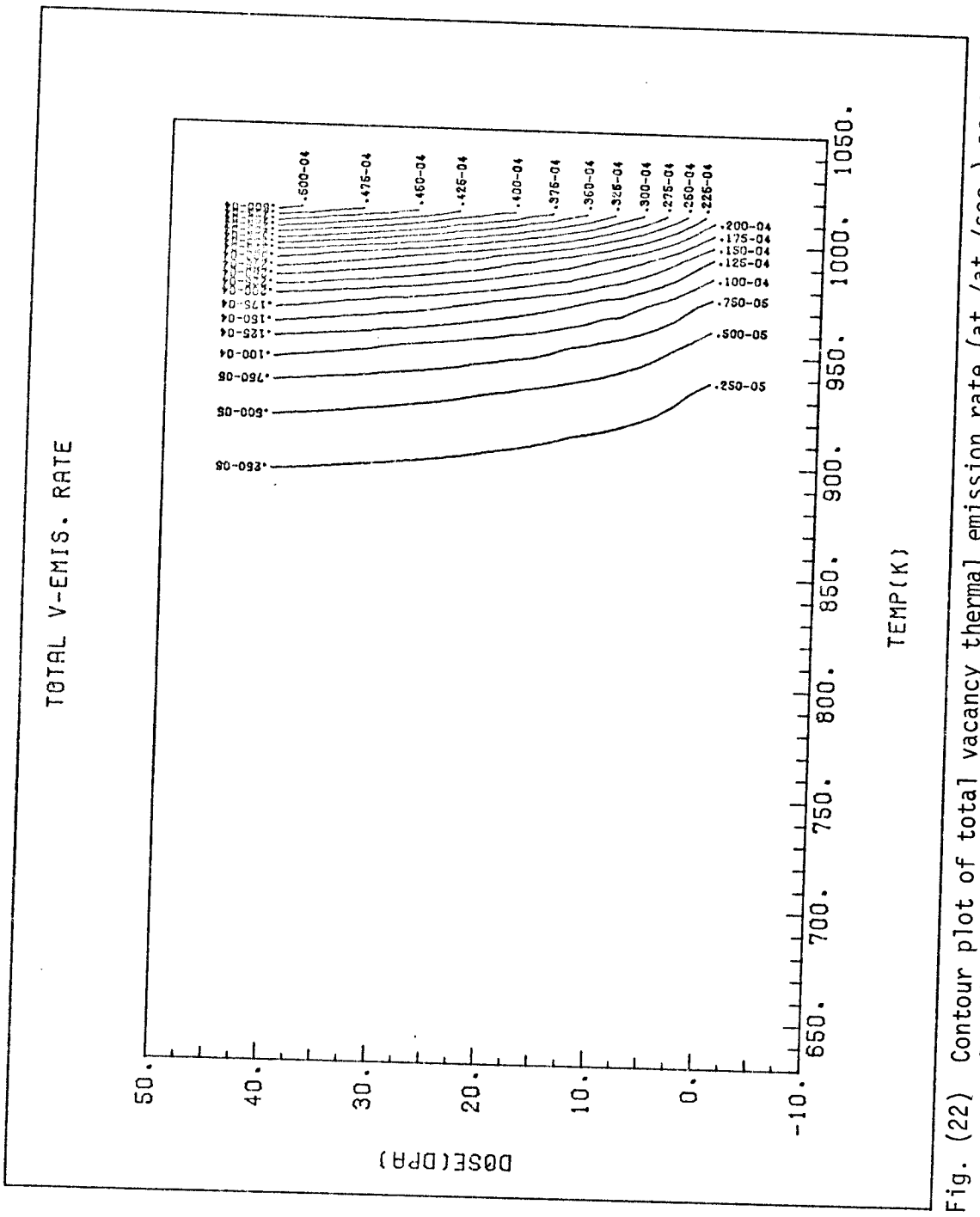

Fig. (22) Contour plot of total vacancy thermal emission rate (at./at./sec.) as a function of dose and temperature in ST stainless steel. The dose rate is 10^{-3} dpa/sec and the cascade efficiency is 0.01.

ii. Point Defect Sink Removal Rates

Sink removal rates are defined as the rates at which different types of sinks (i.e., i-loops, edge dislocations, v-loops, voids, ... , etc.) remove point defects from the matrix. Point defect concentrations are determined by the balance between their production (via irradiation or thermal emission) and their removal (via different sinks or recombination).

We will concentrate here on the total rate at which various sinks remove point defects. The quantity displayed in Figures (23) and (24) is given by:

$$\text{Vacancy Removal Rate} = D_v C_v \{4\pi N_c R_c + \rho_d\} \quad (7)$$

where ρ_d is the total dislocation density.

The results of the present work show that the vacancy removal rate is not a strong function of temperature or dose except for a transient at $\sim$ 650 - 750^{o}K and up to a few dpa. This transient occurs because of the rapid buildup of vacancy loops in the first few hundredths of a dpa followed by rapid vacancy emission which add vacancies to those already being produced by irradiation. The time steps between the updating of defect concentrations needs to be very small to detect the initial buildup and then the longer decay of the defect concentrations.*

The slight decrease of this removal rate with temperature is due to the dominance of the temperature dependence of the sink term in Equation (7) over the vacancy flux ($D_v C_v$). The increase of the removal rate with increasing dose is due to growth of voids and loops with irradiation dose. This feature is seen more clearly at high temperatures in Fig. (24).

Total interstitial sink removal rate is given by:

*In Figures (23-26), (51-52) and (74-76) the dose axis starts at $\sim$0.5 dpa to remove the artificial peaks due to the integration process.

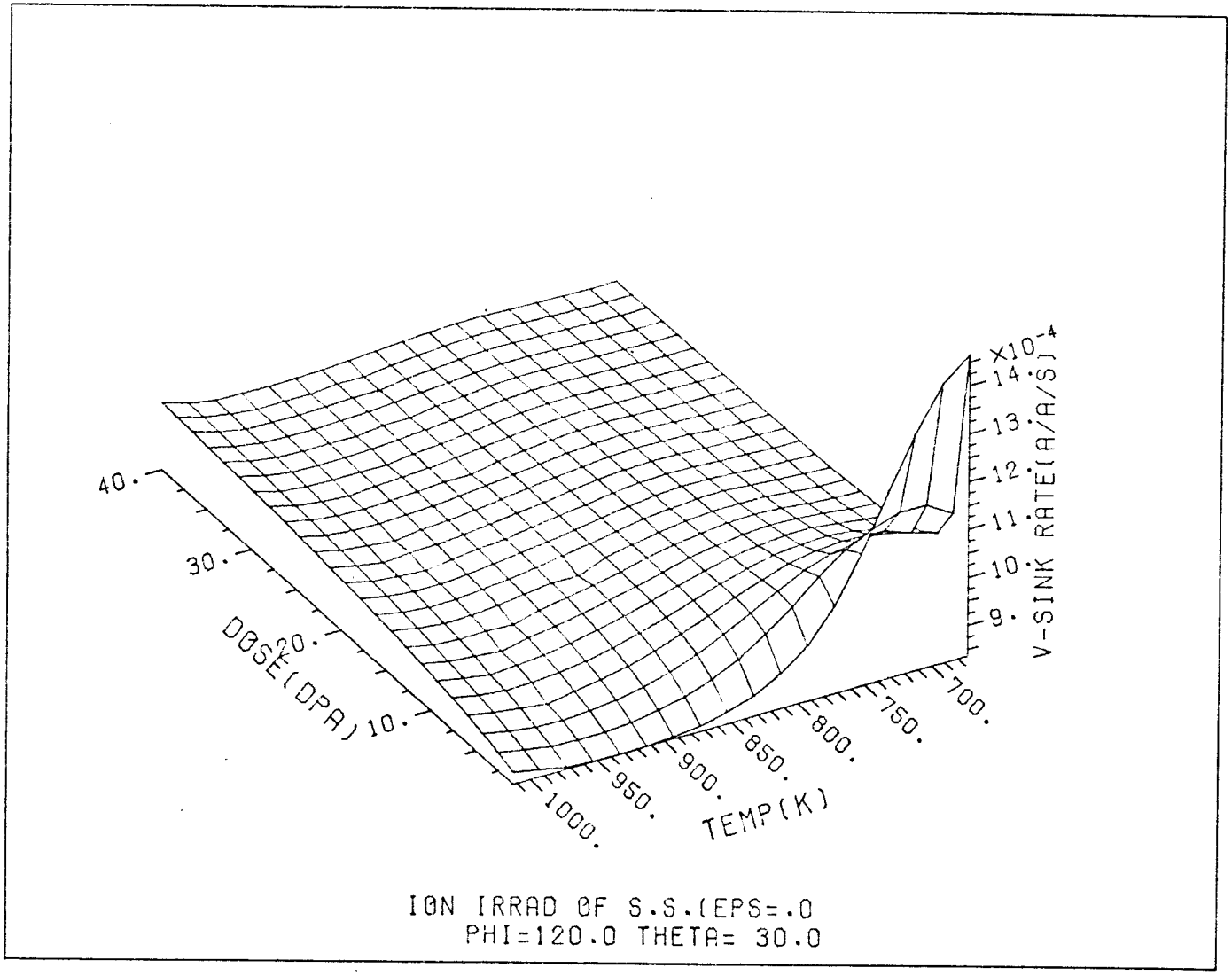

Fig. (23) 3-dimensional plot of vacancy sink removal rate (at./at./sec.) as a function of dose and temperature for ion irradiated ST stainless steel. The dose rate is 10^{-3} dpa/sec and the cascade efficiency is 0.01.

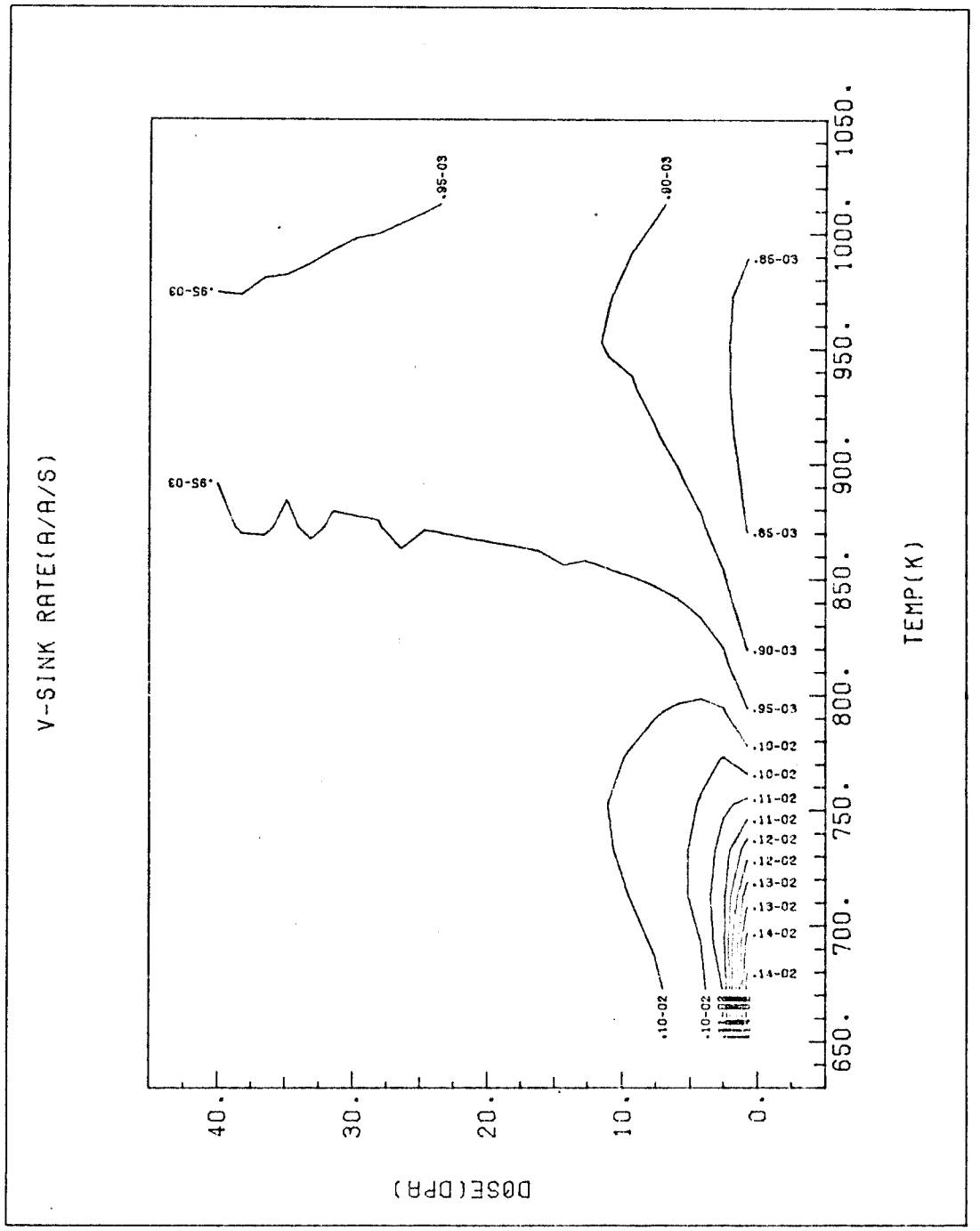

Fig. (24) Contour plot of vacancy sink removal rate (at./at./sec.) as a function of dose and temperature for ion irradiated ST stainless steel. The dose rate is 10^{-3} dpa/sec and the cascade efficiency is 0.01.

$$\text{Interstitial Removal Rate} = D_i C_i \{4\pi N_c R_c^2 + Z_i \rho_d\} . \qquad (8)$$

The behavior of the interstitial sink removal rate is similar to that of the vacancies, the only difference being the thermal vacancy population. See Fig. 25 and 26.

It will be shown later (Figures (37) and (38)) that void equivalent sink strength ($4\pi N_c R_c$) is about 2 orders of magnitude lower than the dislocation sink strength ($Z_i \rho_d$) and, therefore, anything that influences the number and size of dislocation loops (i.e. ε or nucleation agents) will greatly effect the vacancy and interstitial sink strengths.

iii. Point Defects Recombination Rate

The recombination rate for point defects, as shown in Figures (27) and (28) reveal the following behavior: There is a sharp recombination rate transient at low temperature and this transient is less pronounced at high temperatures. Quantitatively, this behavior is described in Table 2.

Table 2

Effectiveness of Recombination as a Means of Removing Point Defects

Temperature °C	% Point Defect Removal by Recombination		
	0 dpa	2.5 dpa	40 dpa
400	50	2	~0
700	40	30	8

The fraction of defects removed by recombination is about equal to that of the total sink removal rate at the start of the irradiation, but it drops rapidly after that at low temperatures. Basically, the introduction

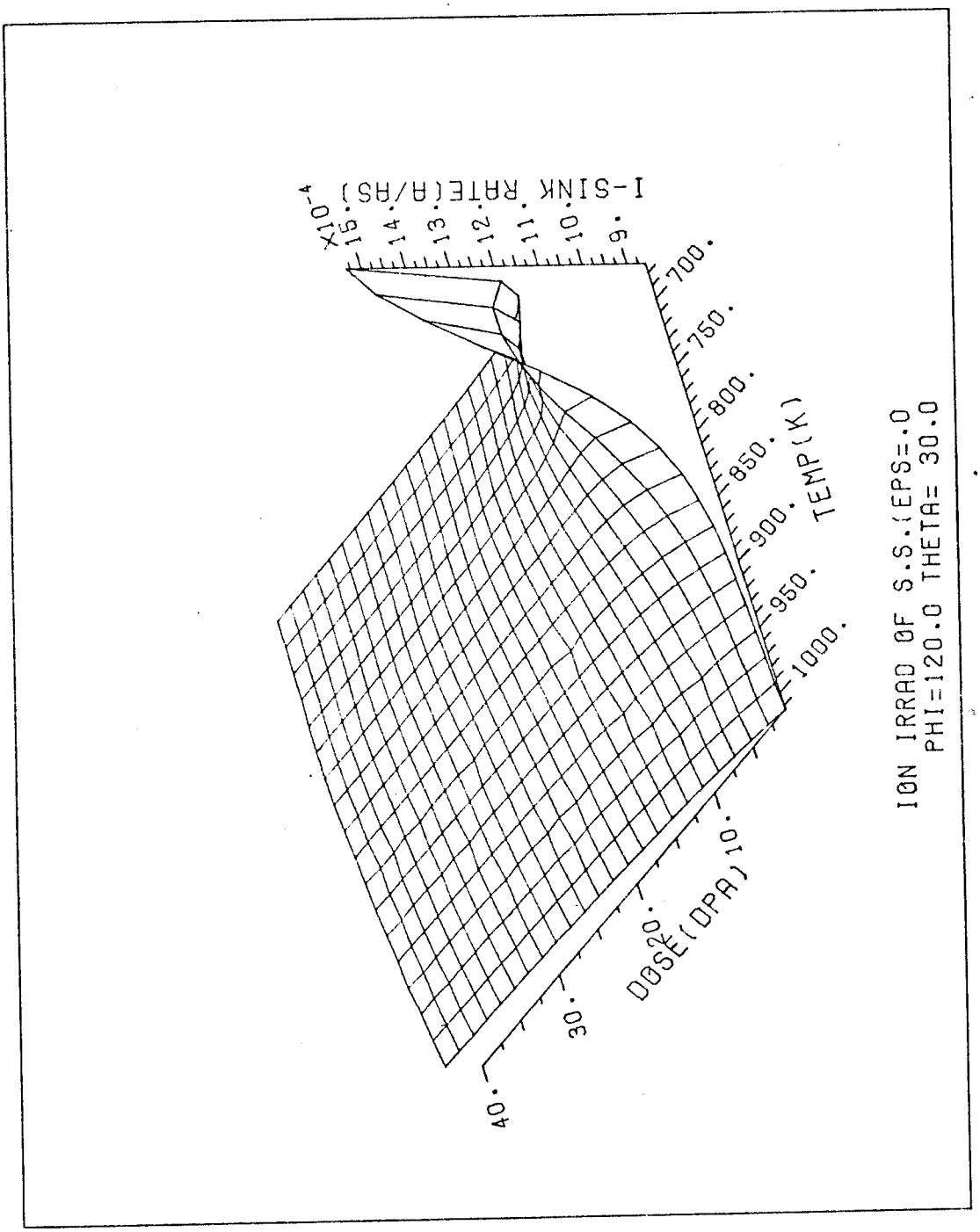

Fig. (25) 3-dimensional plot of interstitial sink removal rate (at./at./sec.) as a function of dose and temperature for ion irradiated ST stainless steel. The dose rate is 10^{-3} dpa/sec and the cascade efficiency is 0.01.

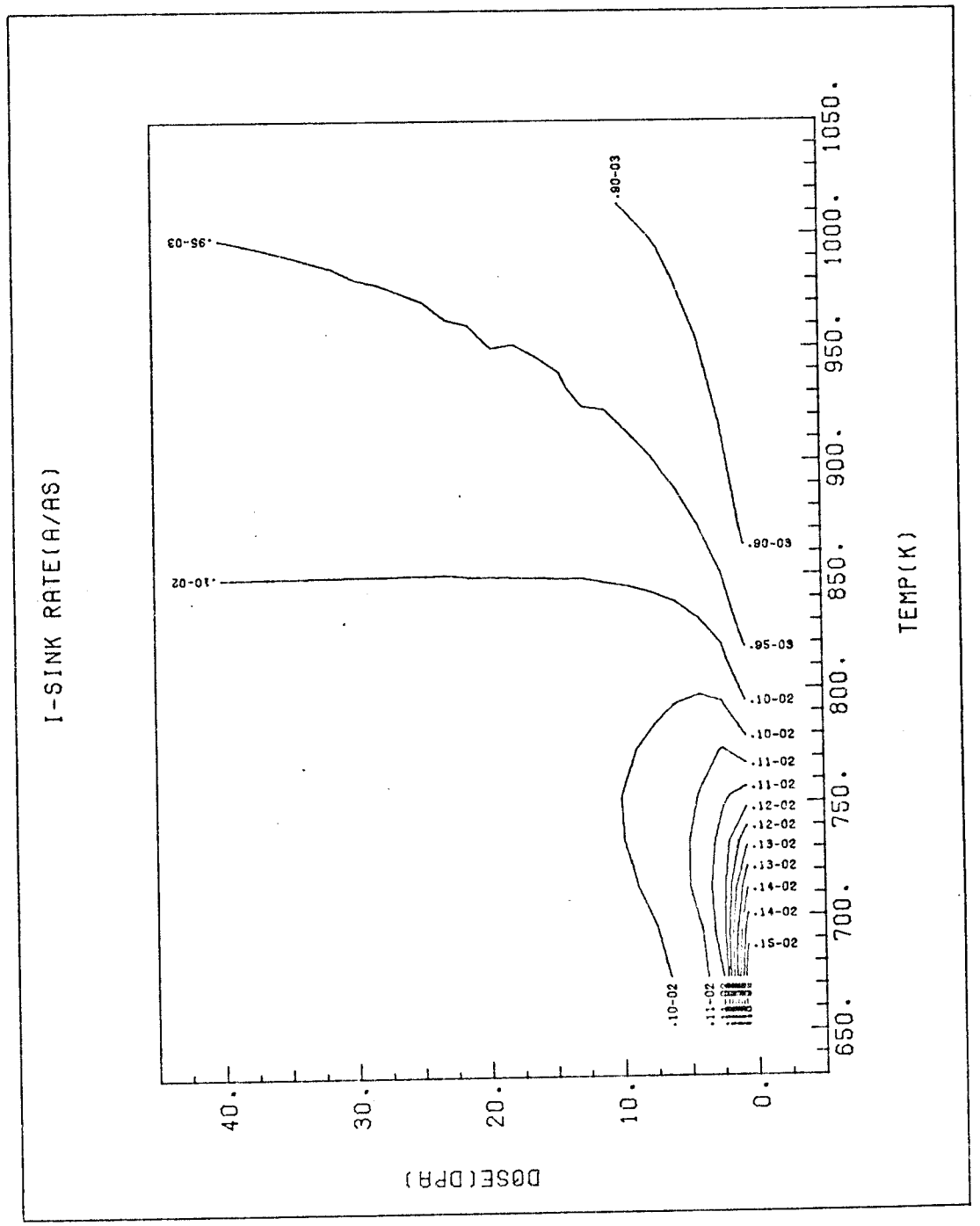

Fig. (26) Contour plot of interstitial sink removal rate (at./at./sec.) as a function of dose and temperature for ion irradiated ST stainless steel. The dose rate is 10^{-3} dpa/sec and the cascade efficiency is 0.01.

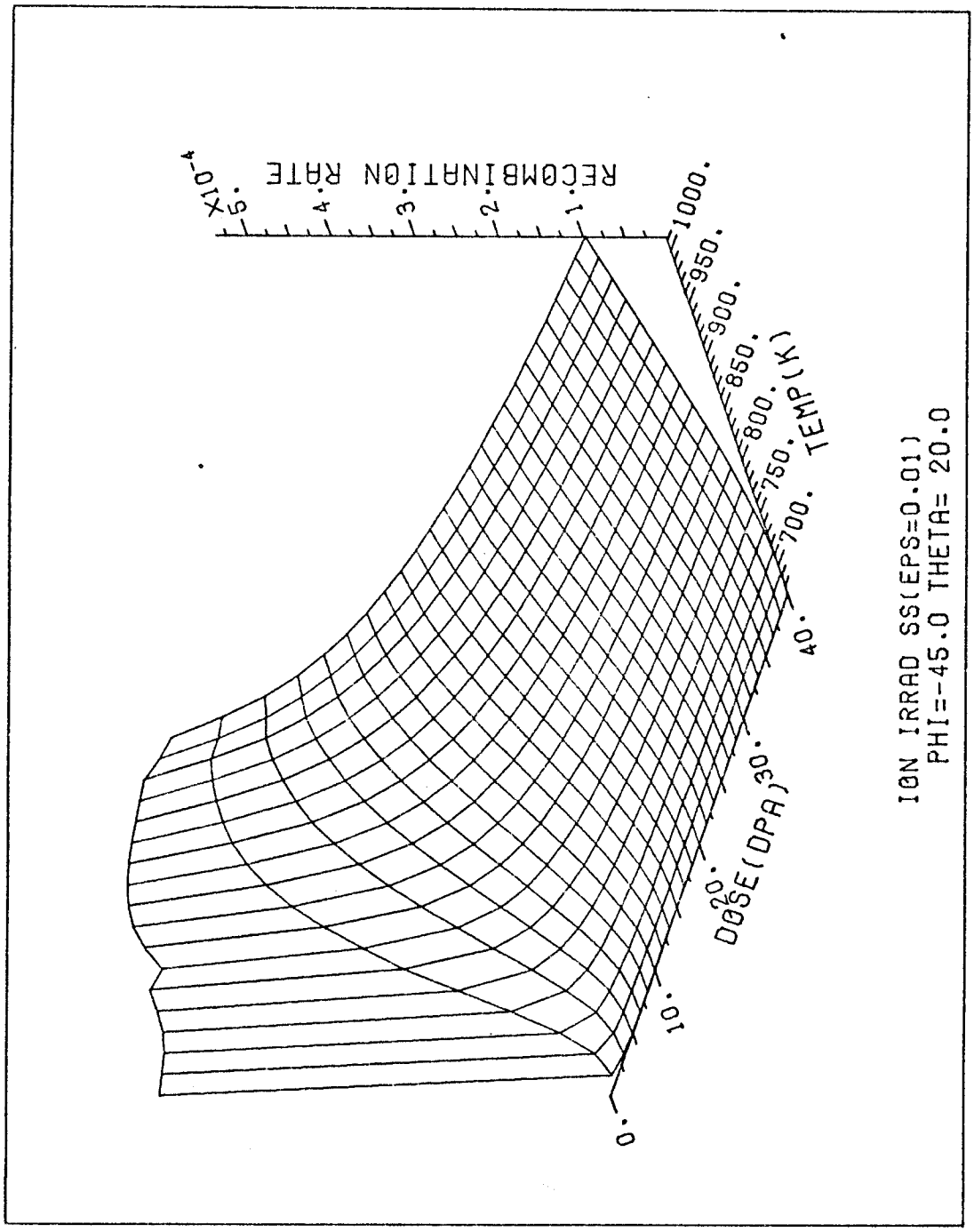

Fig. (27) 3-dimensional plot of point defect recombination rate (at./at./sec.) as a function of dose and temperature for ion irradiated ST stainless steel. The dose rate is 10^{-3} dpa/sec and the cascade efficiency is 0.01.

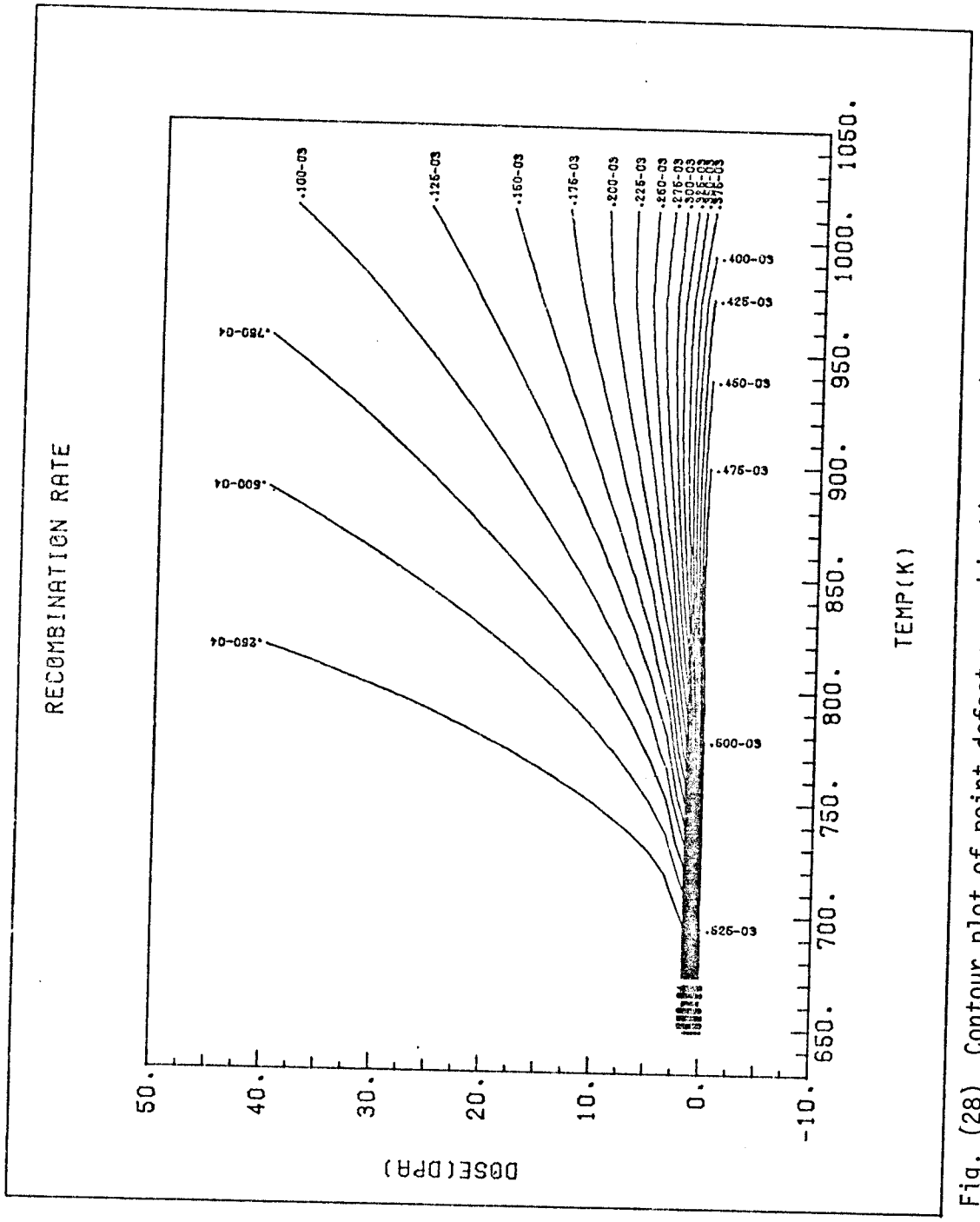

Fig. (28) Contour plot of point defect recombination rate (at./at./sec.) as a function of dose and temperature for ion irradiated ST stainless steel. The dose rate is 10-3 dpa/sec and the cascade efficiency is 0.01.

of a high density of vacancy loops makes it more likely that vacancies and interstitials will find the loops before they find each other. At higher temperatures the drop off in recombination rate with dose also occurs, but it is much less pronounced. This behavior is due to the lower loop line density at the higher temperatures and the higher mobility of the defects.

d. Microstructural Information:

i. Vacancy Loop Line Dislocation Density

The production rates of vacancy loop number density and vacancy fraction in vacancy loops are constant with irradiation (κ_1 and κ_2) while the decay rates (Λ_1 and Λ_2) are acutely temperature dependent. Once vacancy loops are born, they tend always to shrink because of the preferential attraction of interstitials and vacancy emission (evaporation of vacancies from their surfaces). Vacancy emission is also very sensitive to temperature as was pointed out in the section on rate processes (Figure 17). The net result is that the vacancy loop line density is only important at low temperatures (Figures 29 and 30). Another important point is that it takes a long irradiation time for the vacancy dislocation density to saturate at low temperatures while it saturates quickly at high temperatures due to increased shrinkage rates.

The vacancy loop number density is shown in Figures (31) and (32) as a function of dose and temperature (note the log scale). The rapid dropoff in vacancy number density with temperature and the rapid saturation with dose is understandable from our previous discussion.

ii. Interstitial Loop Dislocation Density

The temperature dependence of interstitial loop line density is essentially exponential due to the previously chosen nucleation condition

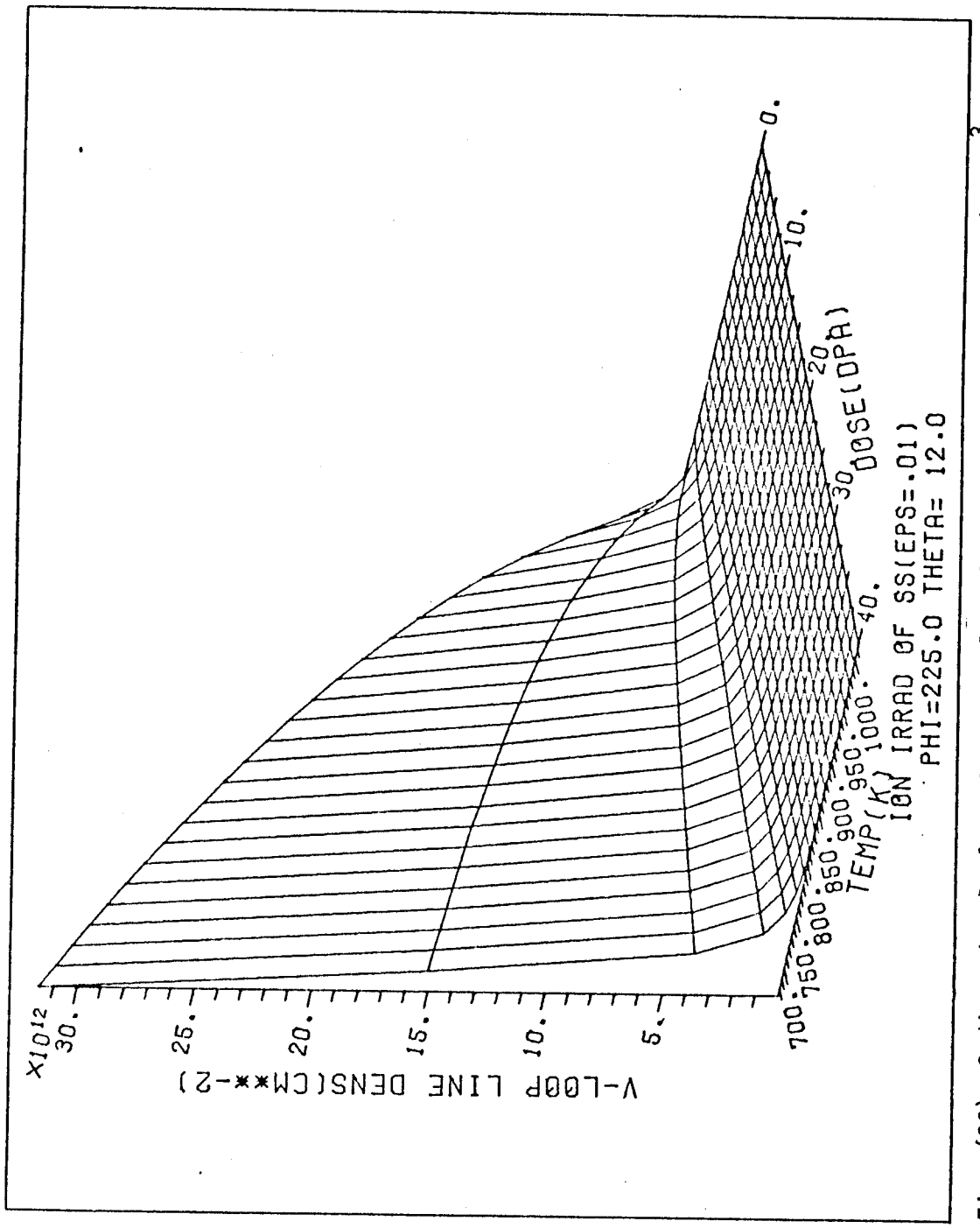

Fig. (29) 3-dimensional plot of vacancy loop line dislocation density (cm/cm^3) as a function of dose and temperature for ion irradiated ST stainless steel. The dose rate is 10^{-3} dpa/sec and the cascade efficiency is 0.01.

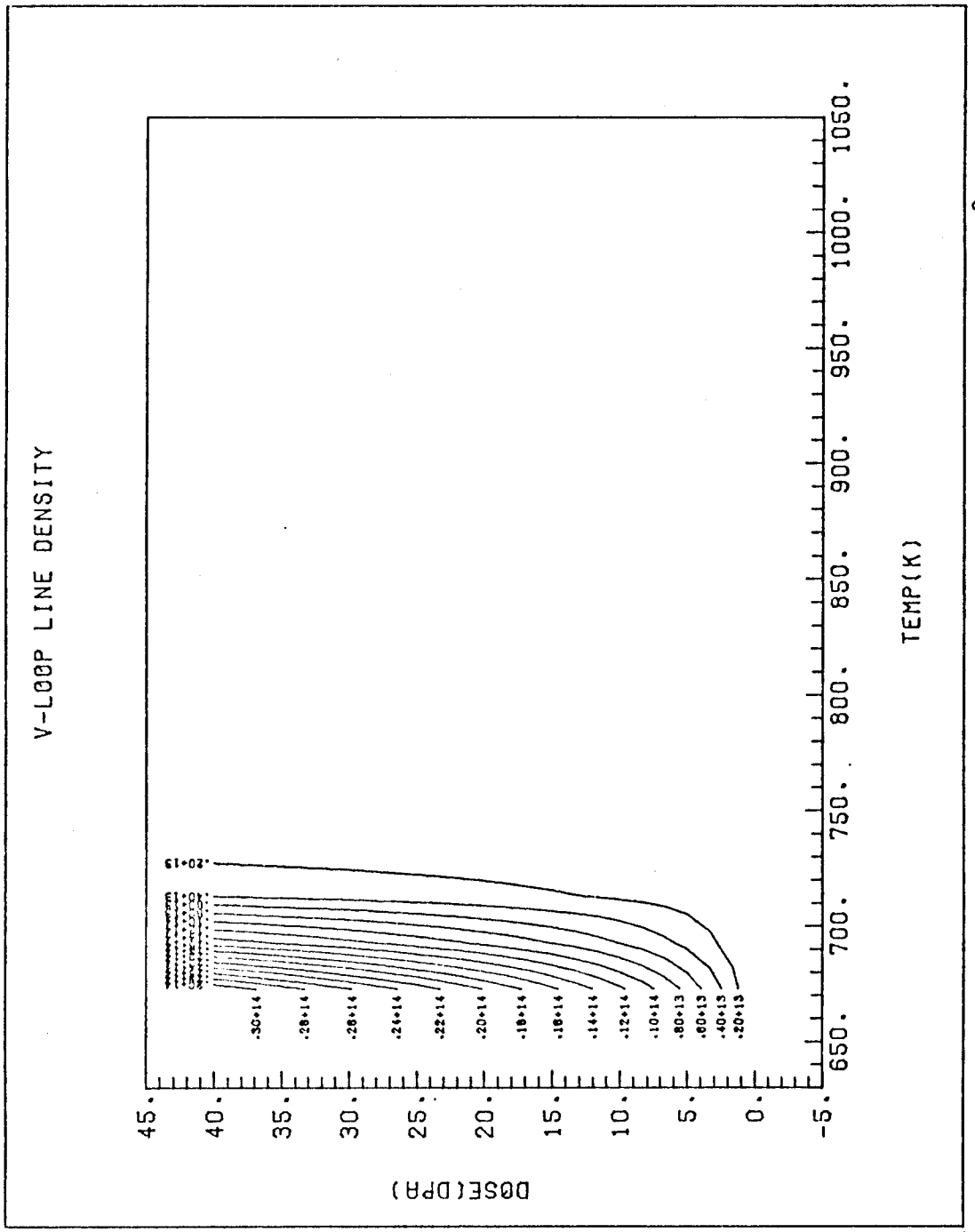

Fig. (30) Contour plot of vacancy loop line dislocation density (cm/cm^3) as a function of dose and temperature for ion irradiated ST stainless steel. The dose rate is 10^{-3} dpa/sec and the cascade efficiency is 0.01.

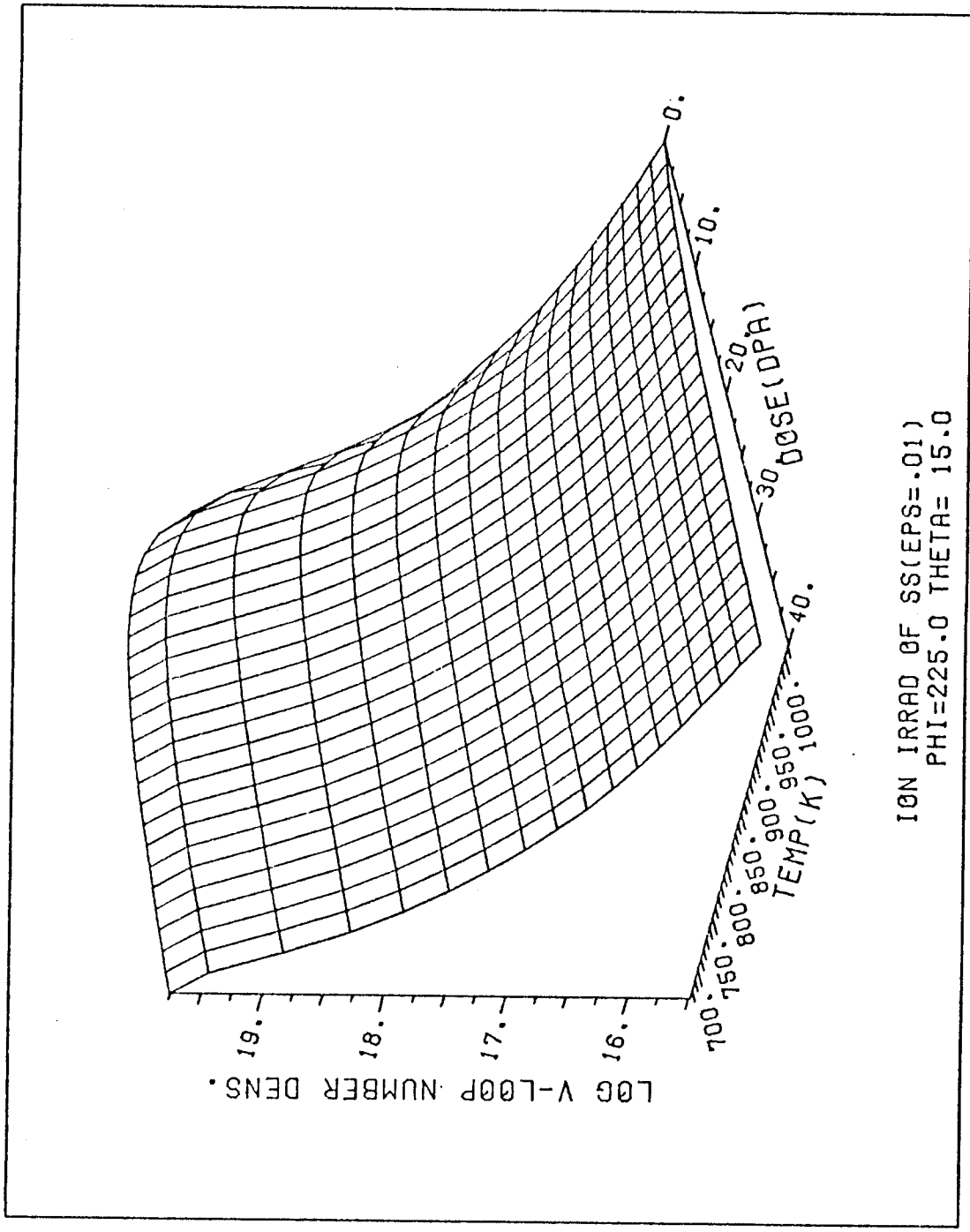

Fig. (31) 3-dimensional plot of vacancy loop number density (cm^{-3}) as a function of dose and temperature for ion irradiated ST stainless steel. The dose rate is 10^{-3} dpa/sec and the cascade efficiency is 0.01.

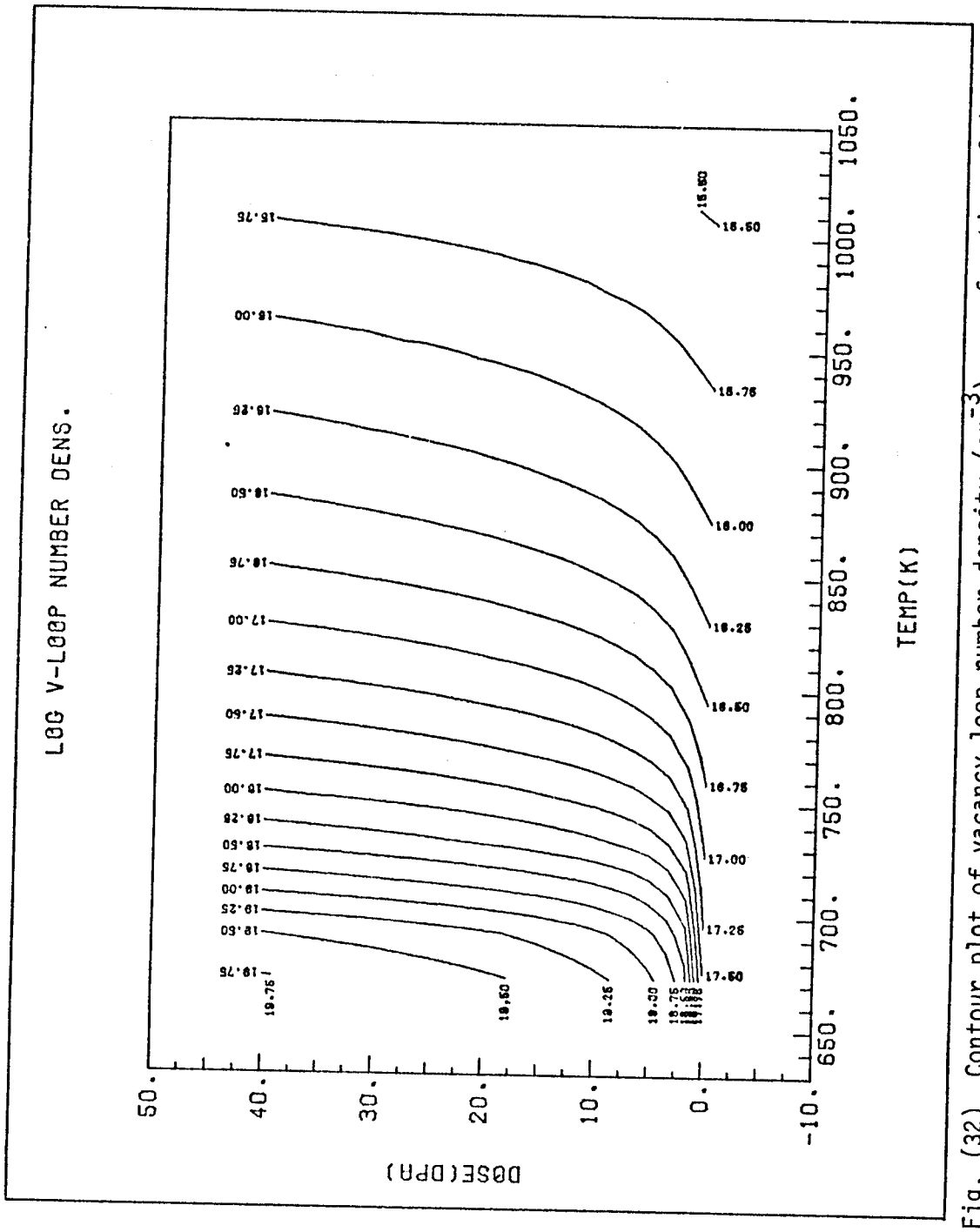

Fig. (32) Contour plot of vacancy loop number density (cm^{-3}) as a function of dose and temperature for ion irradiated ST stainless steel. The dose rate is 10^{-3} dpa/sec and the cascade efficiency is 0.01.

for the number density. Interstitial loops always grow by either receiving an excess flux of interstitials (biased growth) or by thermally emitting vacancies. They exhibit no shrinkage behavior (except at very high temperatures due to abundance of thermal vacancies) because thermal emission of interstitials has a diminishingly small rate due to the large interstitial formation energy. As a consequence of the described physical behavior, interstitial loop dislocation density goes up with increasing dose. The behavior is illustrated in Figures (33) and (34).

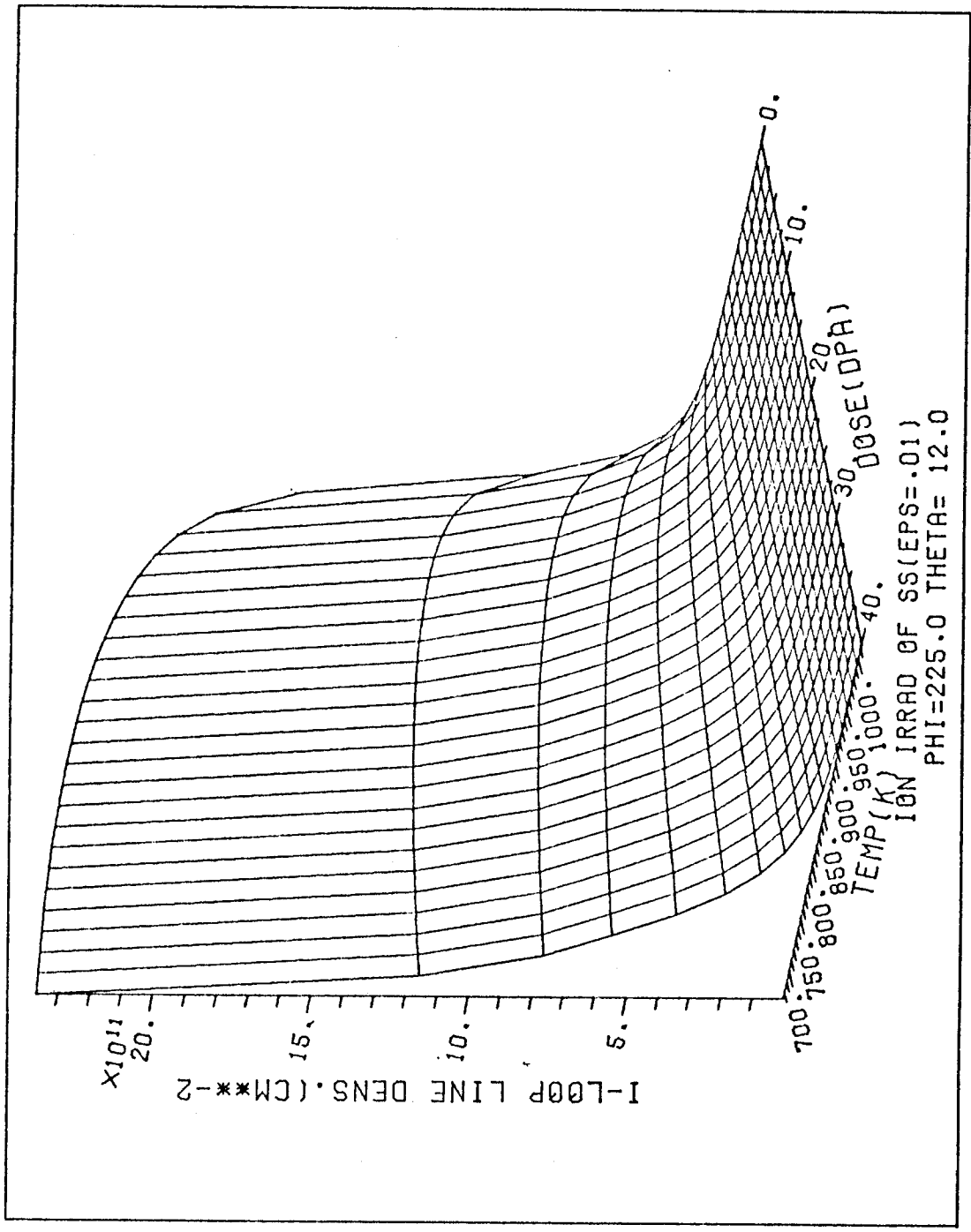

Fig. (33) 3-dimensional plot of interstitial loop line density (cm/cm^3) as a function of dose and temperature for ion irradiated ST stainless steel. The dose rate is 10^{-3} dpa/sec and the cascade efficiency is 0.01.

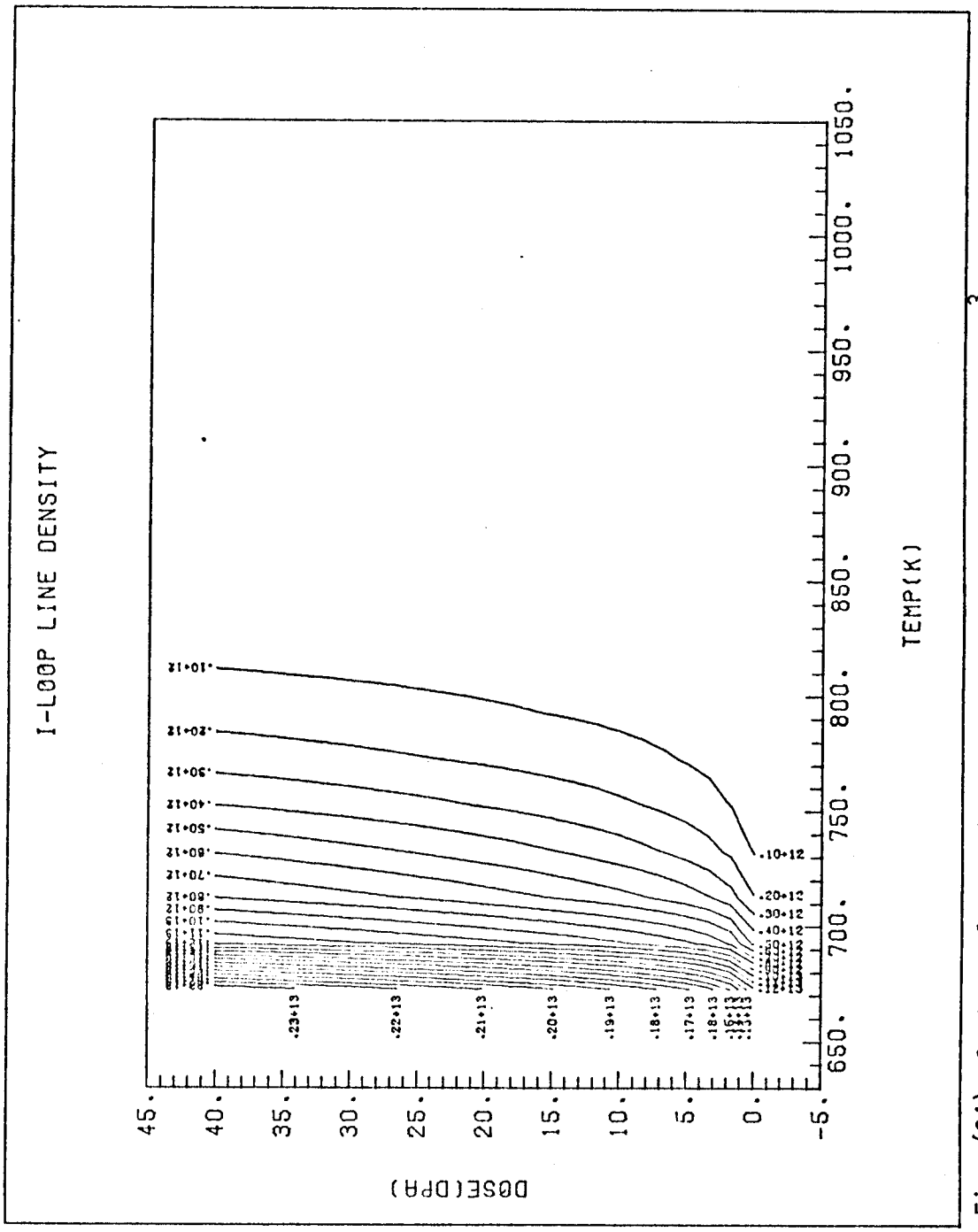

Fig. (34) Contour plot of interstitial loop line density (cm/cm^3) as a function of dose and temperature for ion irradiated ST stainless steel. The dose rate is 10-3 dpa/sec and the cascade efficiency is 0.01.

iii. Total Dislocation Density

The total dislocation density (Figures 35 and 36) is the algebraic sum of three components: (1) Initial deformation produced dislocations (10^8 lines/cm^2 in this case), (2) vacancy loop line dislocation density (Figures 29 and 30), and (3) interstitial loop line dislocation density (Figures 33 and 34). A comparison of Figures (29) and (35) shows that the major contribution to the total dislocation density is from vacancy loops. Obviously, it is extremely important as to what value of ε is used for the growth calculation.

iiii. Effective Void Sink Strength ($4\pi R_c N_c$)

This quantity is of special importance in the analysis of metal swelling under irradiation:

(1) It represents the total non-biased sink through which vacancies and interstitials are lost.

(2) It competes with biased surfaces in the matrix (mainly dislocations) to remove point defects.

If this quantity is large compared to the total dislocation density, the swelling rate will be small. This is intuitively understandable since "almost" equal numbers of point defects are dumped into voids and the effect of bias is small. From Figures (37) and (38) one can see that the void equivalent sink is not a sharp function of temperature. If one compares Figures (35) and (37) it is clear that at low temperatures total dislocation line density is 2 orders of magnitude greater than void equivalent sink causing a high growth rate. However, at high temperatures, the dislocation density drops much faster than void equivalent sink.

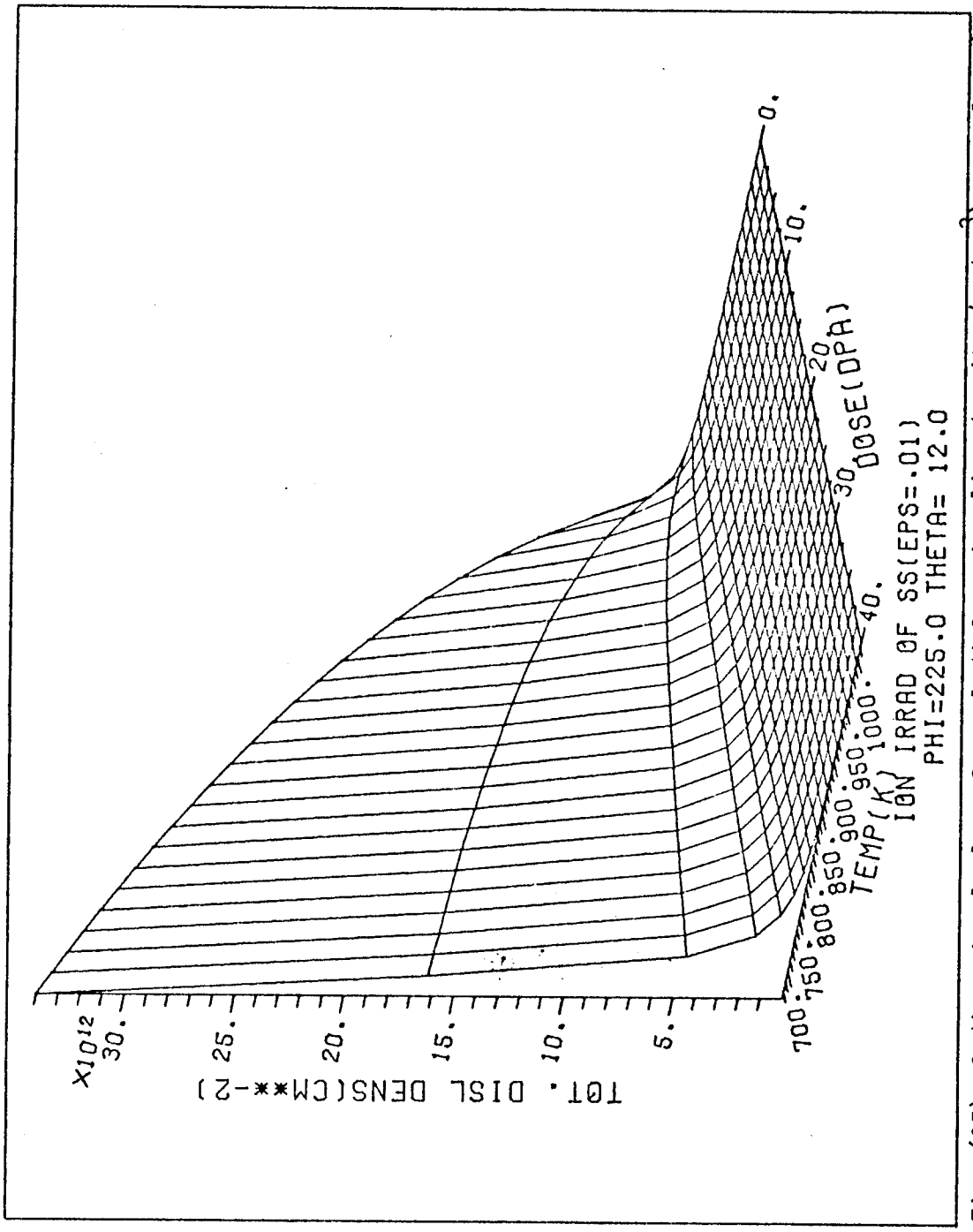

Fig. (35) 3-dimensional plot of total dislocation line density (cm/cm^3) as a function of dose and temperature for ion irradiated ST stainless steel. The dose rate is 10^{-3} dpa/sec and the cascade efficiency is 0.01.

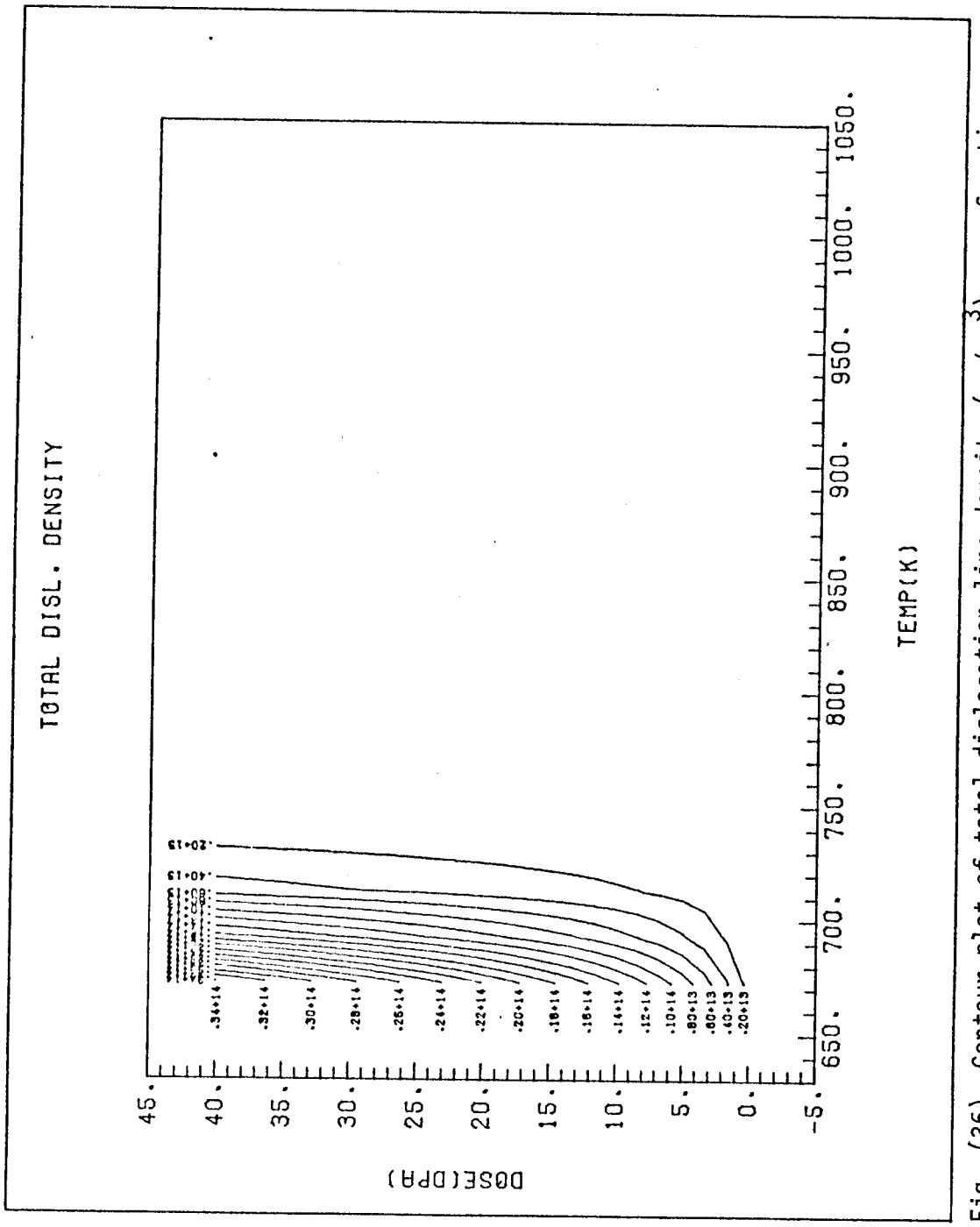

Fig. (36) Contour plot of total dislocation line density (cm/cm^3) as a function of dose and temperature for ion irradiated ST stainless steel. The dose rate is 10^{-3} dpa/sec and the cascade efficiency is 0.01.

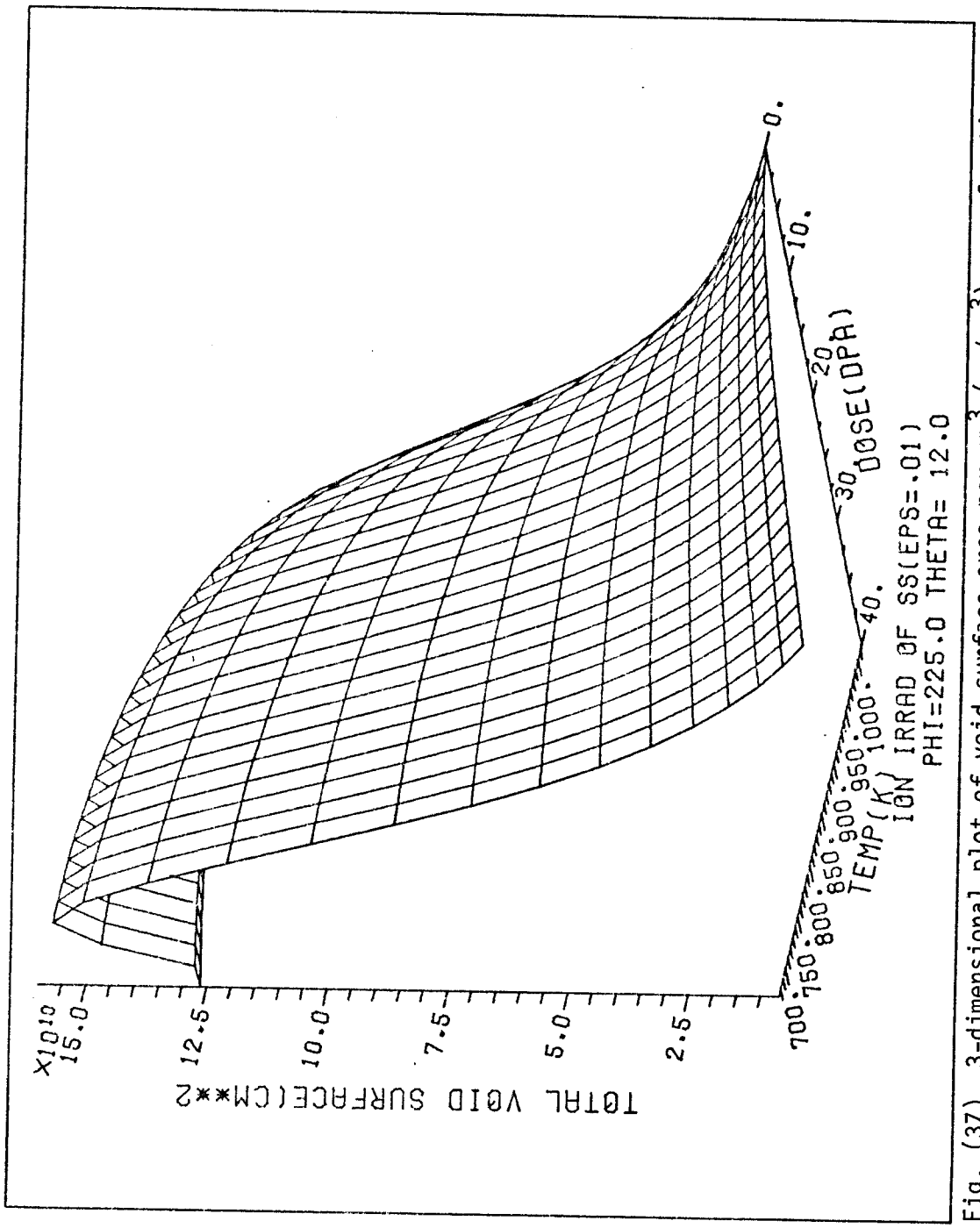

Fig. (37) 3-dimensional plot of void surface area per cm^3 (cm/cm^3) as a function of dose and temperature for ion irradiated ST stainless steel. The dose rate is 10^{-3} dpa/sec and the cascade efficiency is 0.01.

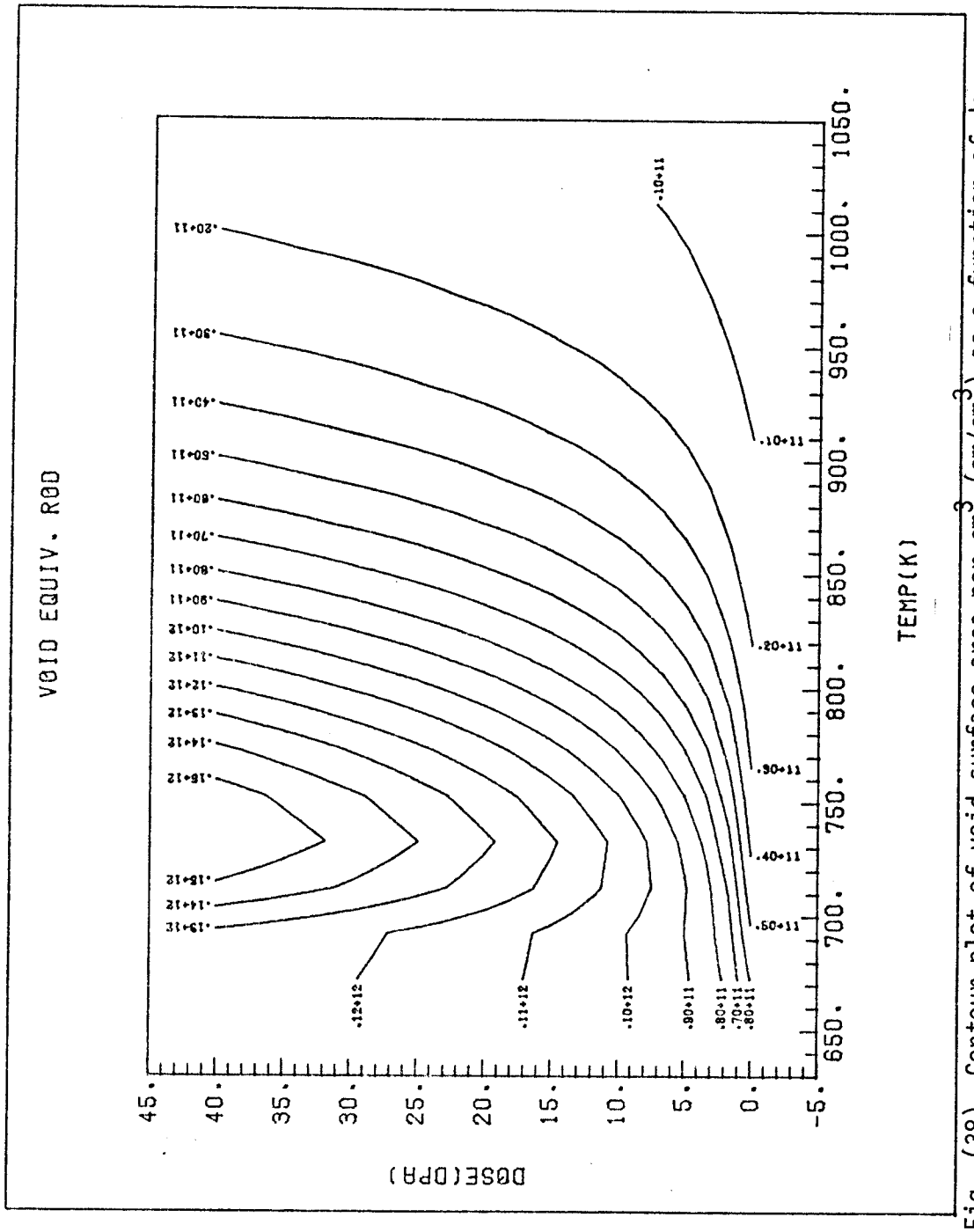

Fig. (38) Contour plot of void surface area per cm^3 (cm/cm^3) as a function of dose and temperature for ion irradiated ST stainless steel. The dose rate is 10^{-3} dpa/sec and the cascade efficiency is 0.01.

2. Accelerator Conditions With Low Cascade Production Efficiency (ε = 0.001 and P = 10^{-3} dpa/sec).

Reducing the cascade collapse efficiency leads to releasing more free vacancies. As a consequence, void swelling is enhanced. Figures (39) and (40) for the mean void radius as a function of dose and temperature show that the general behavior is the same as in the previous case (Figures (12) and (13)), but the mean void radius is large for ε = 0.001.

The swelling behavior is the same as before as a function of temperature and dose. However, there is an enhancement of swelling with an increase of about 15% at the peak over the ε = 0.01 value as shown in Figures (41) and (42).

In Figures (43) and (44) interstitial loop dislocation density is shown to be larger than the ε = 0.01 case (Fig. (33) and (34)). This is expected because interstitial loops receive the flux of interstitials, which would have normally gone to the vacancy loops. For the same reason, there are now more vacancies in the matrix and these cause more swelling.

Although we have reduced the cascade collapse efficiency by only an order of magnitude, the vacancy loop line density is found to go down by a factor of $\sim$ 30 as shown in Figures (45) and (46). Besides the reduction in the vacancy loop generation rate, their chance of destruction is increased with the presence of a higher interstitial flux in the matrix.

The total vacancy emission rate as shown in Figures (47) and (48) is reduced by 10-20% from the value associated with ε = 0.01 displayed in Figures (21) and (22). This slight reduction is due to a smaller number of vacancy loops that thermally emit vacancies.

3. Accelerator Conditions With High Cascade Efficiency (ε = 0.044 and P = 10^{-3} dpa/sec).

Comparison of Figures (49) and (50) with Figures (27) and (28) shows that increasing the cascade collapse efficiency by a factor of 4.4 from the reference case of ε = 0.01 reduces the recombination coefficient by about a factor of 2-3. The use of a higher cascade efficiency tends to remove more

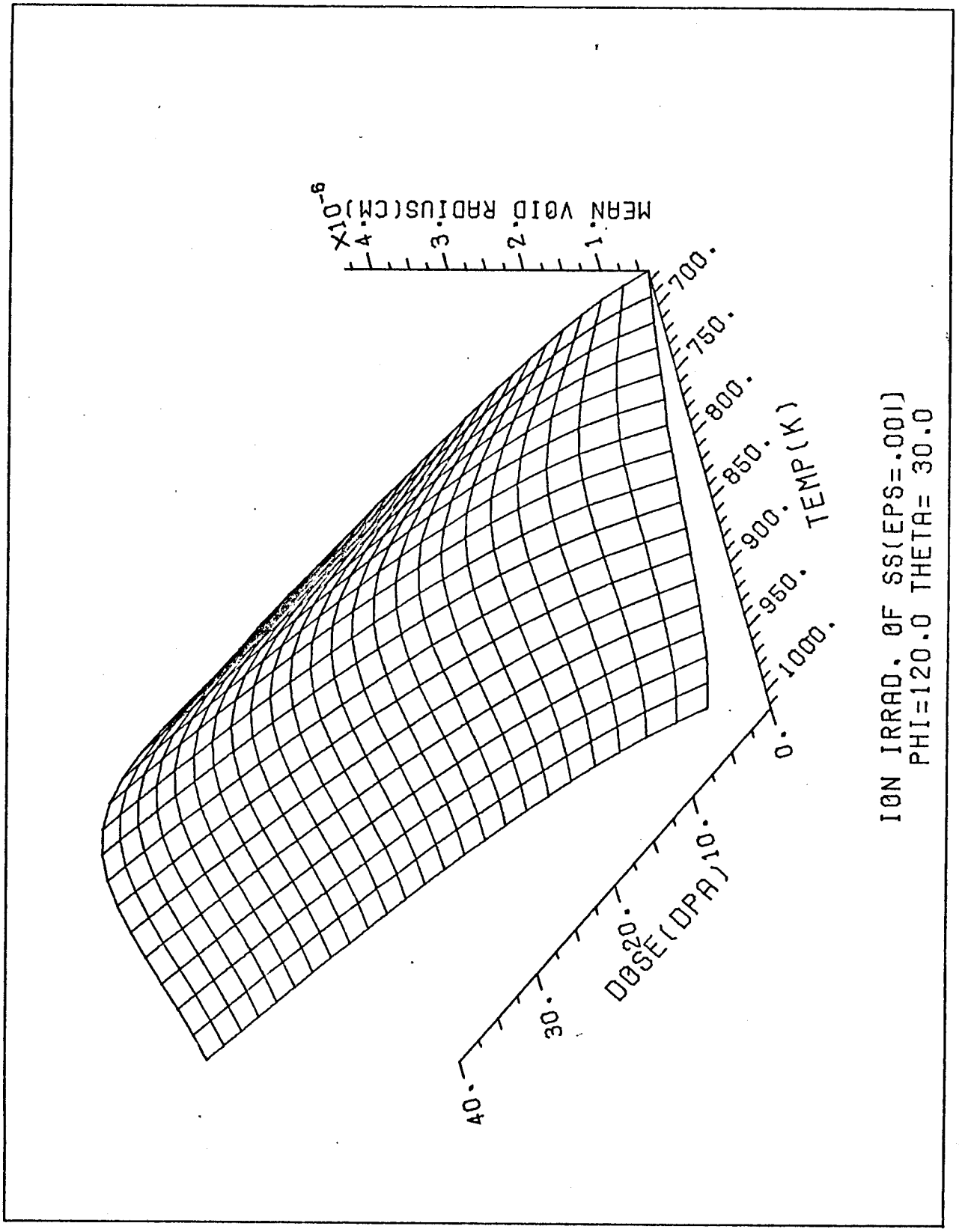

Fig. (39) 3-dimensional plot of mean void radius as a function of dose and temperature for ion irradiated ST stainless steel. The dose rate is 10^{-3} dpa/sec and the cascade efficiency is 0.001.

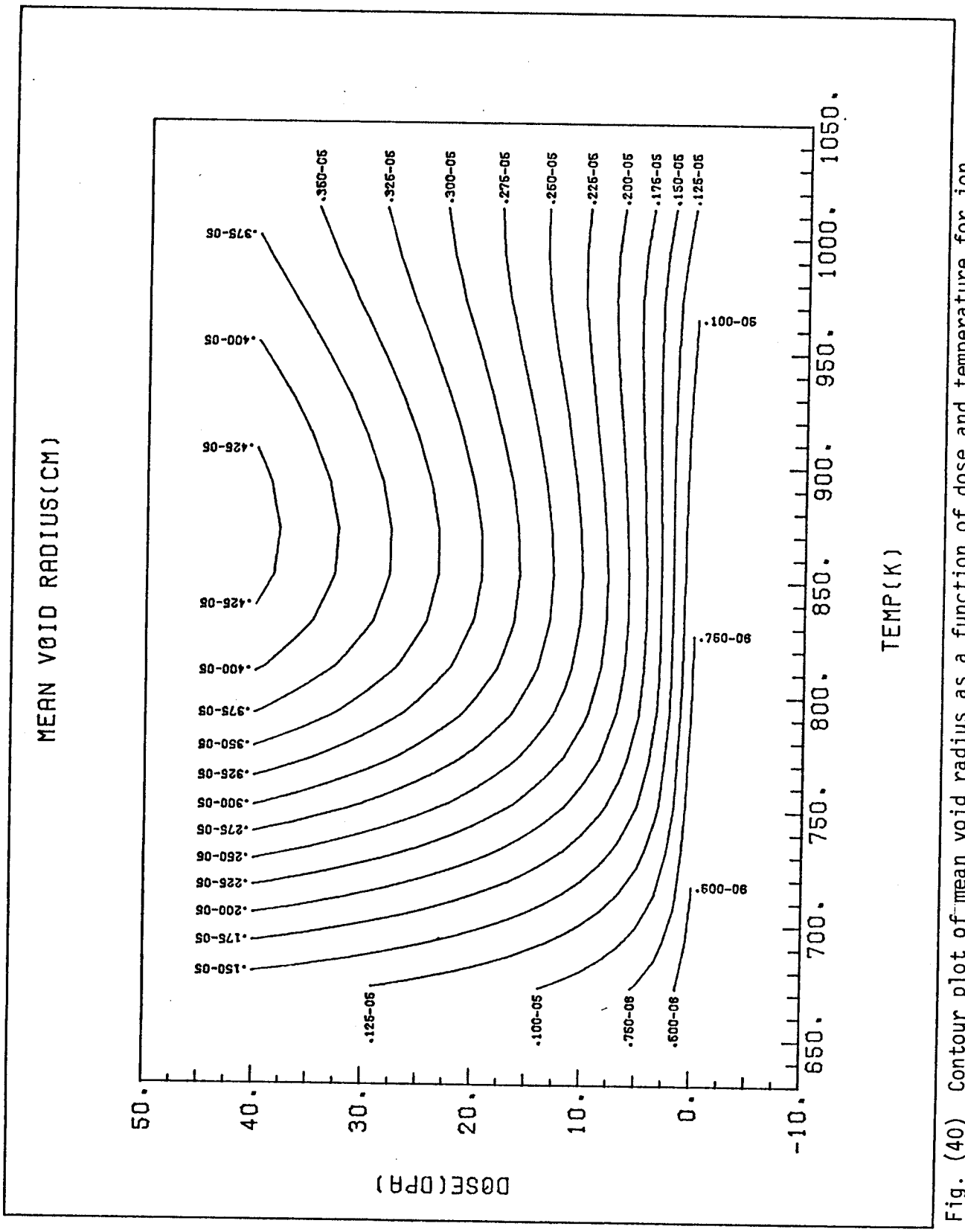

Fig. (40) Contour plot of mean void radius as a function of dose and temperature for ion irradiated ST stainless steel. The dose rate is 10^{-3} dpa/sec and the cascade efficiency is 0.001.

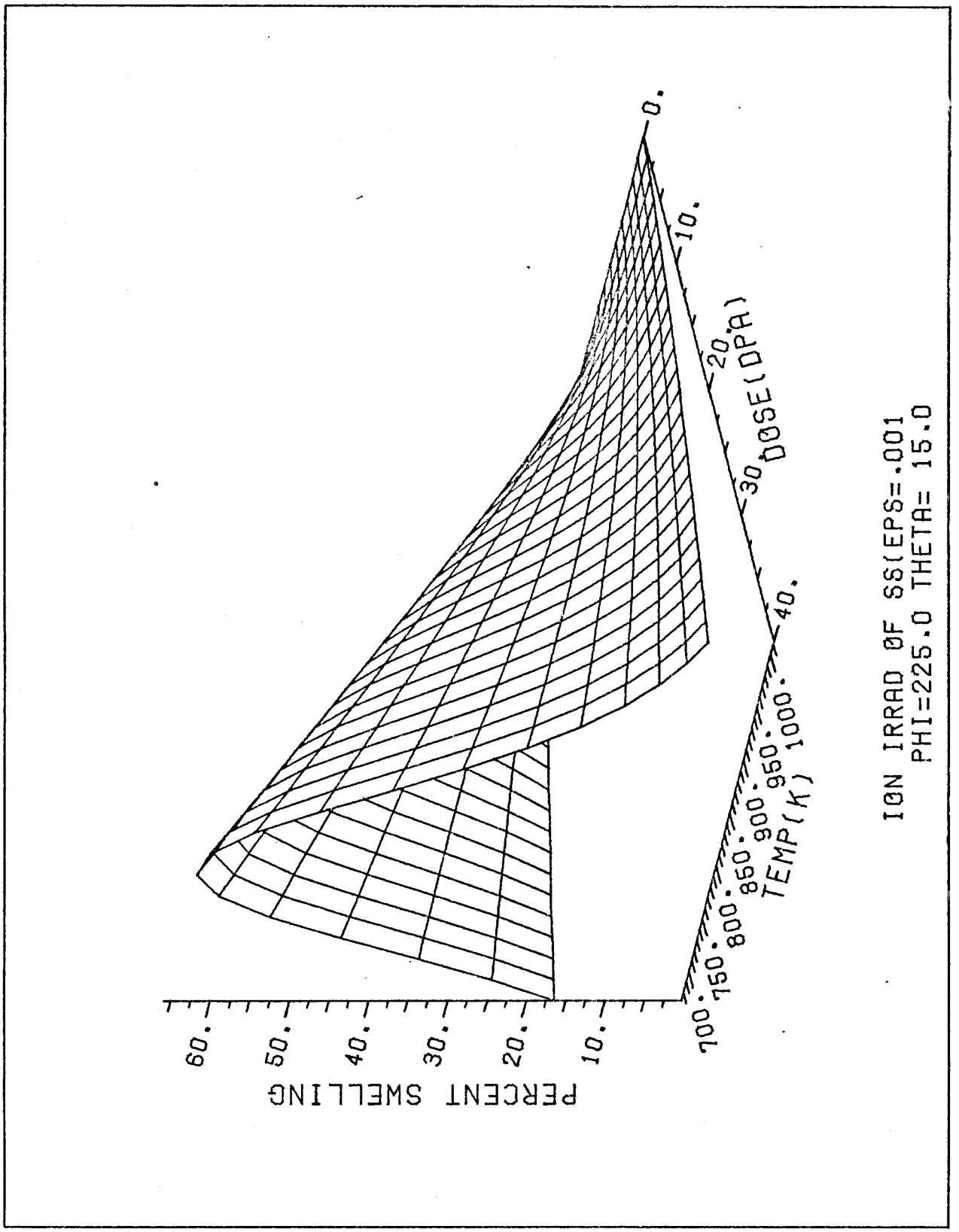

Fig. (41) 3-dimensional plot of percent swelling as a function of dose and temperature for ion irradiated ST stainless steel. The dose rate is 10^{-3} dpa/sec and the cascade efficiency is 0.001.

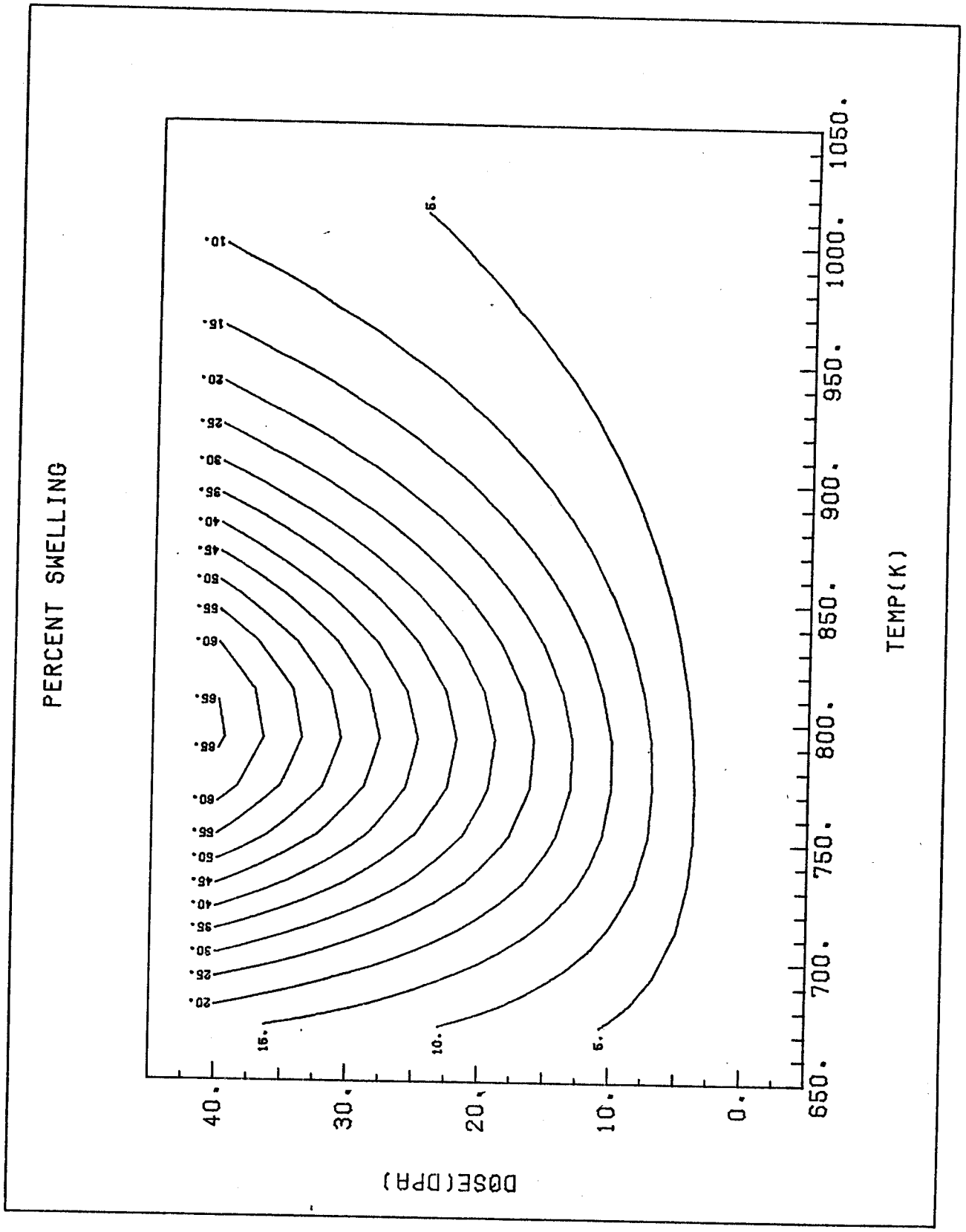

Fig. (42) Contour plot of percent swelling as a function of dose and temperature for ion irradiated ST stainless steel. The dose rate is 10^{-3} dpa/sec and the cascade efficiency is 0.001.

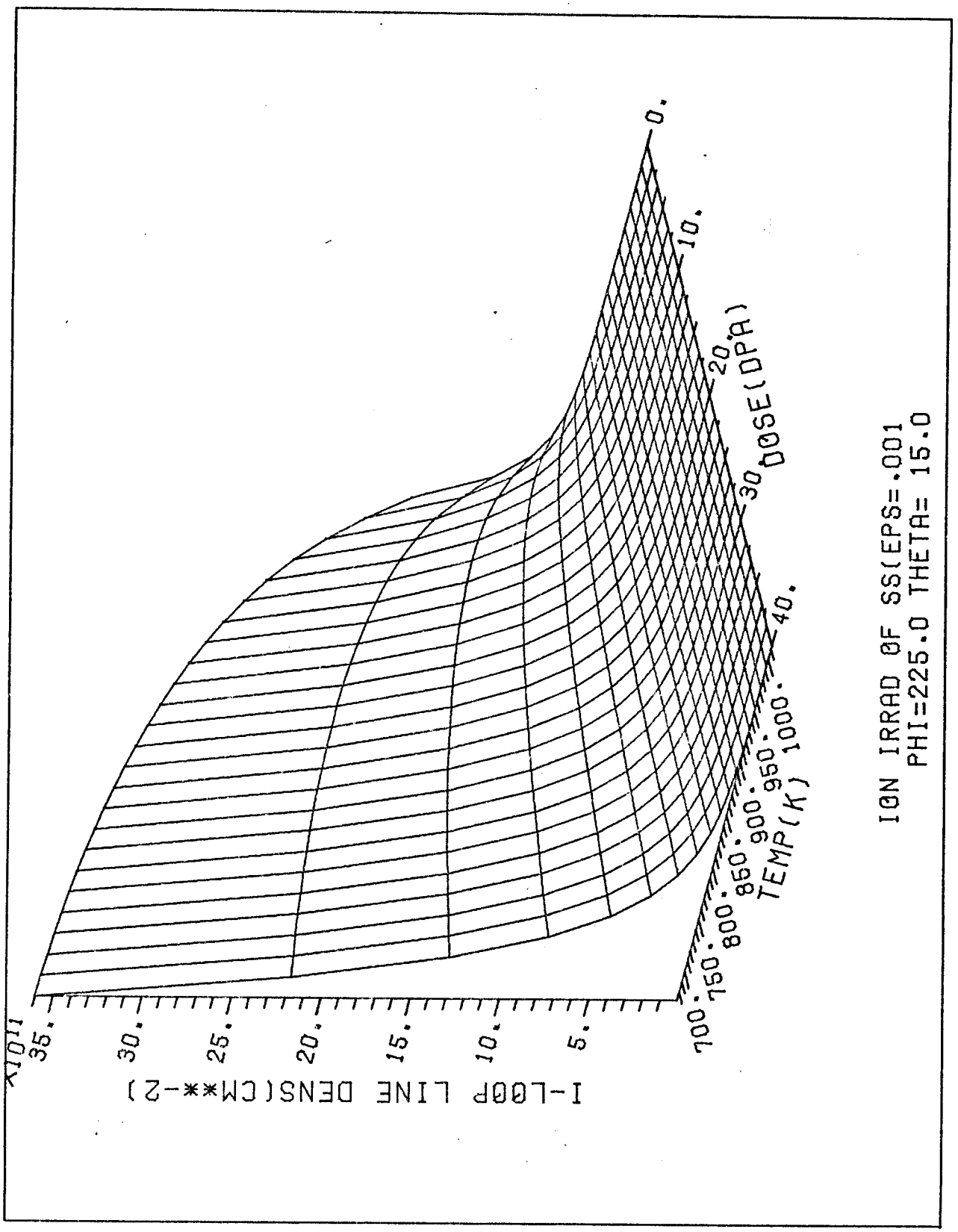

Fig. (43) 3-dimensional plot of interstitial loop line density (cm/cm^3) as a function of dose and temperature for ion irradiated ST stainless steel. The dose rate is 10^{-3} dpa/sec and the cascade efficiency is 0.001.

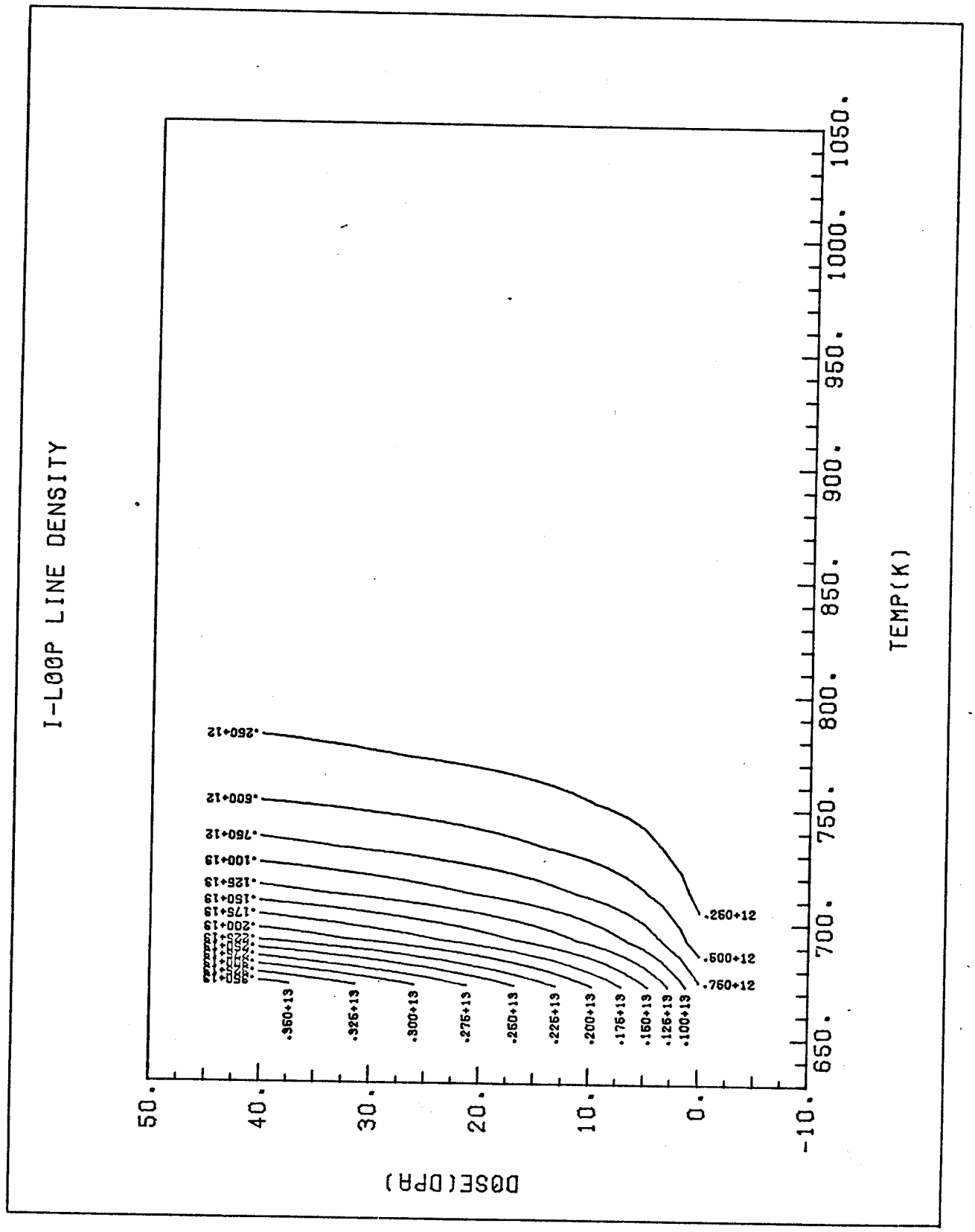

Fig. (44) Contour plot of interstitial loop line density (cm/cm^3) as a function of dose and temperature for ion irradiated ST stainless steel. The dose rate is 10^{-3} dpa/sec and the cascade efficiency is 0.001.

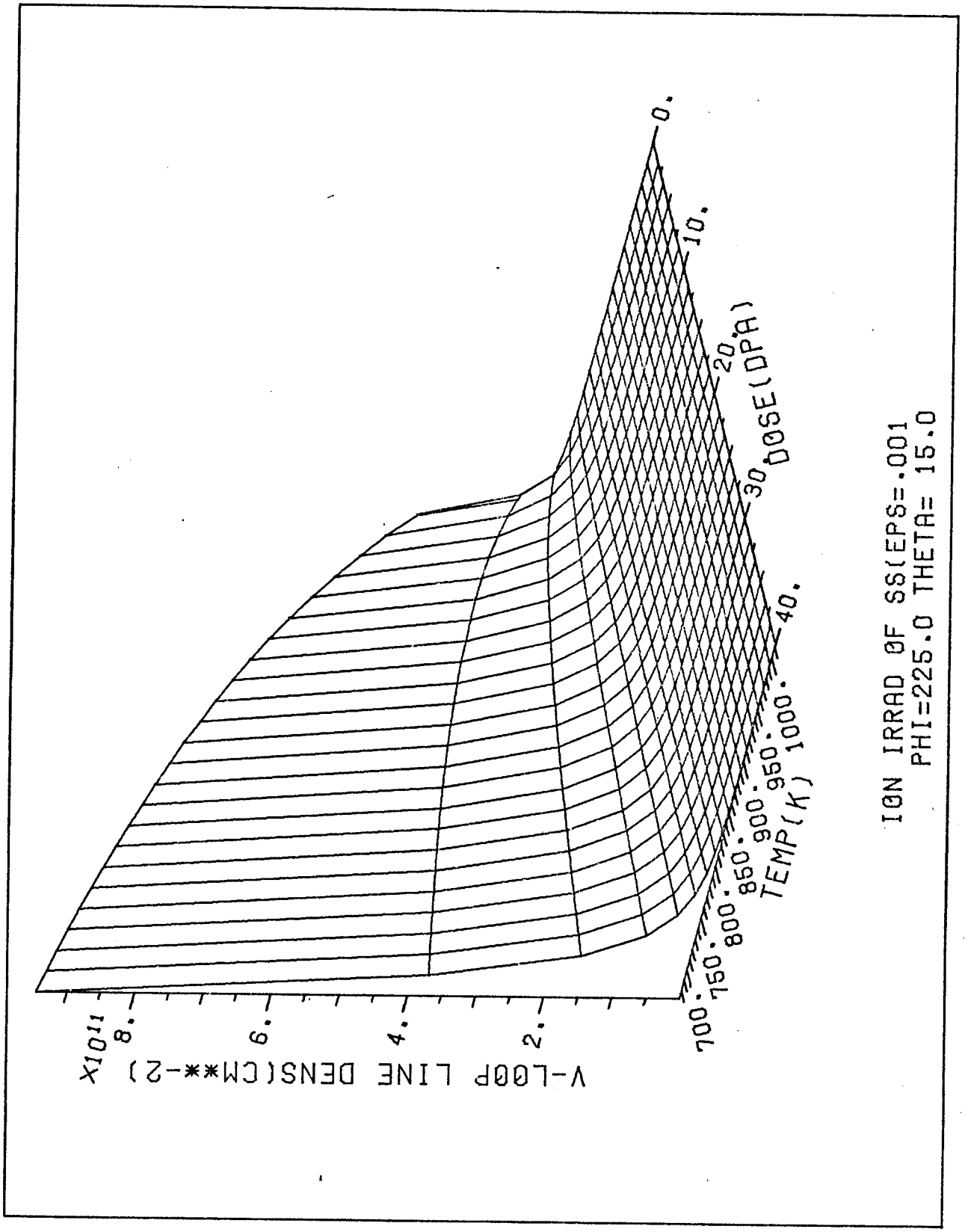

Fig. (45) 3-dimensional plot of vacancy loop line density (cm/cm^3) as a function of dose and temperature for ion irradiated ST stainless steel. The dose rate is 10^{-3} dpa/sec and the cascade efficiency is 0.001.

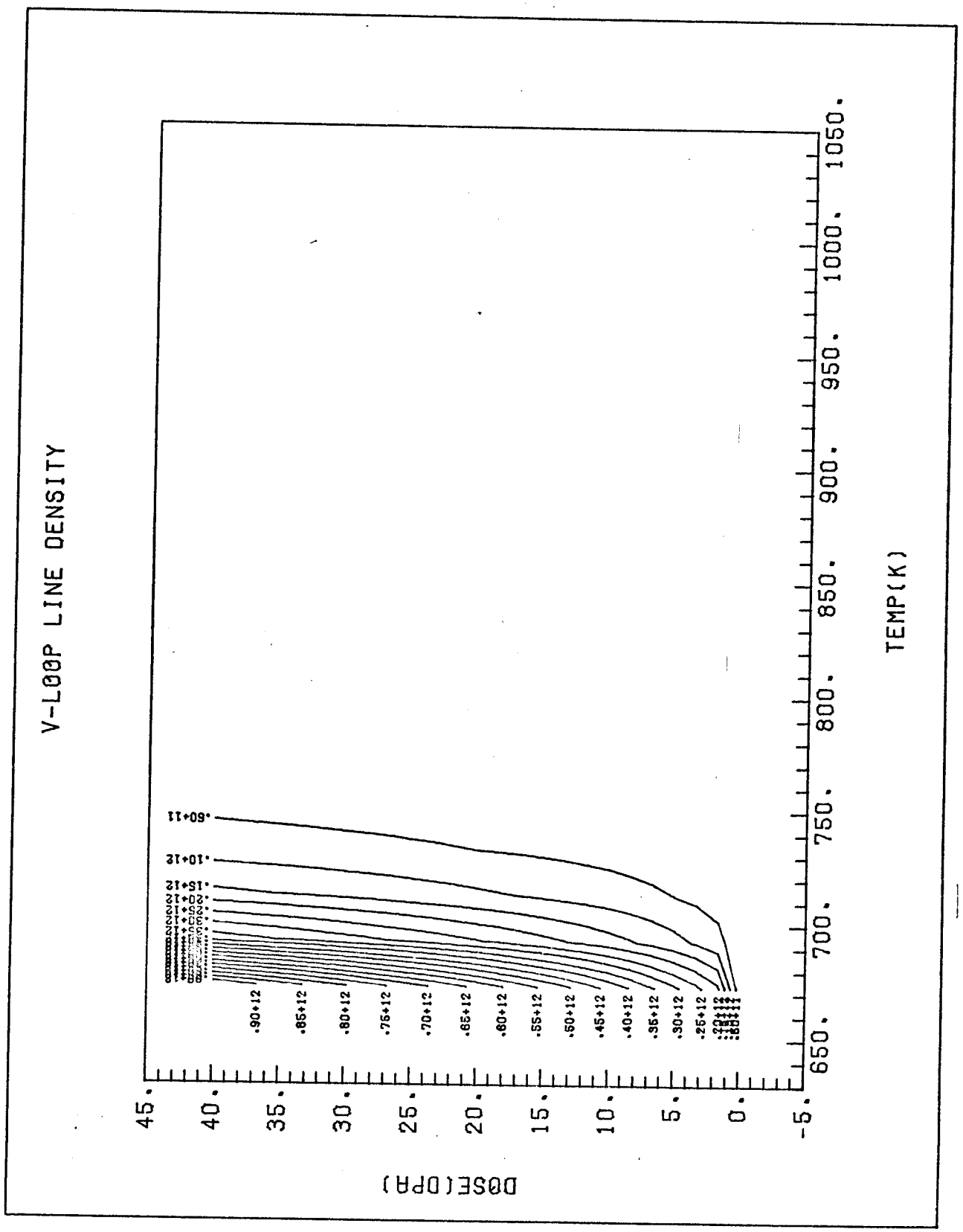

Fig. (46) Contour plot of vacancy loop line density (cm/cm^3) as a function of dose and temperature for ion irradiated ST stainless steel. The dose rate is 10^{-3} dpa/sec and the cascade efficiency is 0.001.

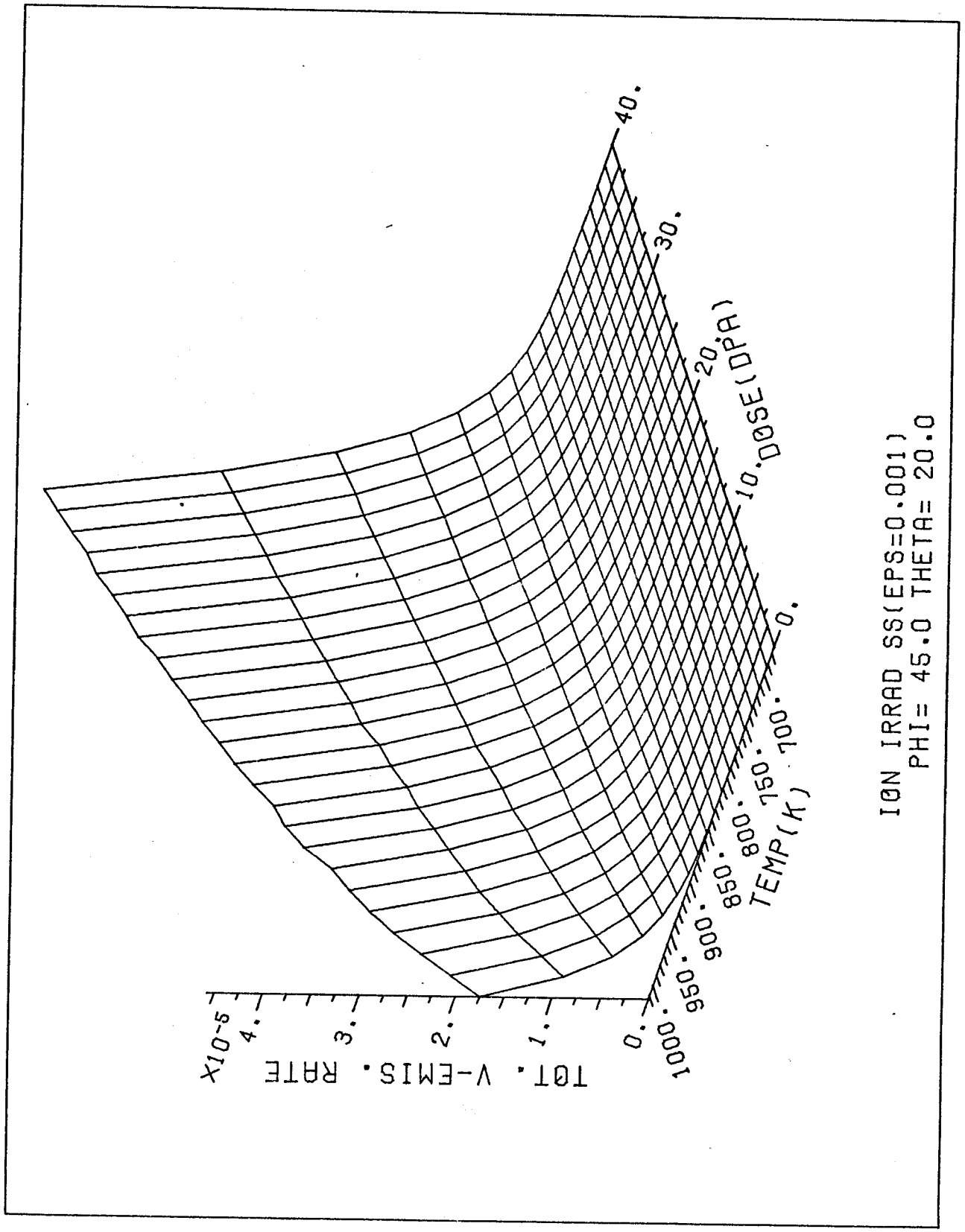

Fig. (47) 3-dimensional plot of total vacancy emission rate (at/at/s) as a function of dose and temperature for ion irradiated ST stainless steel. The dose rate is 10^{-3} dpa/sec and the cascade efficiency is 0.001.

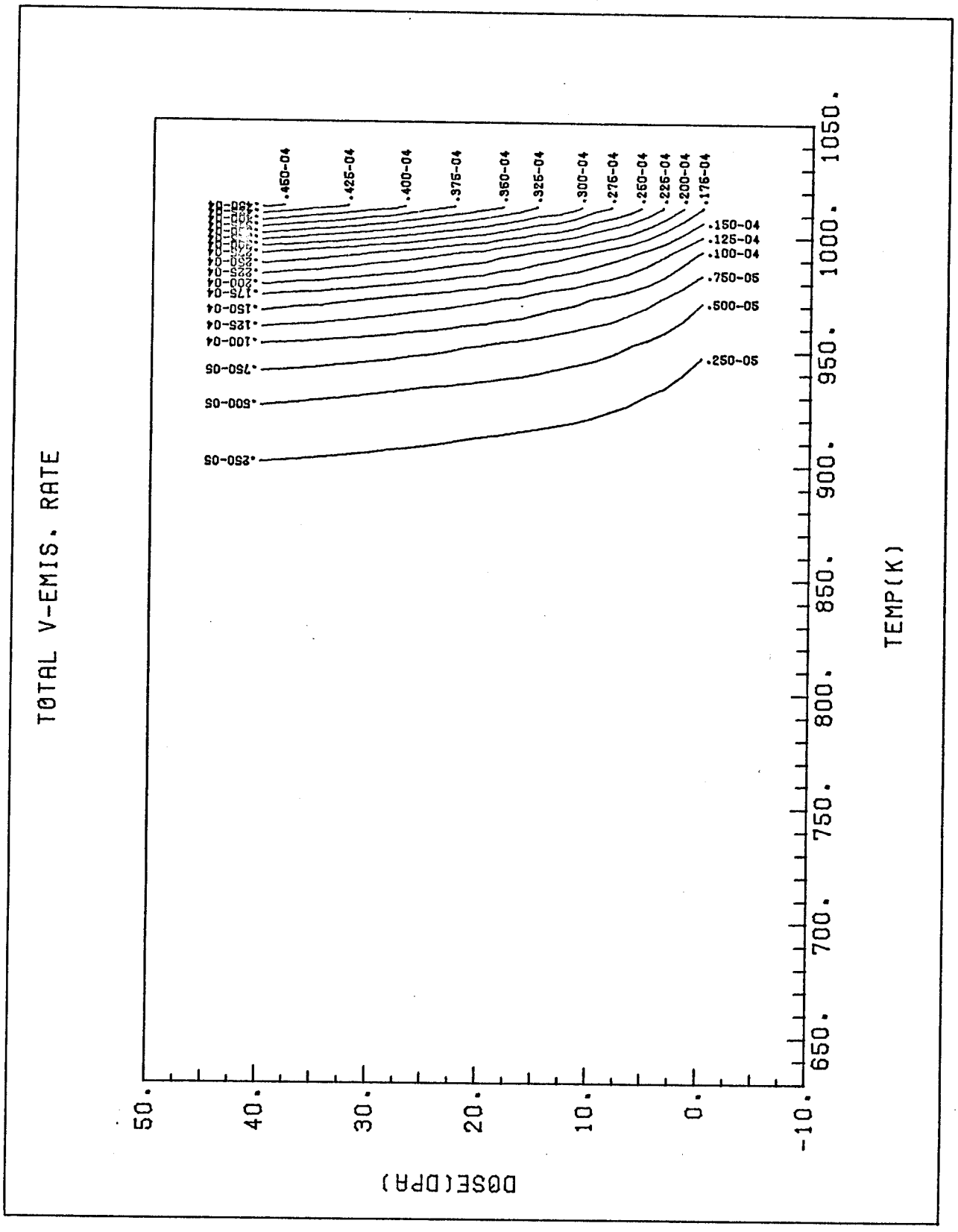

Fig. (48) Contour plot of total vacancy emission rate (at/at/s) as a function of dose and temperature for ion irradiated ST stainless steel. The dose rate is 10^{-3} dpa/sec and the cascade efficiency is 0.001.

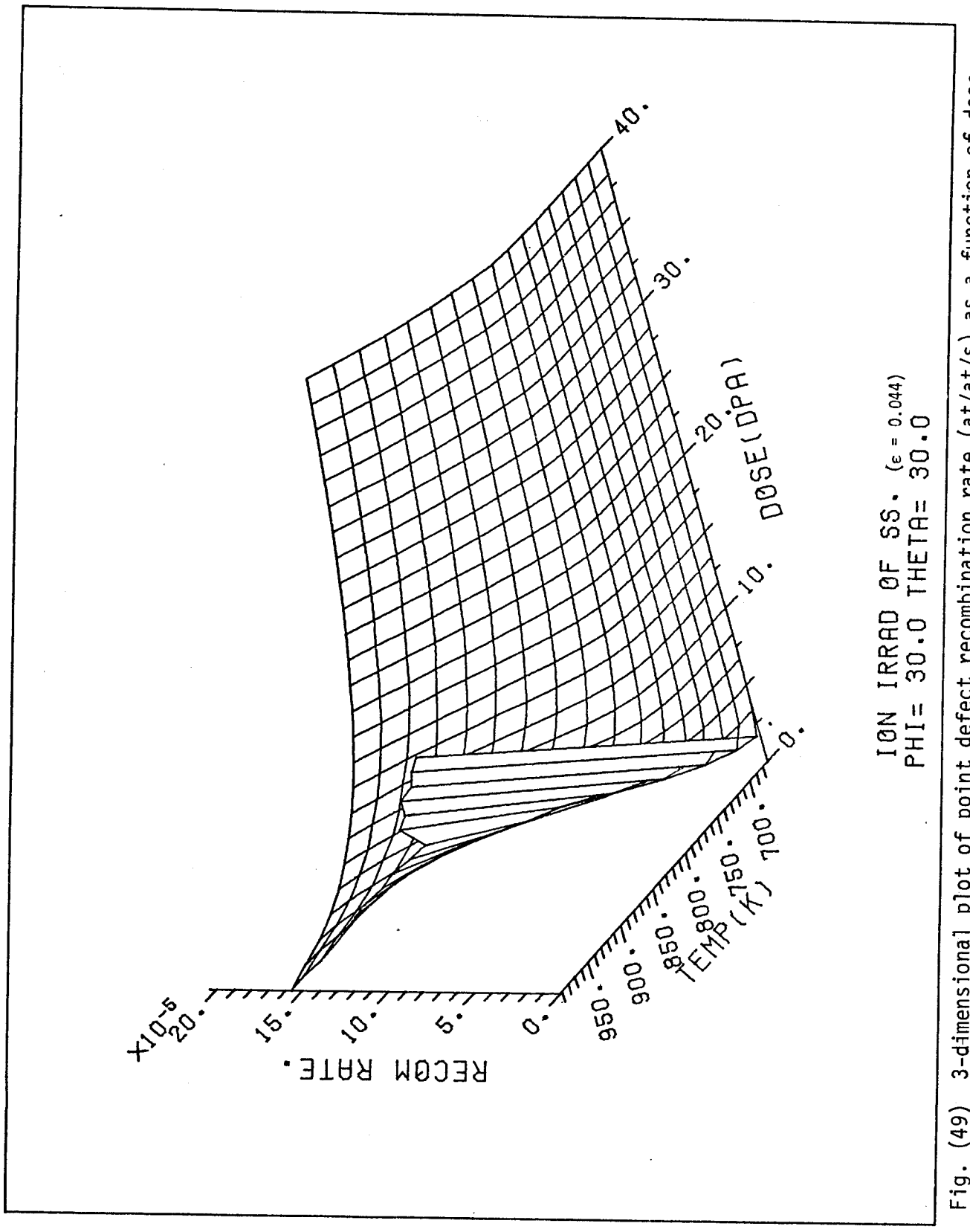

Fig. (49) 3-dimensional plot of point defect recombination rate (at/at/s) as a function of dose and temperature for ion irradiated ST stainless steel. The dose rate is 10^{-3} dpa/sec and the cascade efficiency is 0.044.

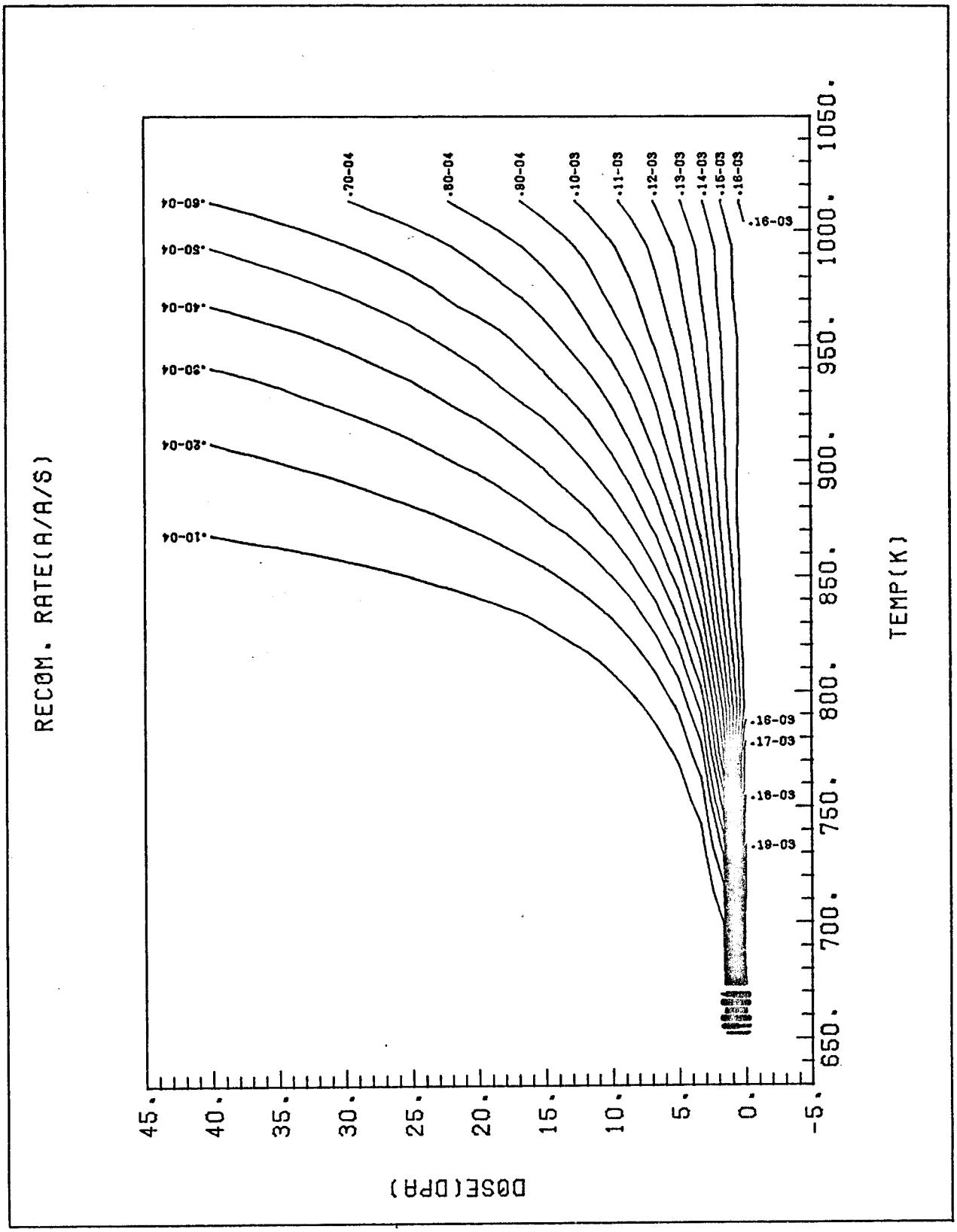

Fig. (50) Contour plot of point defect recombination rate (at/at/s) as a function of dose and temperature for ion irradiated ST stainless steel. The dose rate is 10^{-3} dpa/sec and the cascade efficiency is 0.044.

defects from the matrix, thus lowering the vacancy concentration. The increased absorption of vacnacies and interstitials by dislocation loops (especially vacancy loops), as illustrated in Figures (51) and (52), completely dominates the defect removal process and one can safely neglect the recombination rates.

The mean void radius shown in Figures (53) and (54) and also the subsequent swelling in Figures (55) and (56) are lower than the previously studied cases. This is mainly due to the lower vacancy flux because of smaller C_v. Swelling is inhibited roughly by a factor of 4-5 from the $\varepsilon = 0.01$ case to a maximum of $\sim$ 12% at 40 dpa and 600°C.

Comparison of Figures (57) and (58) with Figures (29) and (30) readily shows that the vacancy loop line dislocation density has increased at all temperatures and doses by increasing ε, but the temperature dependence is much less pronounced. Evidently the increased loop production rate is more important than the increased shrinkage rate.

The equivalent void sink ($4\pi R_c N_c$) is displayed in Figures (59) and (60). It shows the same general characteristics as before but its absolute level is reduced in this case by the presence of a large biased sink (mainly vacancy loops).

III.C. Reactor Conditions

1. Reactor Conditions with Low Cascade Efficiency

1. ($\varepsilon = 0.001$ and $P = 10^{-6}$ dpa/sec).

Under reactor conditions a major item of concern is the vacancy thermal emission rate because it is in the same order of magnitude as the vacancy production by irradiation. This behavior is highly sensitive to temperature and at high temperatures (above > 550°C) irradiation at 10^{-6} dpa s^{-1} is comparable to the thermal generation of vacancies.

In Figures (61) and (62) the mean void radius as a function of dose and temperature is shown. One can readily see that voids have a much more difficult time growing at high temperatures than when the displacement rate was 10^{-3} dpa s^{-1}.

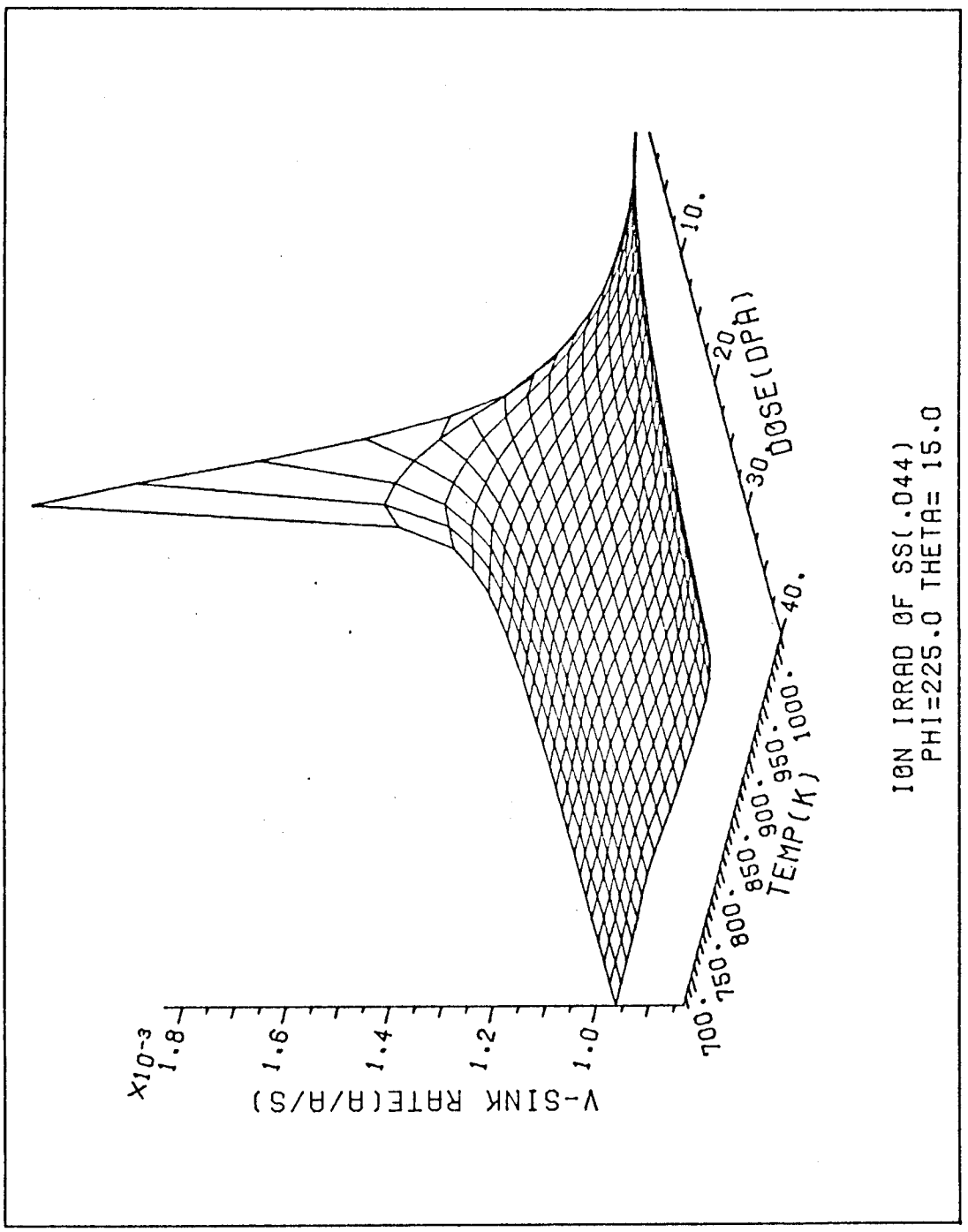

Fig. (51) 3-dimensional plot of vacancy sink removal rate (at/at/s) as a function of dose and temperature for ion irradiated ST stainless steel. The dose rate is 10^{-3} dpa/sec and the cascade efficiency is 0.044.

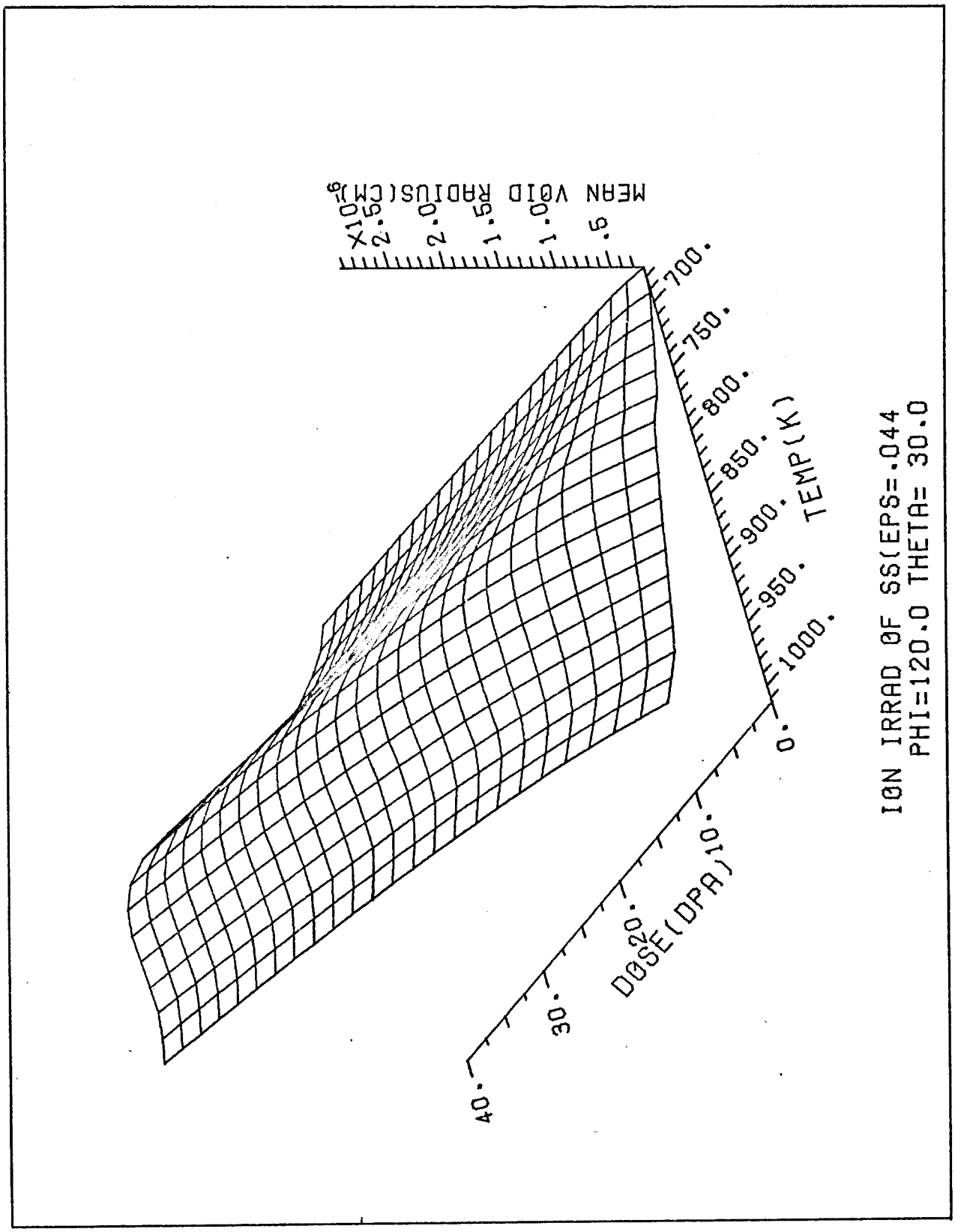

Fig. (53) 3-dimensional plot of mean void radius as a function of dose and temperature for ion irradiated ST stainless steel. The dose rate is 10^{-3} dpa/sec and the cascade efficiency is 0.044.

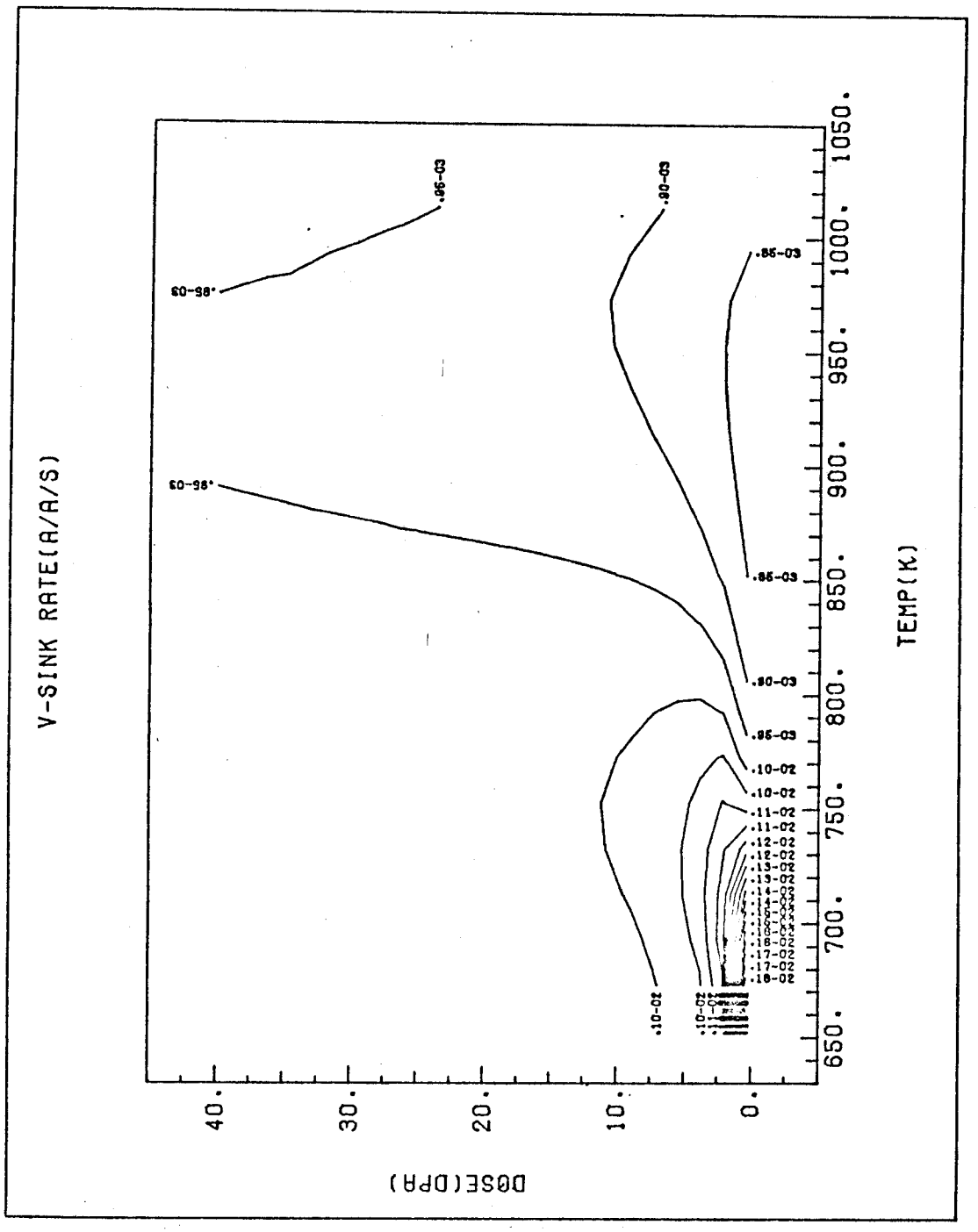

Fig. (52) Contour plot of vacancy sink removal rate (at/at/s) as a function of dose and temperature for ion irradiated ST stainless steel. The dose rate is 10-3 dpa/sec and the cascade efficiency is 0.044.

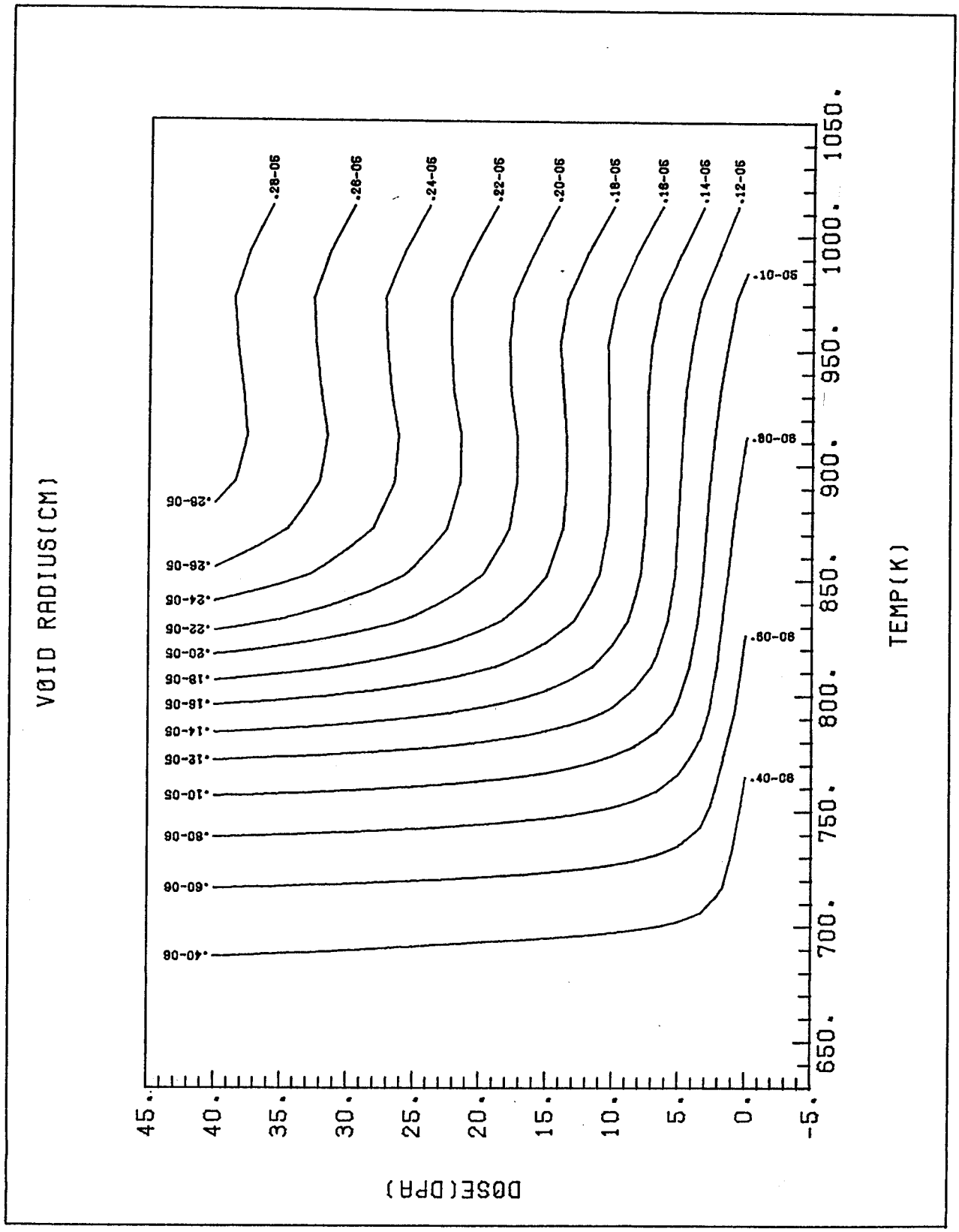

Fig. (54) Contour plot of mean void radius as a function of dose and temperature for ion irradiated ST stainless steel. The dose rate is 10^{-3} dpa/sec and the cascade efficiency is 0.044.

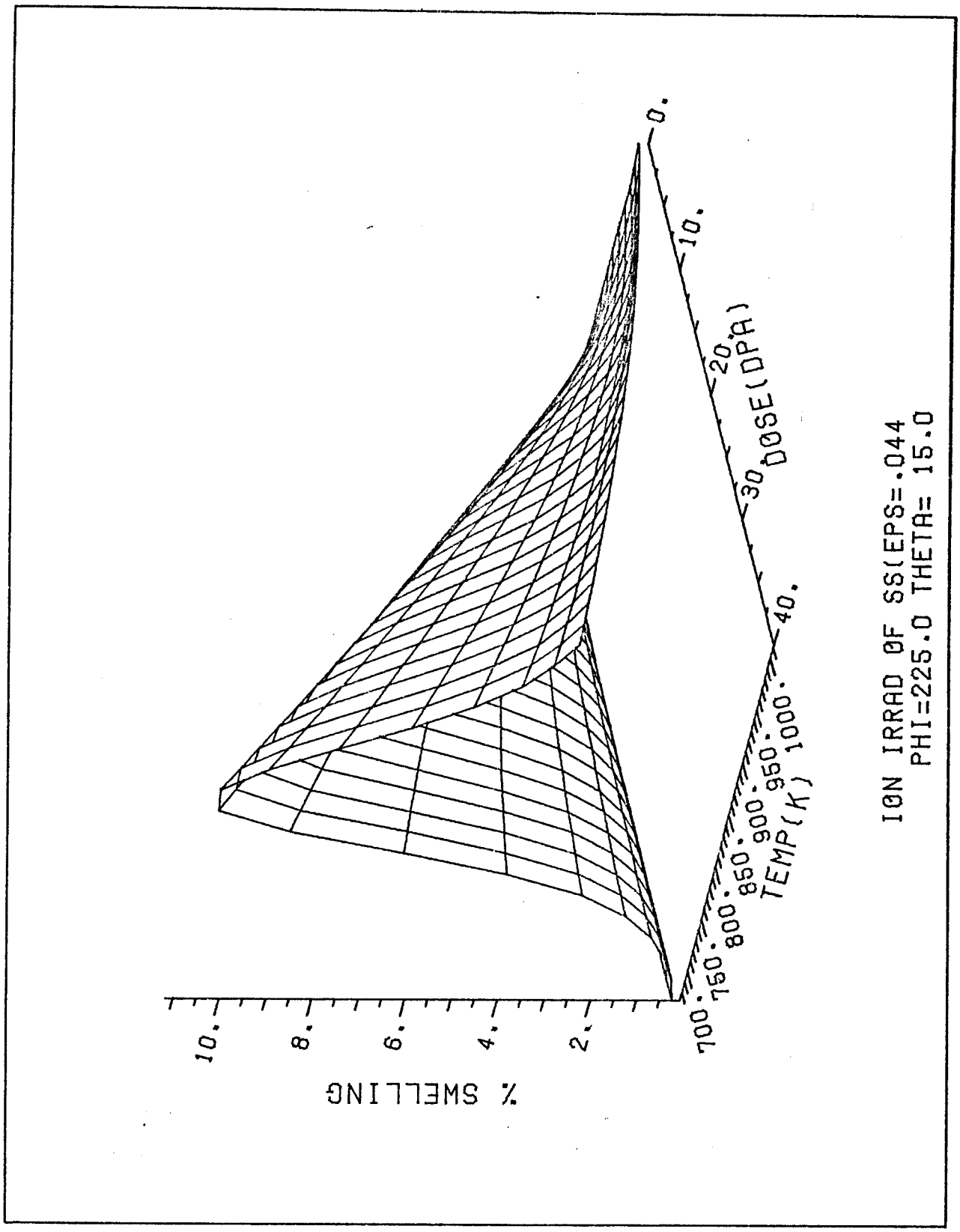

Fig. (55) 3-dimensional plot of percent swelling as a function of dose and temperature for ion irradiated ST stainless steel. The dose rate is 10^{-3} dpa/sec and the cascade efficiency is 0.044.

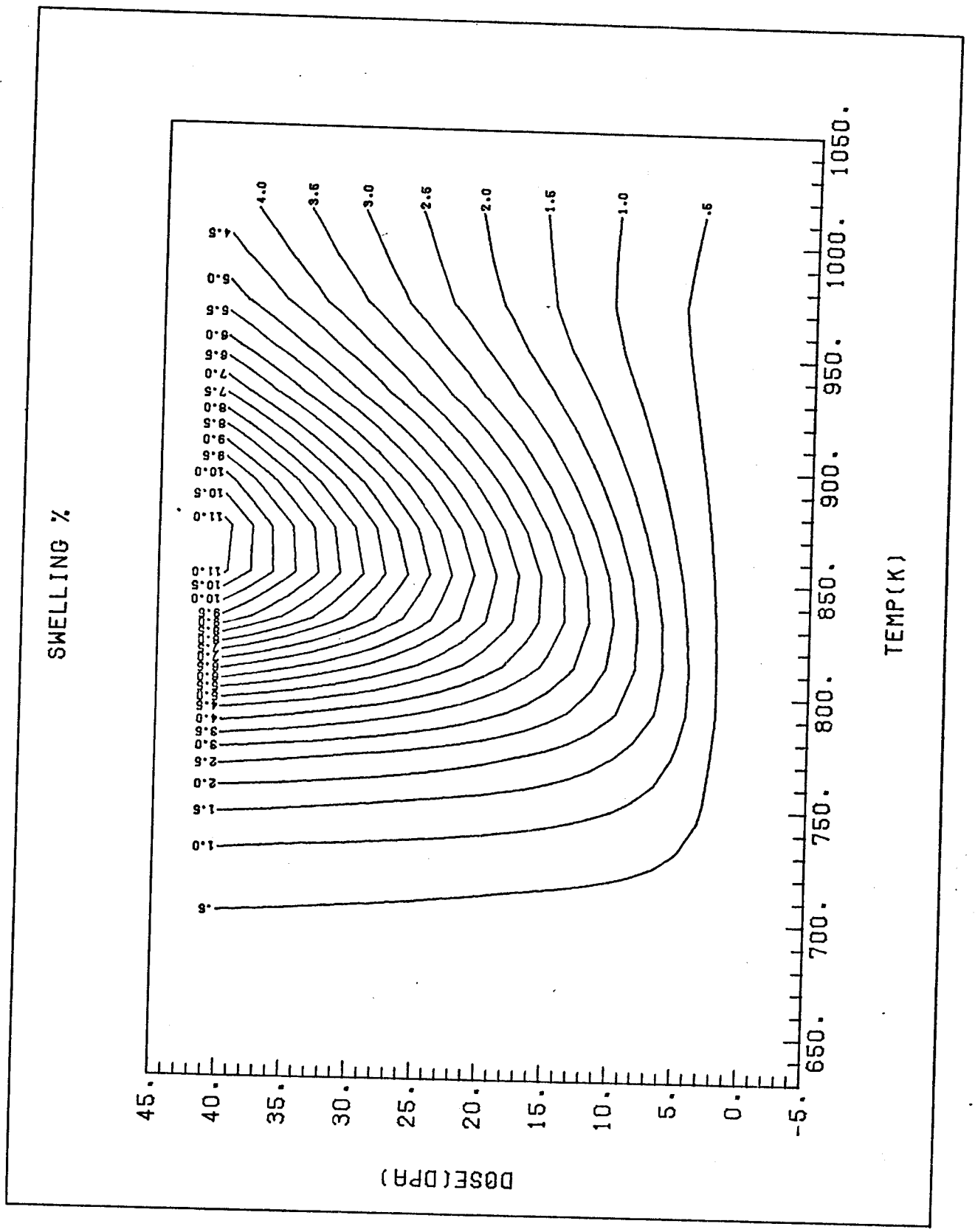

Fig. (56) Contour plot of percent swelling as a function of dose and temperature for ion irradiated ST stainless steel. The dose rate is 10^{-3} dpa/sec and the cascade efficiency is 0.044.

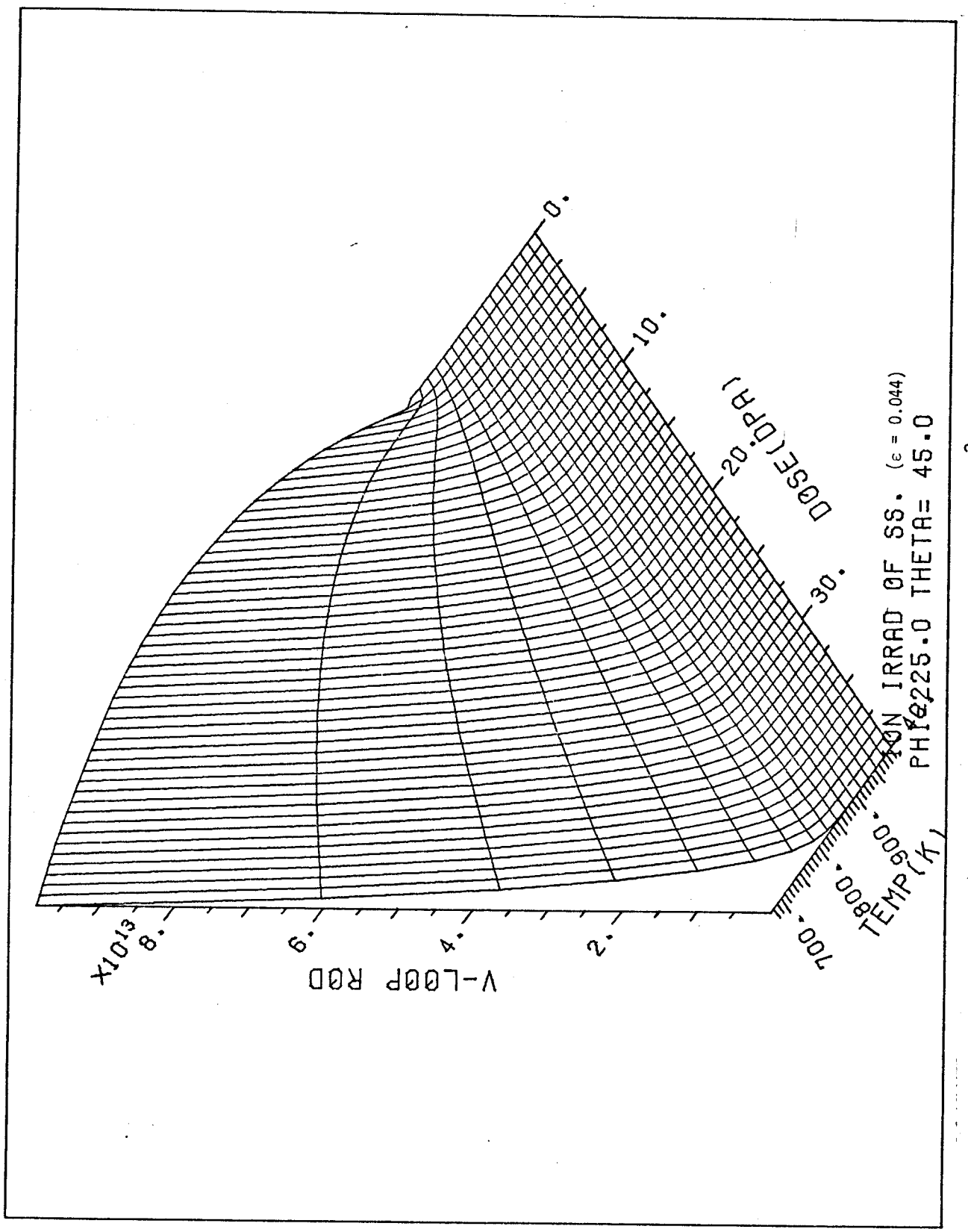

Fig. (57) 3-dimensional plot of vacancy loop line density (cm/cm^3) as a function of dose and temperature for ion irradiated ST stainless steel. The dose rate is 10^{-3} dpa/sec and the cascade efficiency is 0.044.

Fig. (58) Contour plot of vacancy loop line density (cm/cm^3) as a function of dose and temperature for ion irradiated ST stainless steel. The dose rate is 10^{-3} dpa/sec and the cascade efficiency is 0.044.

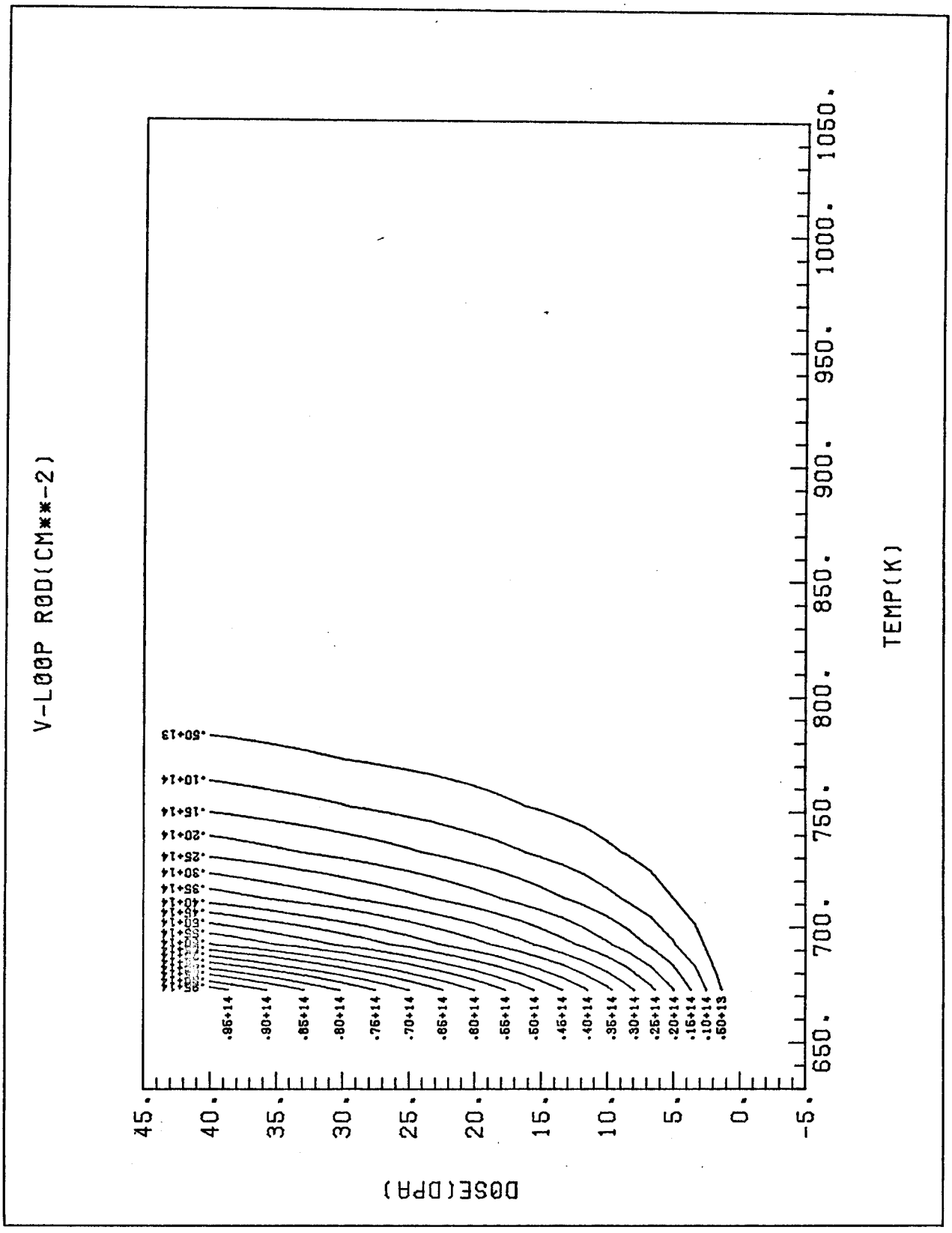

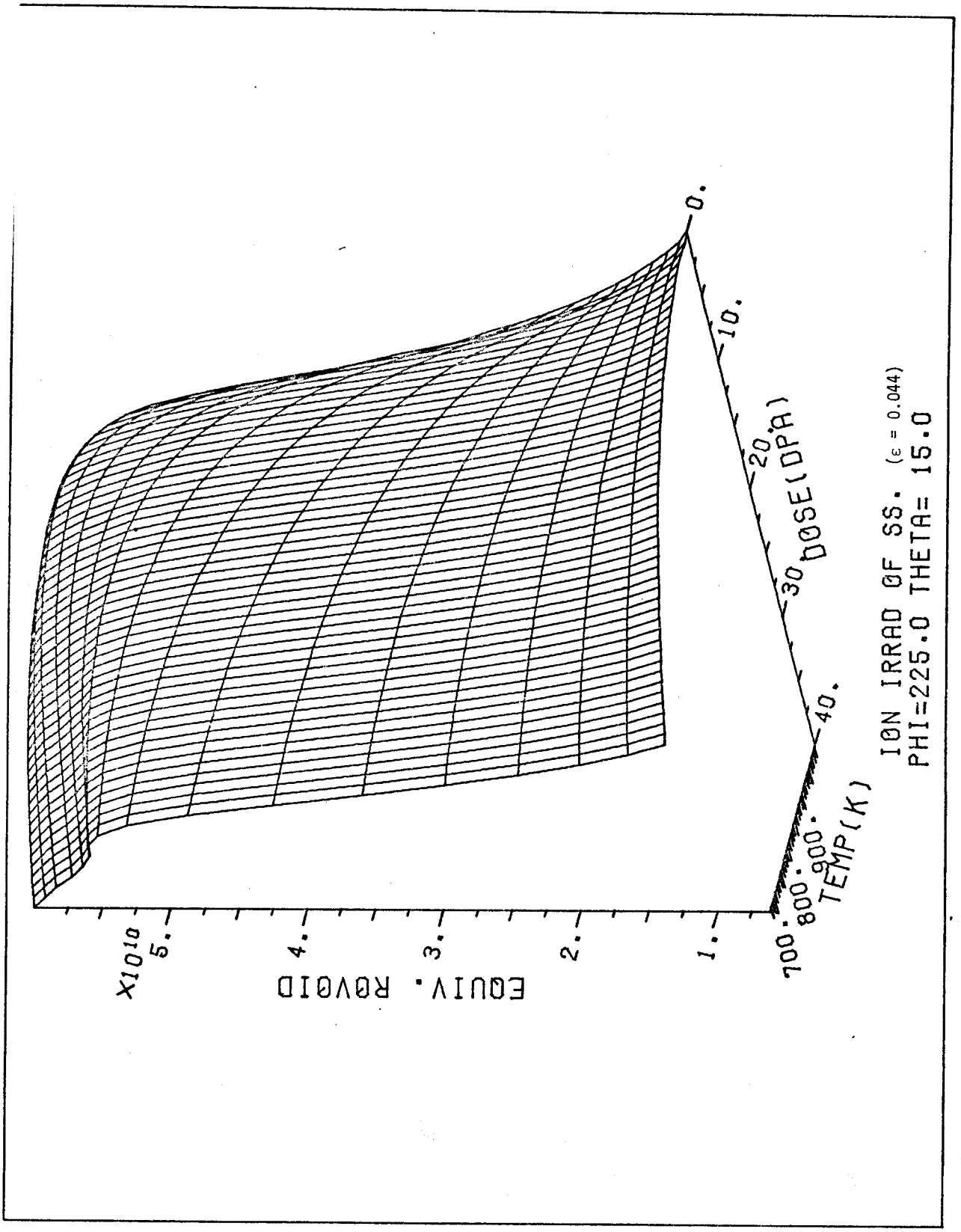

Fig. (59) 3-dimensional plot of equivalent void sink (cm/cm^3) as a function of dose and temperature for ion irradiated ST stainless steel. The dose rate is 10-3 dpa/sec and the cascade efficiency is 0.044.

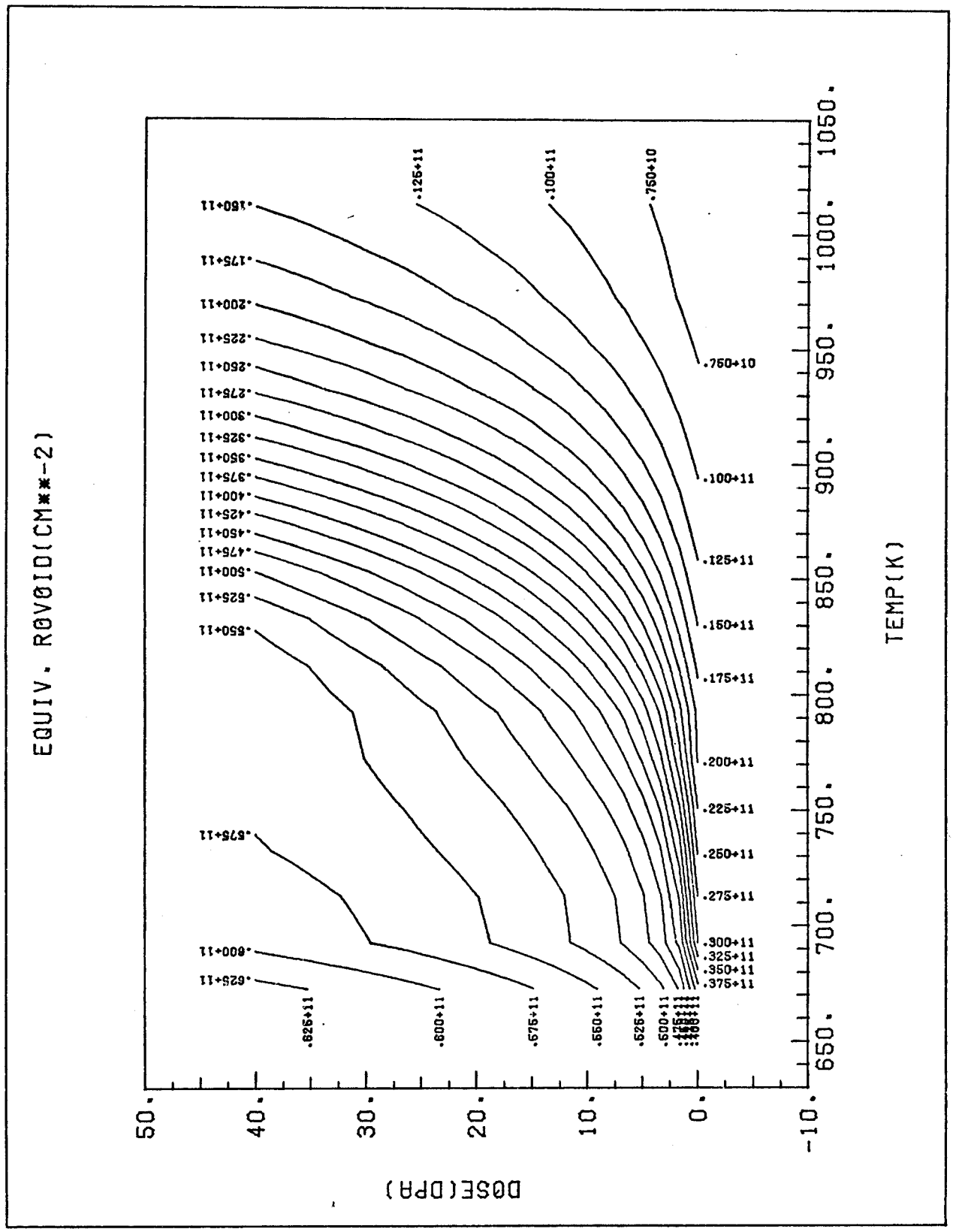

Fig. (60) Contour plot of equivalent void sink (cm/cm^3) as a function of dose and temperature for ion irradiated ST stainless steel. The dose rate is 10^{-3} dpa/sec and the cascade efficiency is 0.044.

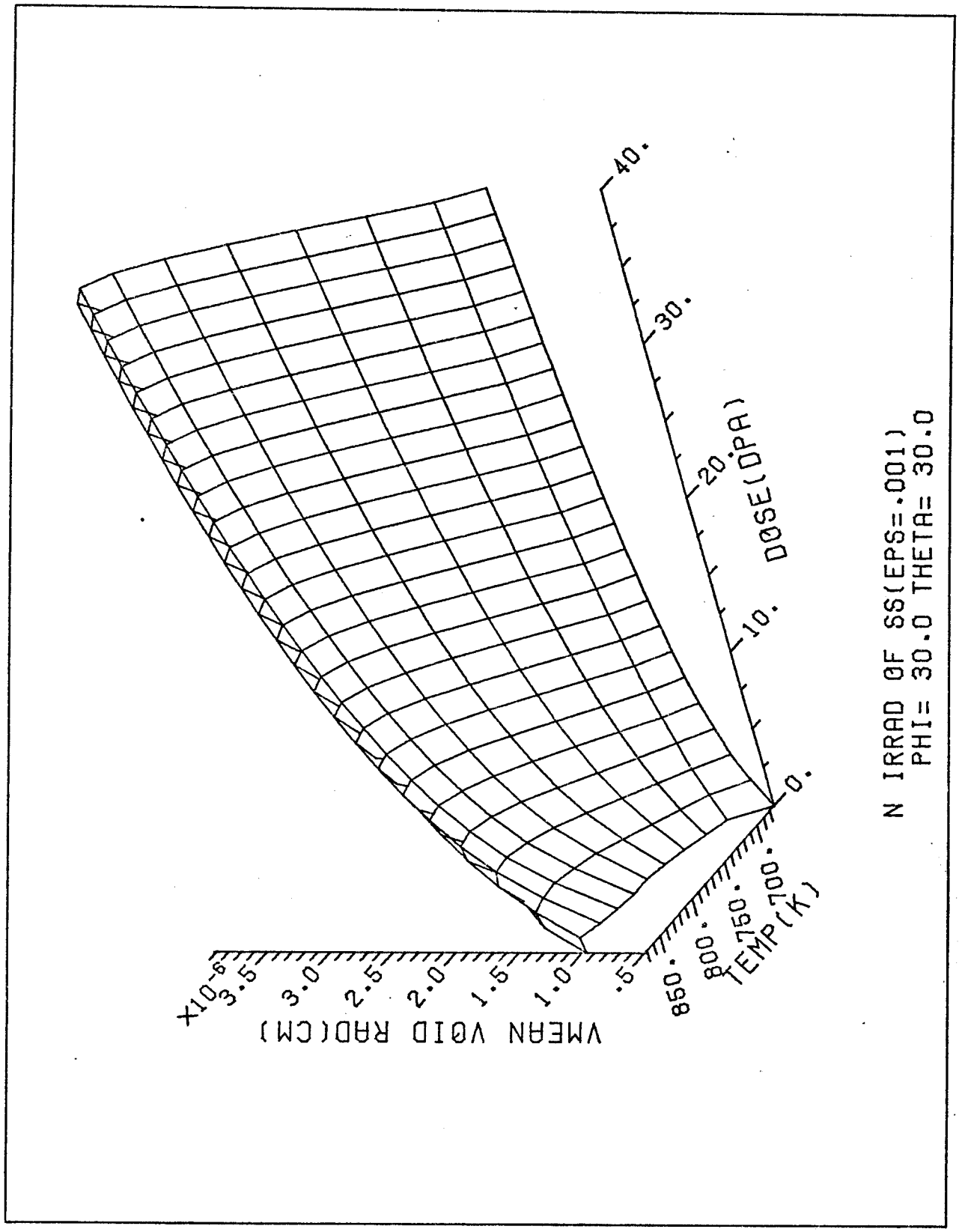

Fig. (61) 3-dimensional plot of mean void radius as a function of dose and temperature for neutron irradiated ST stainless steel. The dose rate is 10^{-6} dpa/sec and the cascade efficiency is 0.001.

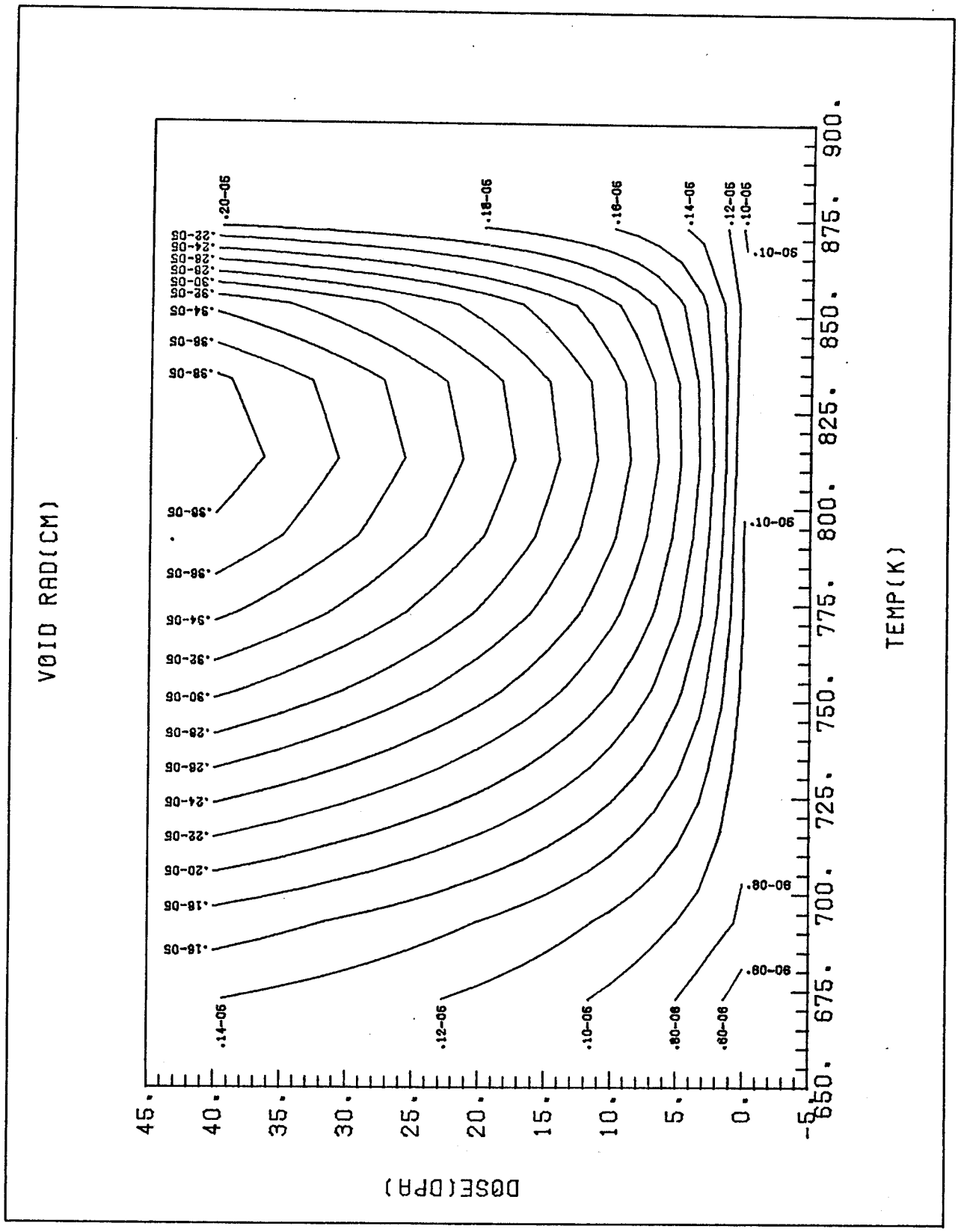

Fig. (62) Contour plot of mean void radius as a function of dose and temperature for neutron irradiated ST stainless steel. The dose rate is 10-6 dpa/sec and the cascade efficiency is 0.001.

As a result, swelling as shown in Figures (63), (64) and (65) shows a sharp drop in magnitude at high temperature. It is worthwhile to notice that no gas generation was assumed in this particular set of calculations. The presence of a large amount of gas atoms in voids would lead to gas driven swelling at high temperatures under reactor conditions.

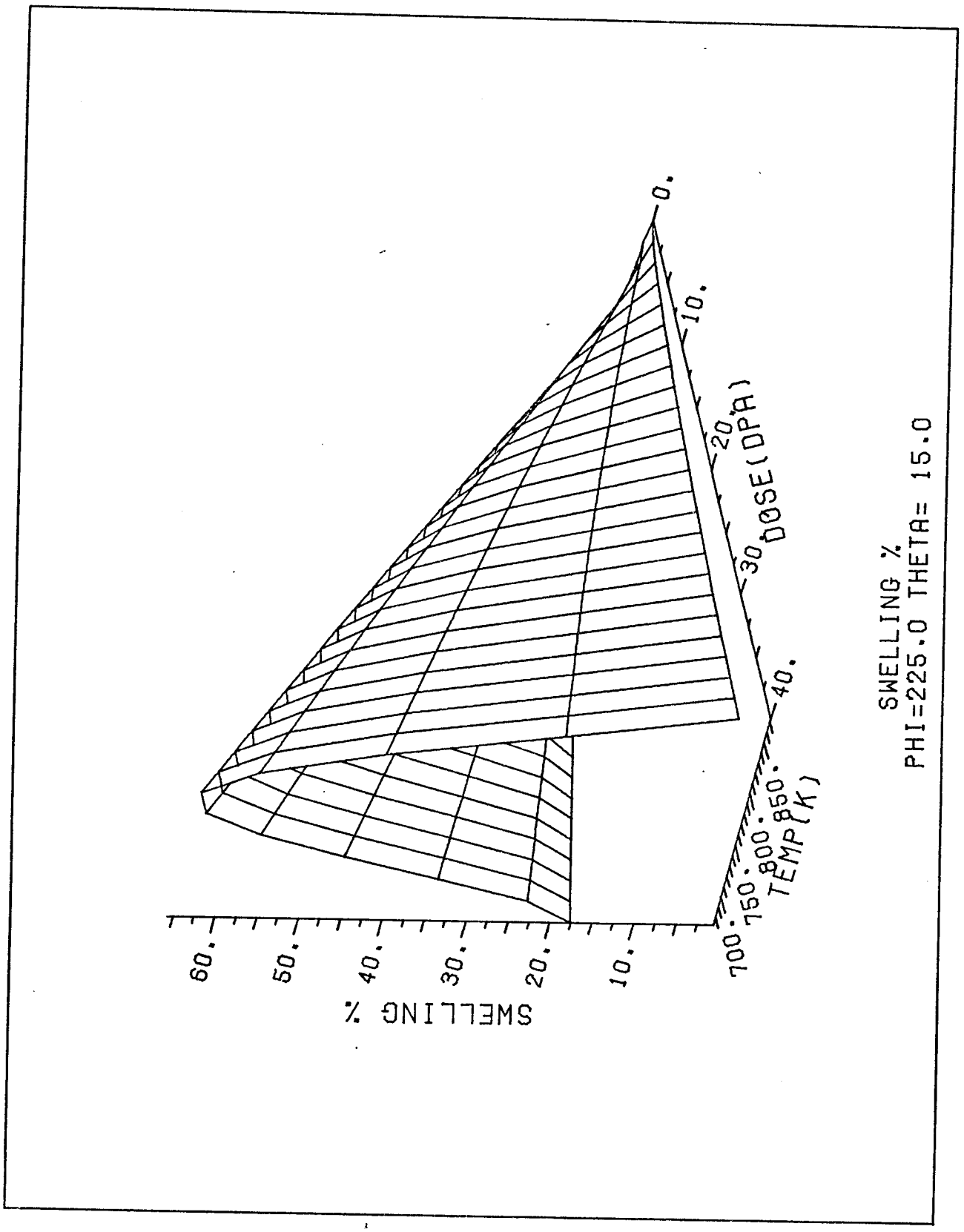

Fig. (63) 3-dimensional plot of percent swelling as a function of dose and temperature for neutron irradiated ST stainless steel. The dose rate is 10^{-6} dpa/sec and the cascade efficiency is 0.001.

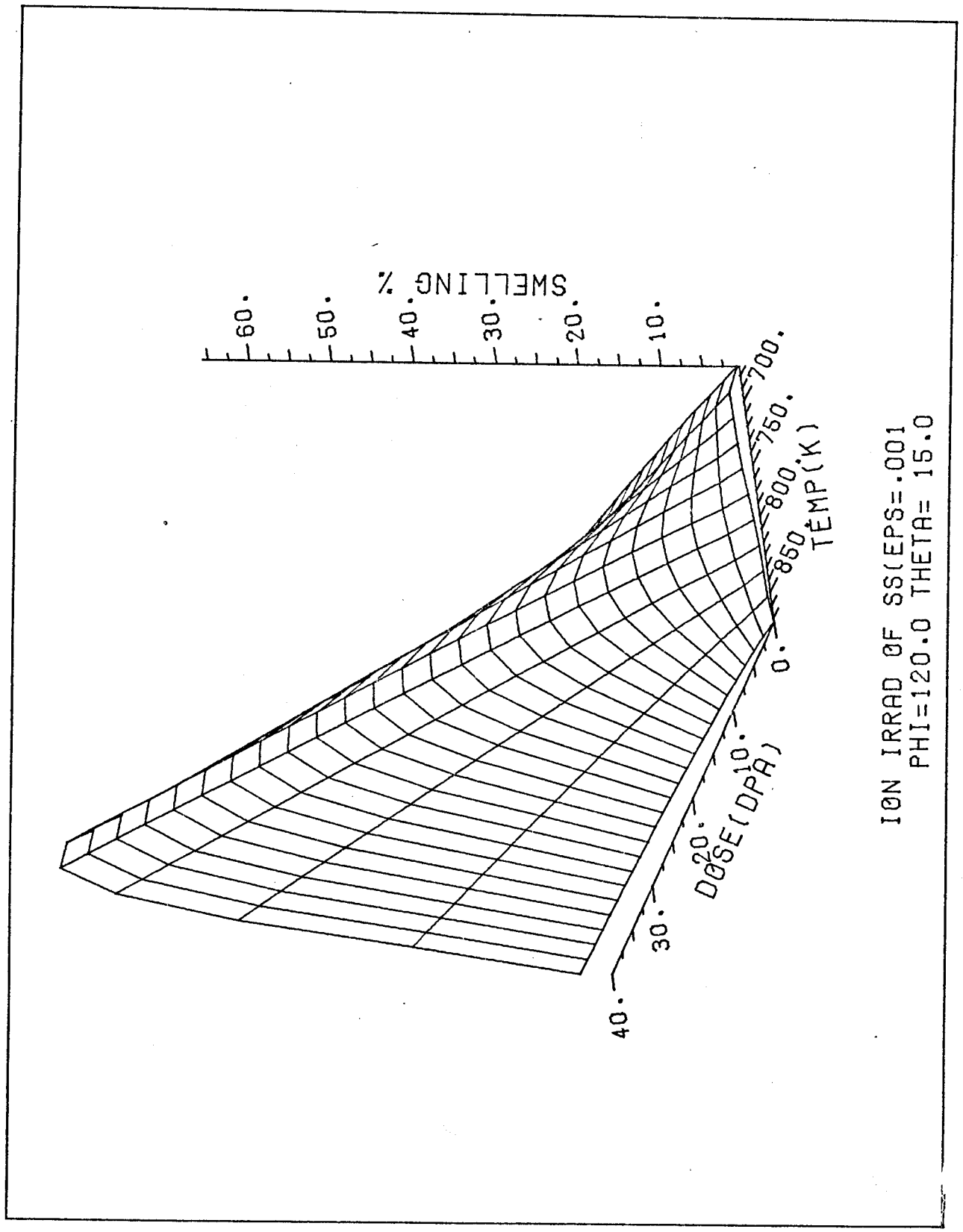

Fig. (64) 3-dimensional plot of percent swelling as a function of dose and temperature for neutron irradiated ST stainless steel. The dose rate is 10^{-6} dpa/sec and the cascade efficiency is 0.001.

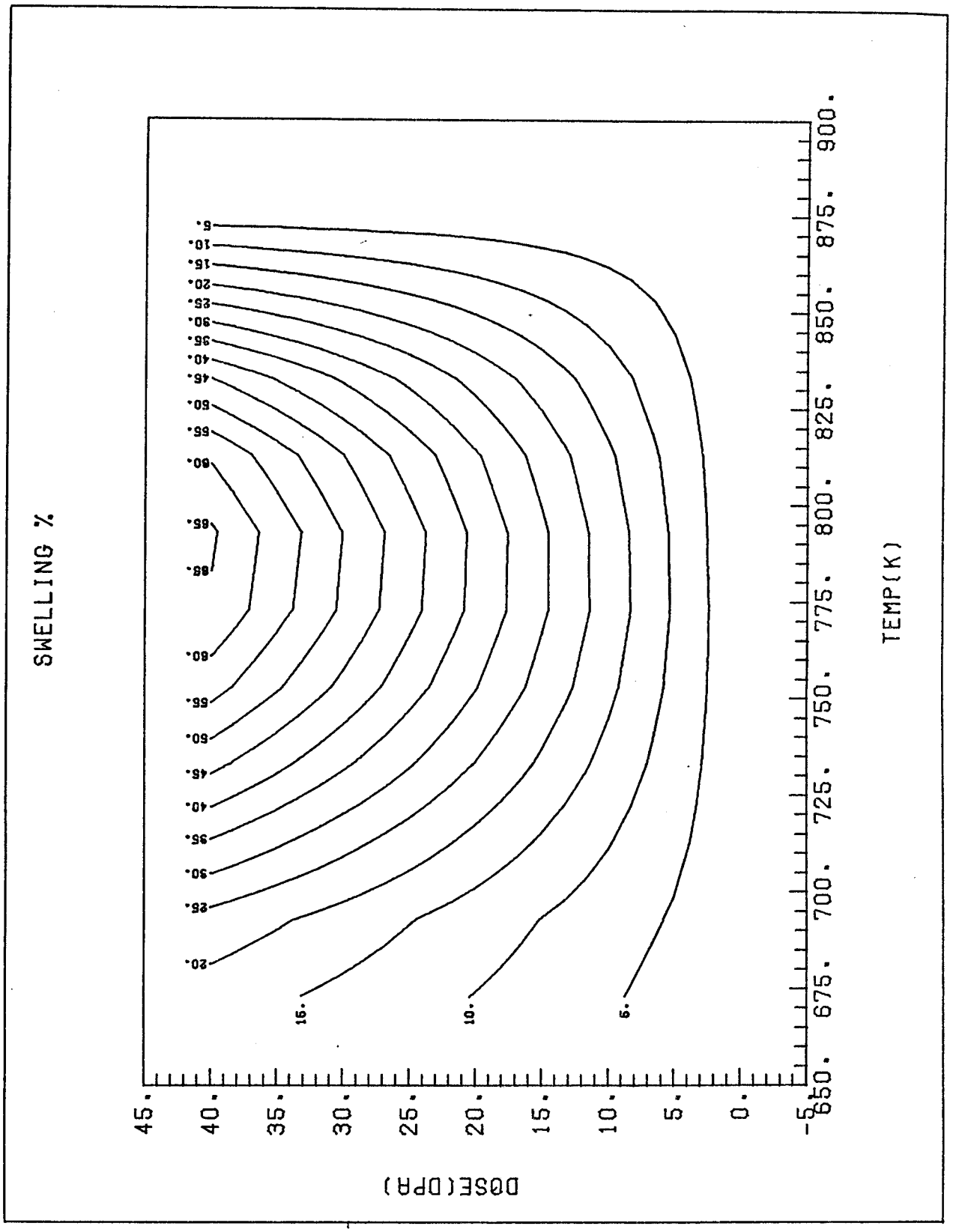

Fig. (65) Contour plot of percent swelling as a function of dose and temperature for neutron irradiated ST stainless steel. The dose rate is 10^{-6} dpa/sec and the cascade efficiency is 0.001.

The equivalent void sink strength is compared to the total dislocation density in Figures (66-69). Total dislocation density is about an order of magnitude larger than void surface area per cm^3 at low temperatures, then it drops faster at high temperature. This is another factor in slowing down void growth at high temperatures since point defects migrate more to the non-biased sink (voids) than the biased sink (dislocations).

The total vacancy emission rate (at/at/sec) as shown in Figures (70) and (71) is found to contribute largely to the vacancy population in the matrix. It reaches the high value of ~ 40% of irradiation produced vacancies at a temperature of $600^{o}C$. As demonstrated in all the previously studied cases, void vacancy emission rate (Figures (72) and (73)) constitute the largest portion of total vacancy emission rate. Almost all irradiation produced point defects get absorbed by sinks (voids as well as dislocation loops), as in Figures (74) and (75). Recombination is negligible in this particular case as shown in Figures (76) and (77).

2. Reactor Conditions With High Cascade Efficiency (ε = 0.044 and P = 10^{-6} dpa/sec).

As established previously, swelling is reduced by increasing the cascade efficiency and this is also true at 10^{-6} dpa s^{-1} (Figures 78 and 79). Comparing the swelling curves in Figures (78) and (79) with Figures (55) and (56) we find a temperature shift for the peak swelling of about $50^{o}C$. (T_{max} is lower at the lower displacement rate). Another feature to be noticed is the higher peak swelling value in a reactor condition compared to the corresponding accelerator condition. These differences are attributed to the greater importance of point defect mutual recombination under accelerator conditions due to their higher concentrations.

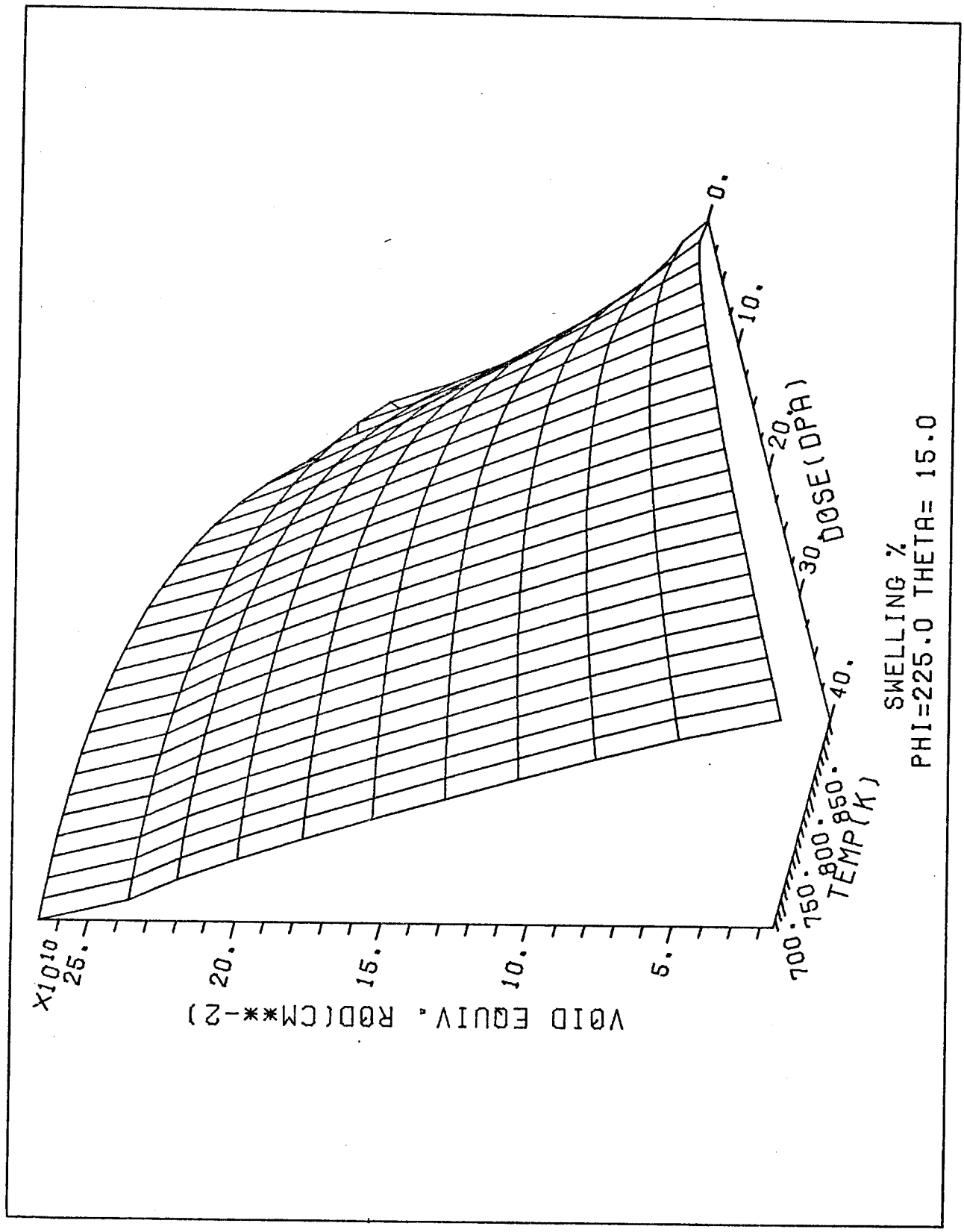

Fig. (66) 3-dimensional plot of void equivalent sink (cm/cm^3) as a function of dose and temperature for neutron irradiated ST stainless steel. The dose rate is 10-6 dpa/sec and the cascade efficiency is 0.001.

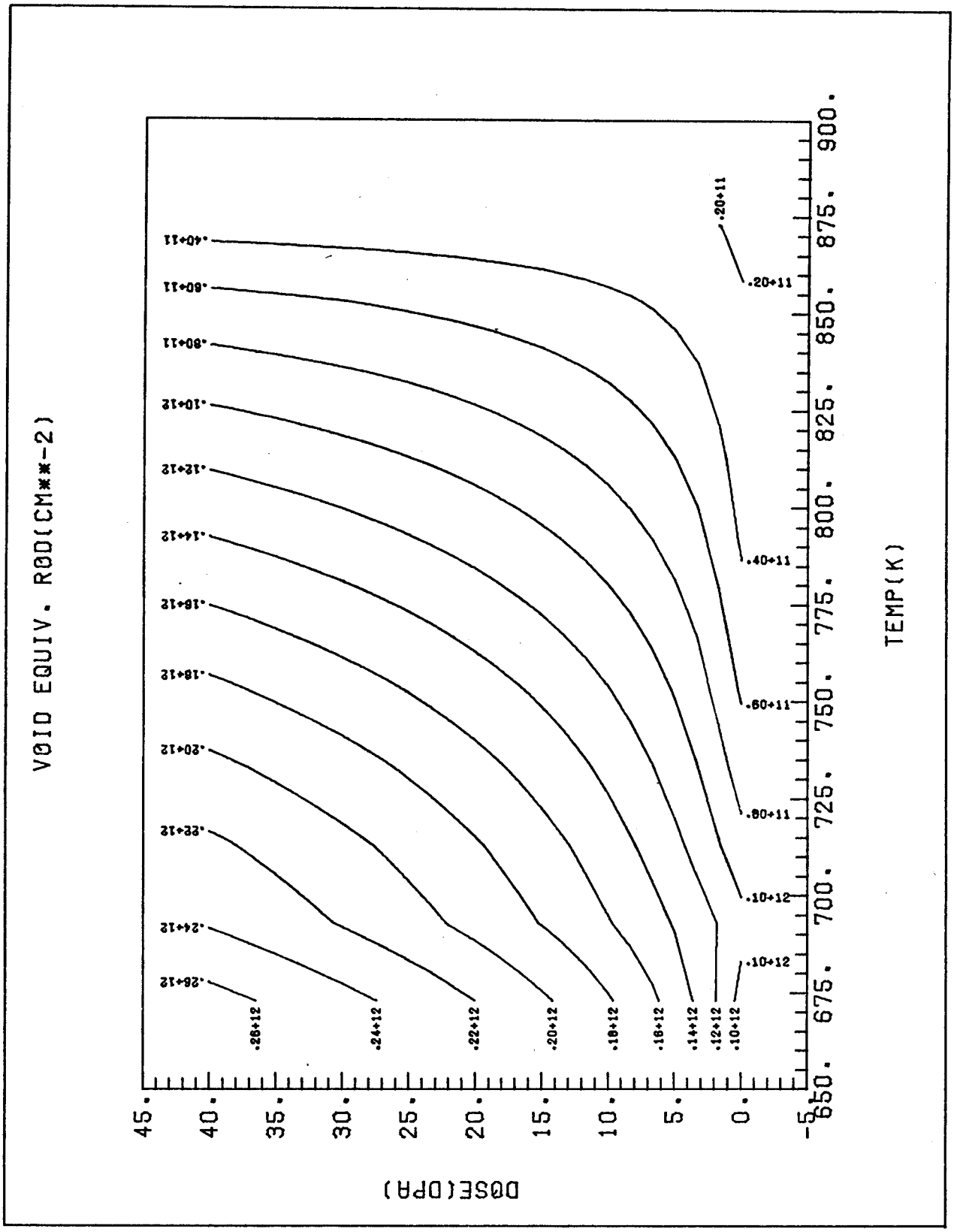

Fig. (67) Contour plot of void equivalent sink (cm/cm^3) as a function of dose and temperature for neutron irradiated ST stainless steel. The dose rate is 10^{-6} dpa/sec and the cascade efficiency is 0.001.

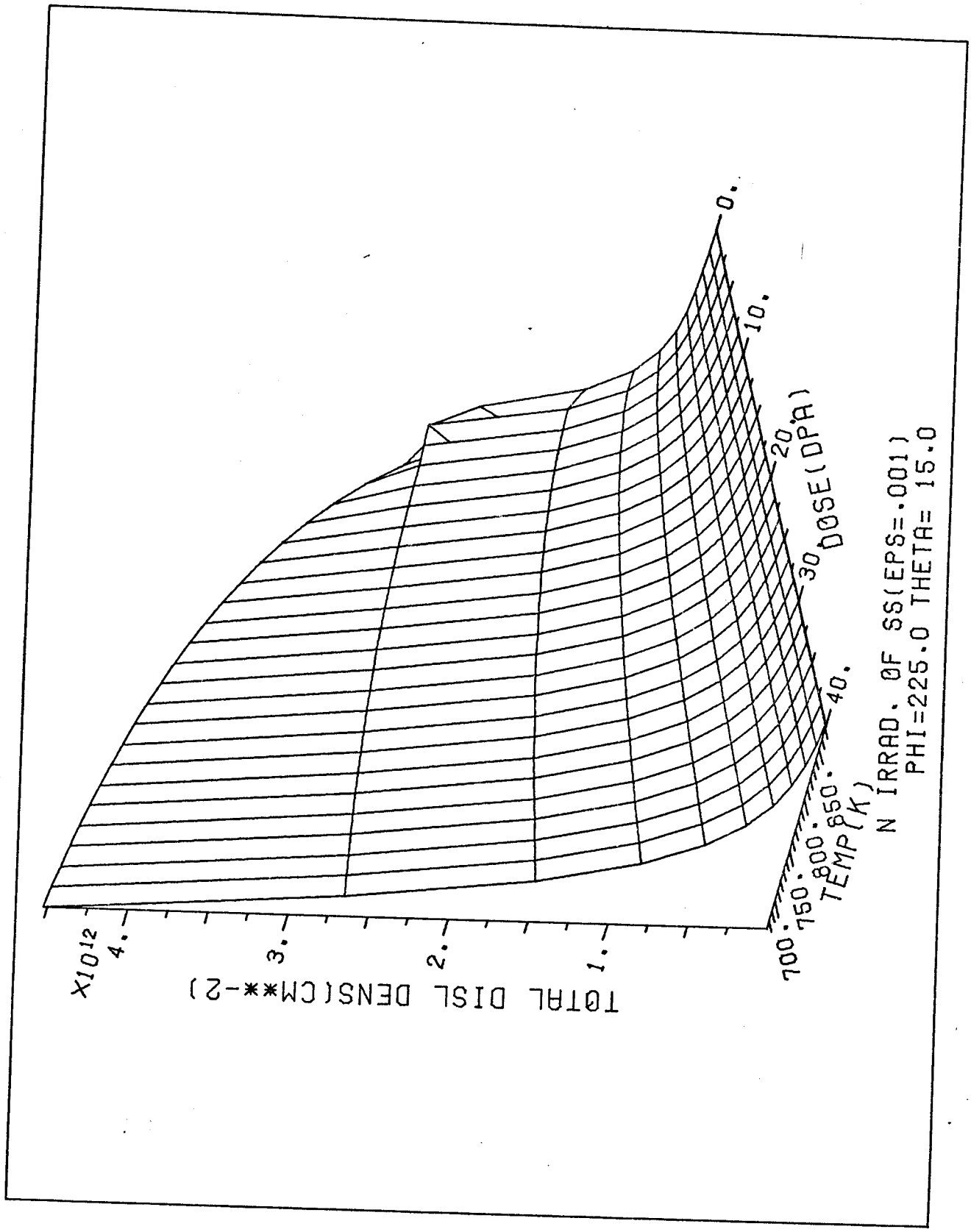

Fig. (68) 3-dimensional plot of total dislocation density (cm/cm^3) as a function of dose and temperature for neutron irradiated ST stainless steel. The dose rate is 10^{-6} dpa/sec and the cascade efficiency is 0.001.

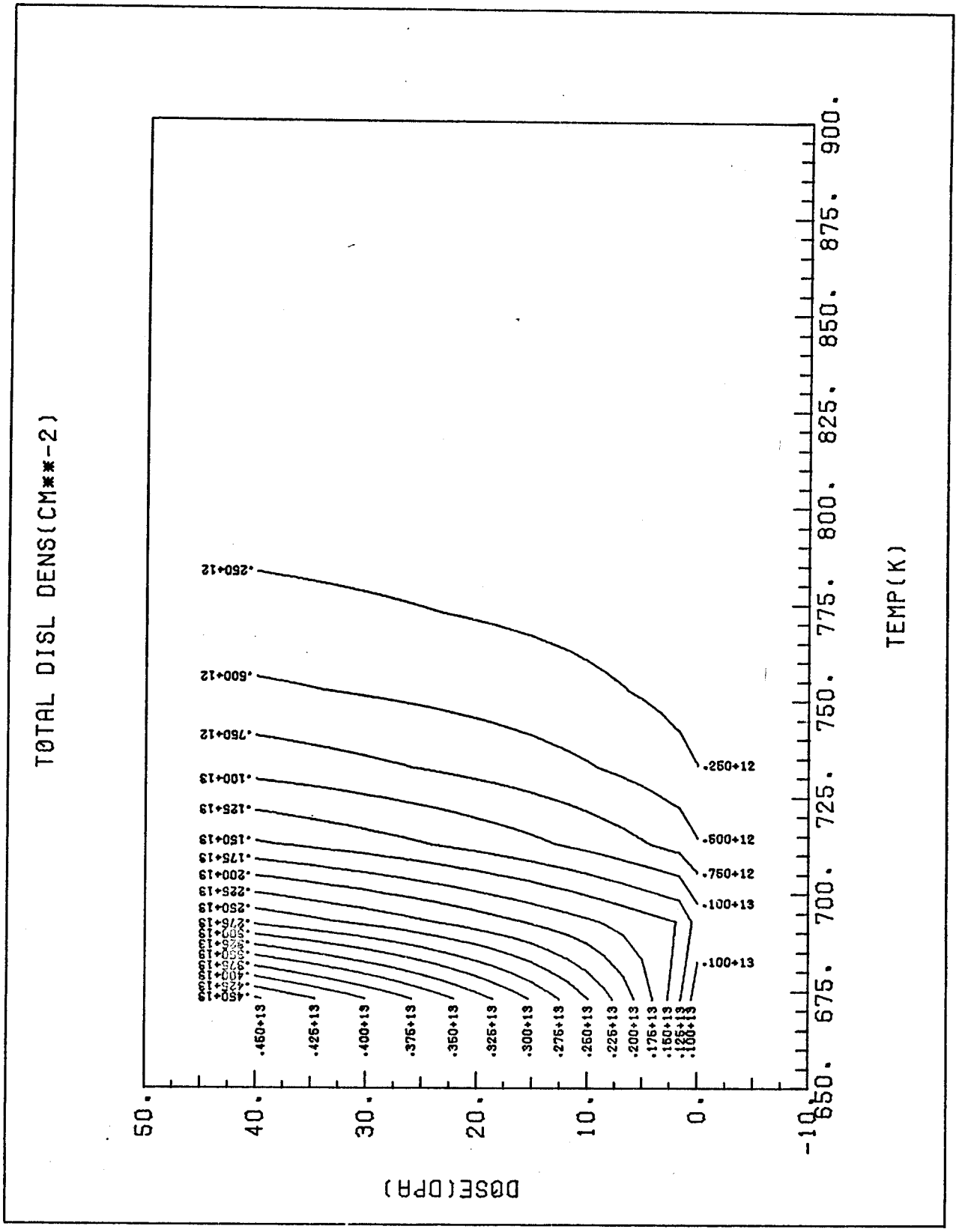

Fig. (69) Contour plot of total dislocation density (cm/cm^3) as a function of dose and temperature for neutron irradiated ST stainless steel. The dose rate is 10^{-6} dpa/sec and the cascade efficiency is 0.001.

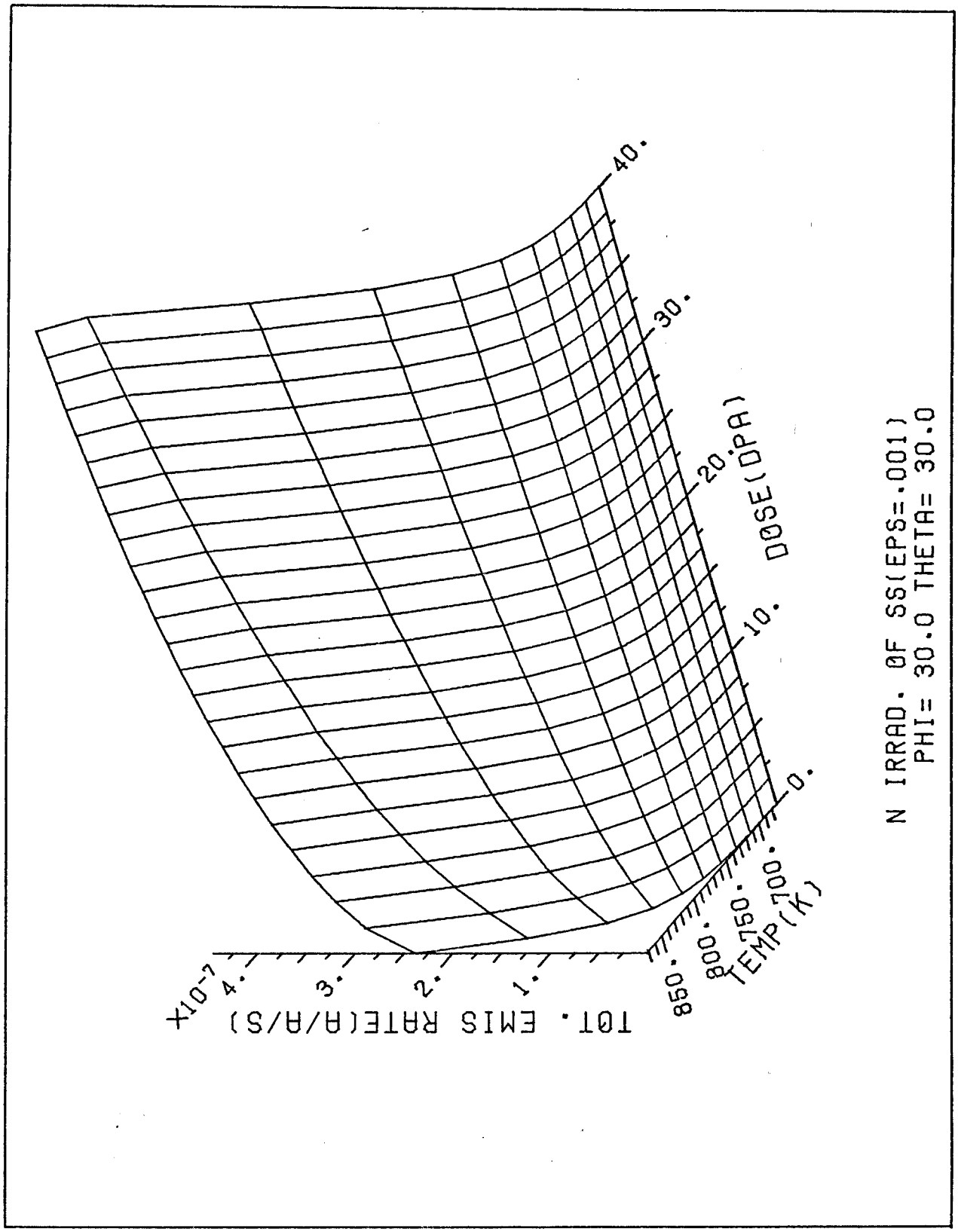

Fig. (70) 3-dimensional plot of total vacancy thermal emission rate (at/at/sec) as a function of dose and temperature for neutron irradiated ST stainless steel. The dose rate is 10^{-6} dpa/sec and the cascade efficiency is 0.001.

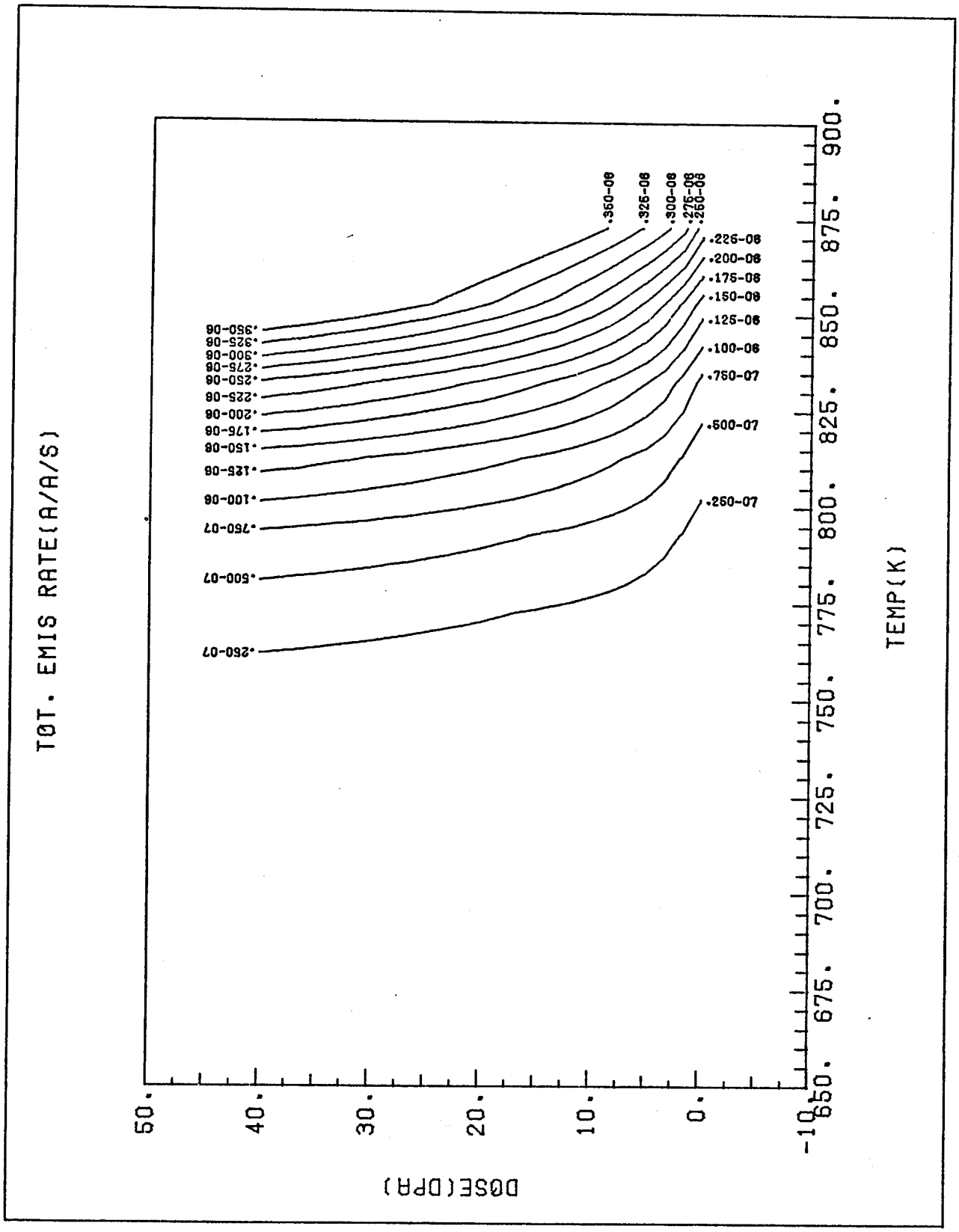

Fig. (71) Contour plot of total vacancy thermal emission rate (at/at/sec) as a function of dose and temperature for neutron irradiated ST stainless steel. The dose rate is 10-6 dpa/sec and the cascade efficiency is 0.001.

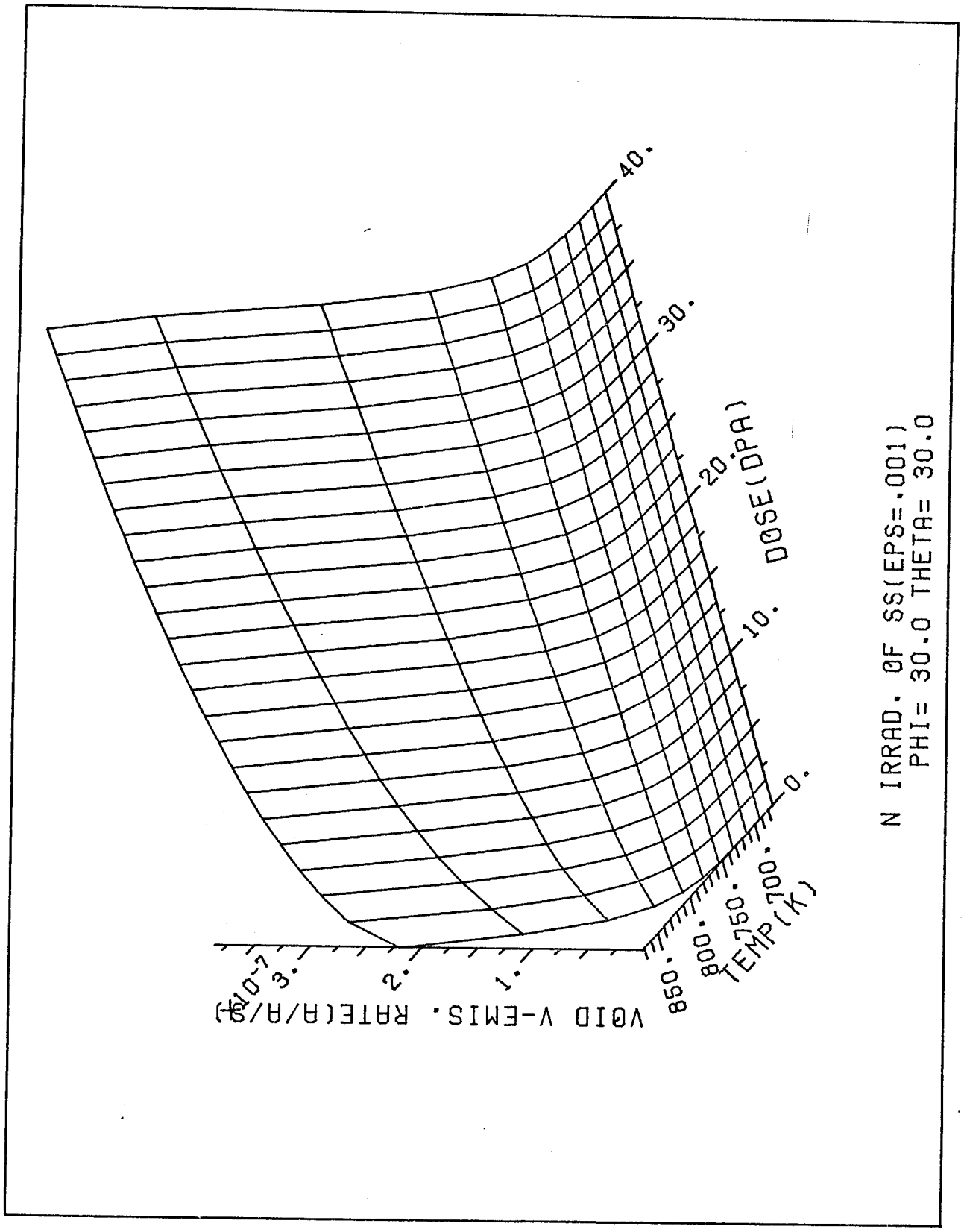

Fig. (72) 3-dimensional plot of void vacancy thermal emission rate (at/at/sec) as a function of dose and temperature for neutron irradiated ST stainless steel. The dose rate is 10^{-6} dpa/sec and the cascade efficiency is 0.001.

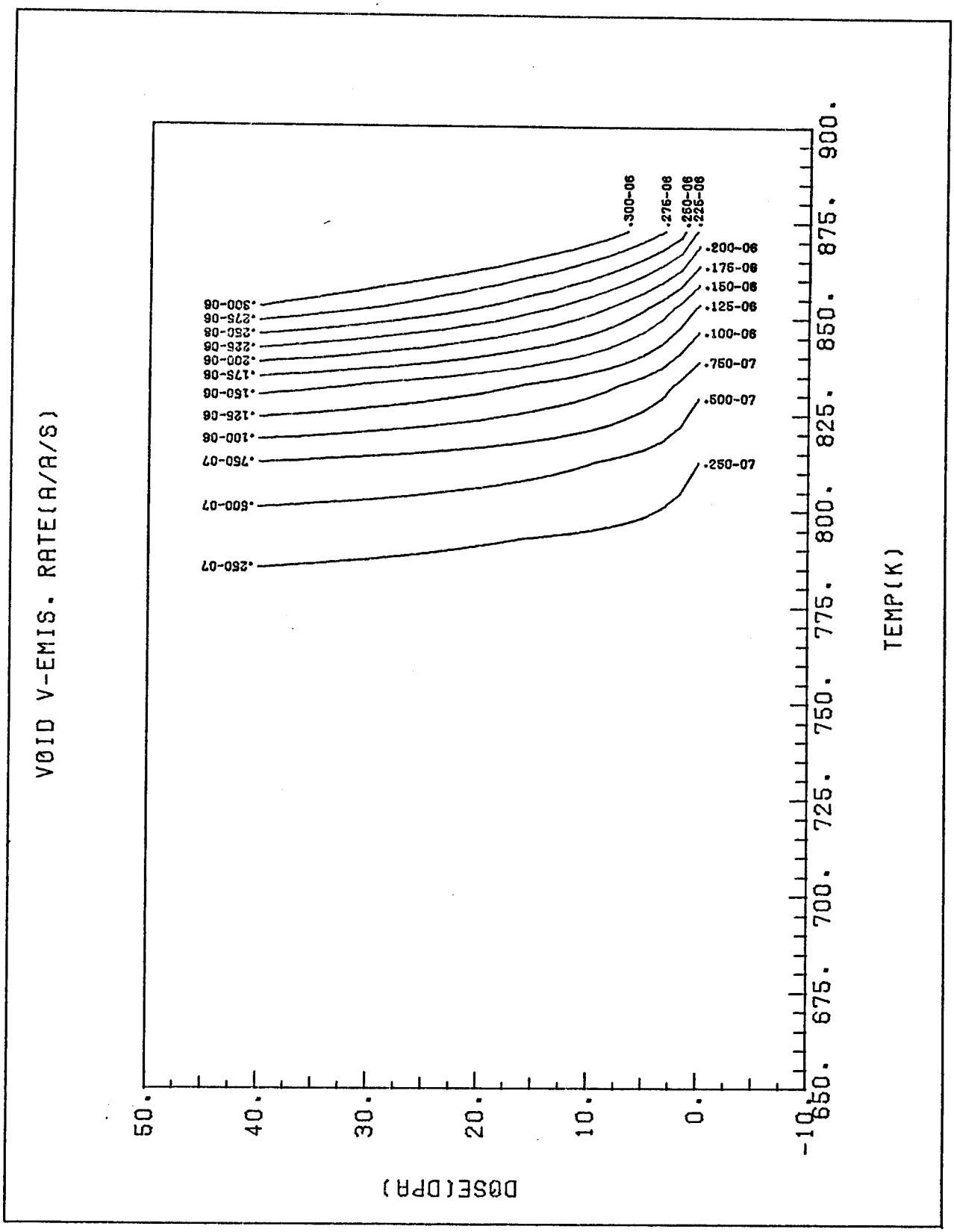

Fig. (73) Contour plot of void vacancy thermal emission rate (at/at/sec) as a function of dose and temperature for neutron irradiated ST stainless steel. The dose rate is 10^{-6} dpa/sec and the cascade efficiency is 0.001.

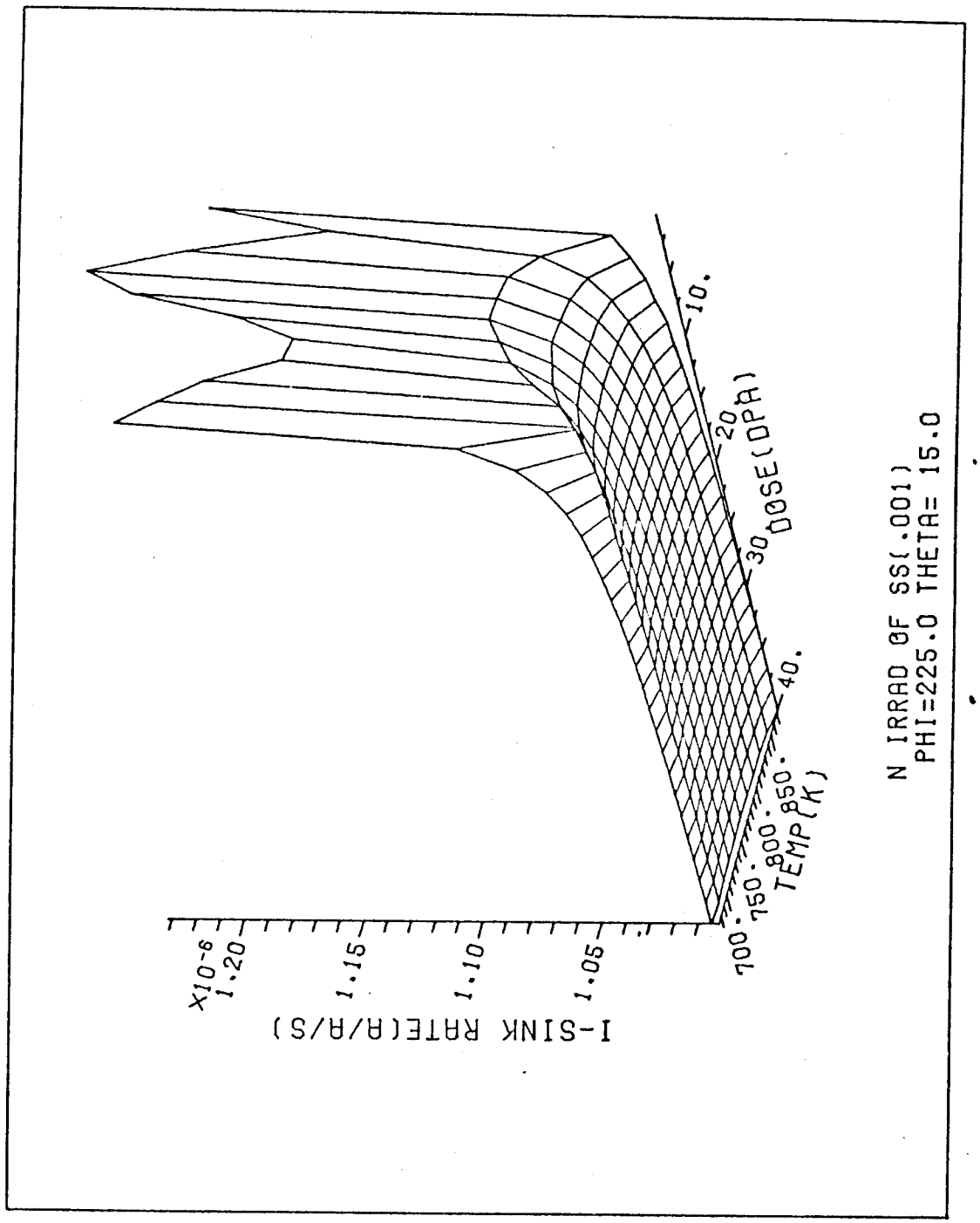

Fig. (74) 3-dimensional plot of interstitial sink removal rate (at/at/sec) as a function of dose and temperature for neutron irradiated ST stainless steel. The dose rate is 10^{-6} dpa/sec and the cascade efficiency is 0.001.

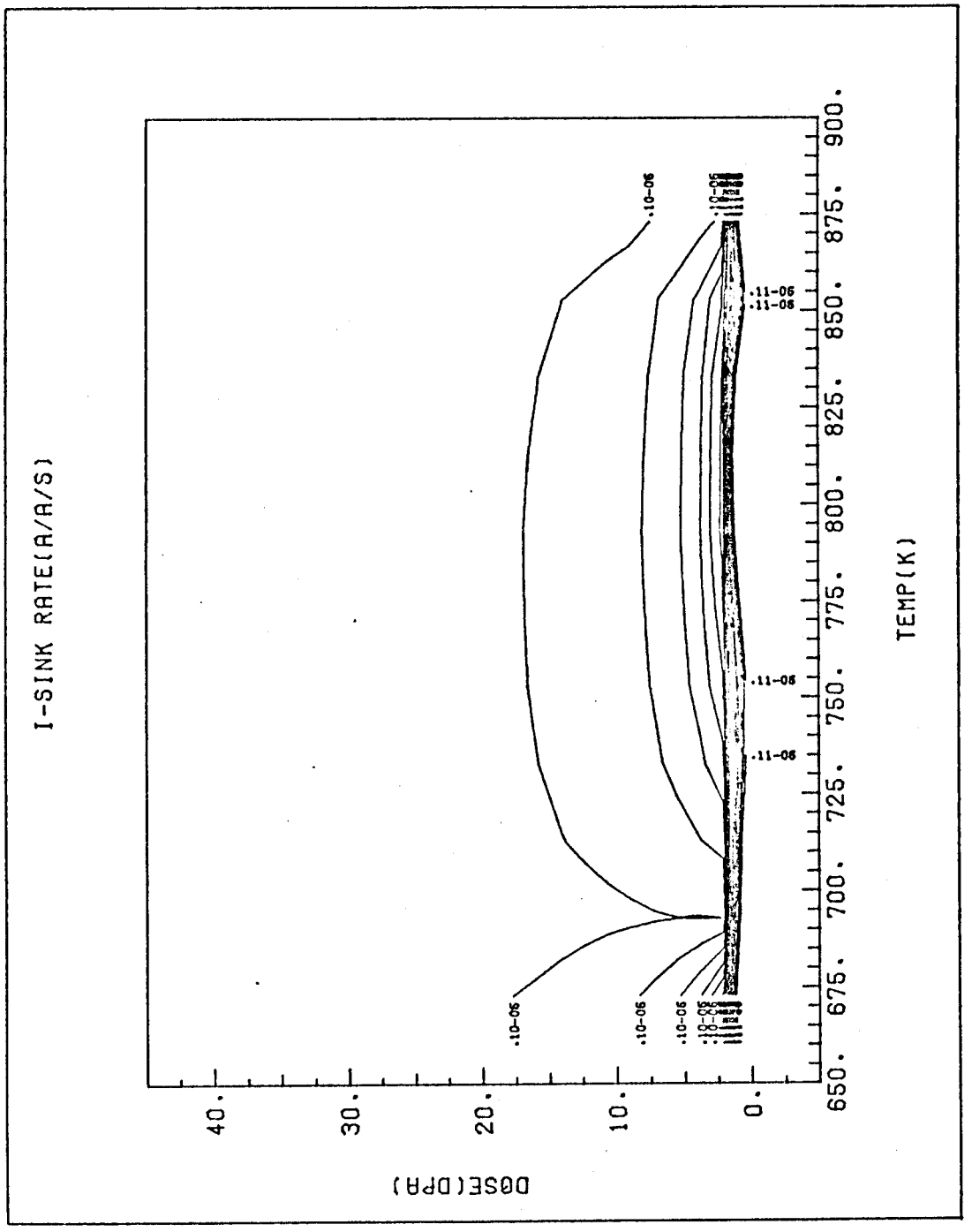

Fig. (75) Contour plot of interstitial sink removal rate (at/at/sec) as a function of dose and temperature for neutron irradiated SS stainless steel. The dose rate is 10-6 dpa/sec and the cascade efficiency is 0.001.

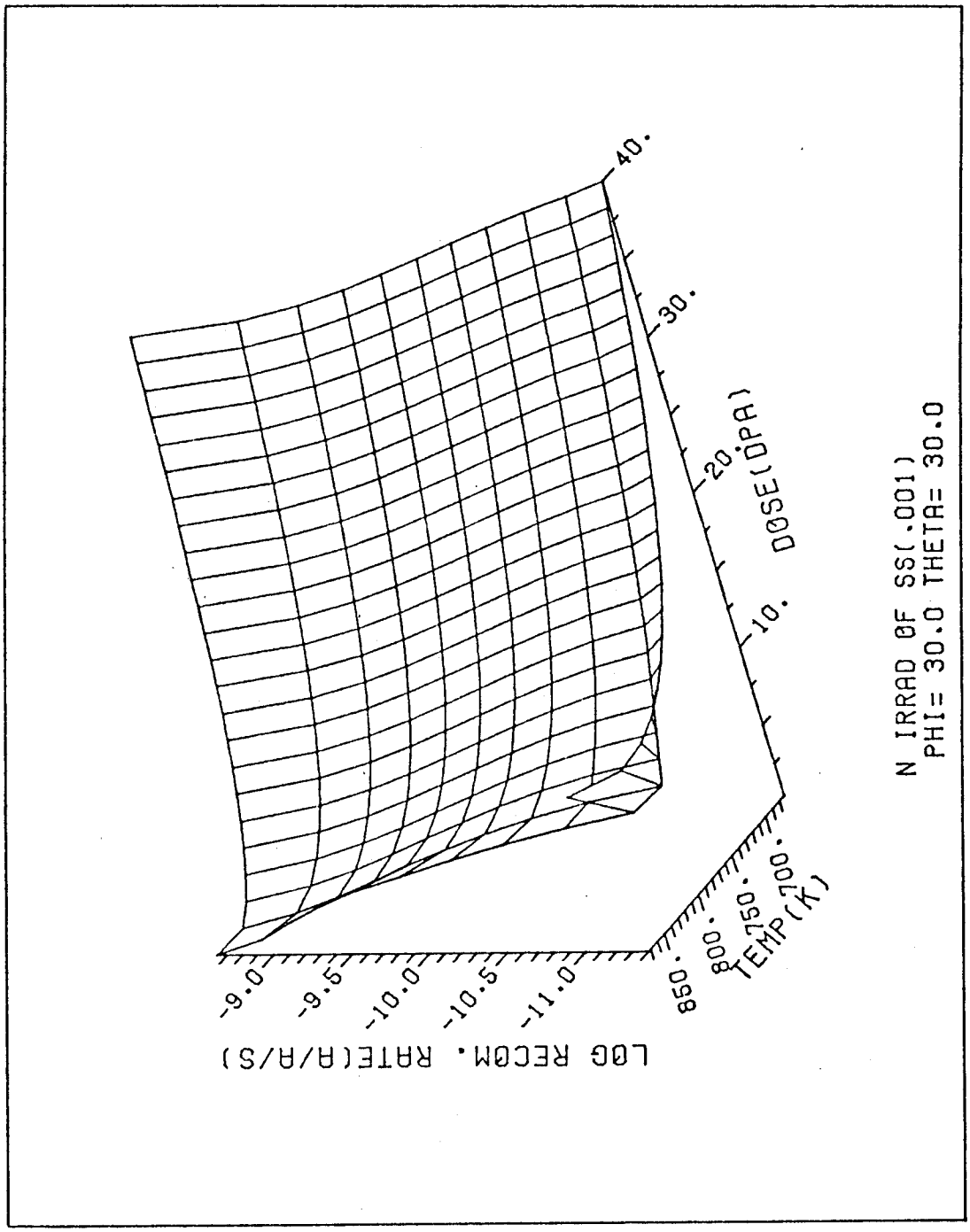

Fig. (76) 3-dimensional plot of point defect recombination rate (at/at/sec) as a function of dose and temperature for neutron irradiated ST stainless steel. The dose rate is 10^{-6} dpa/sec and the cascade efficiency is 0.001.

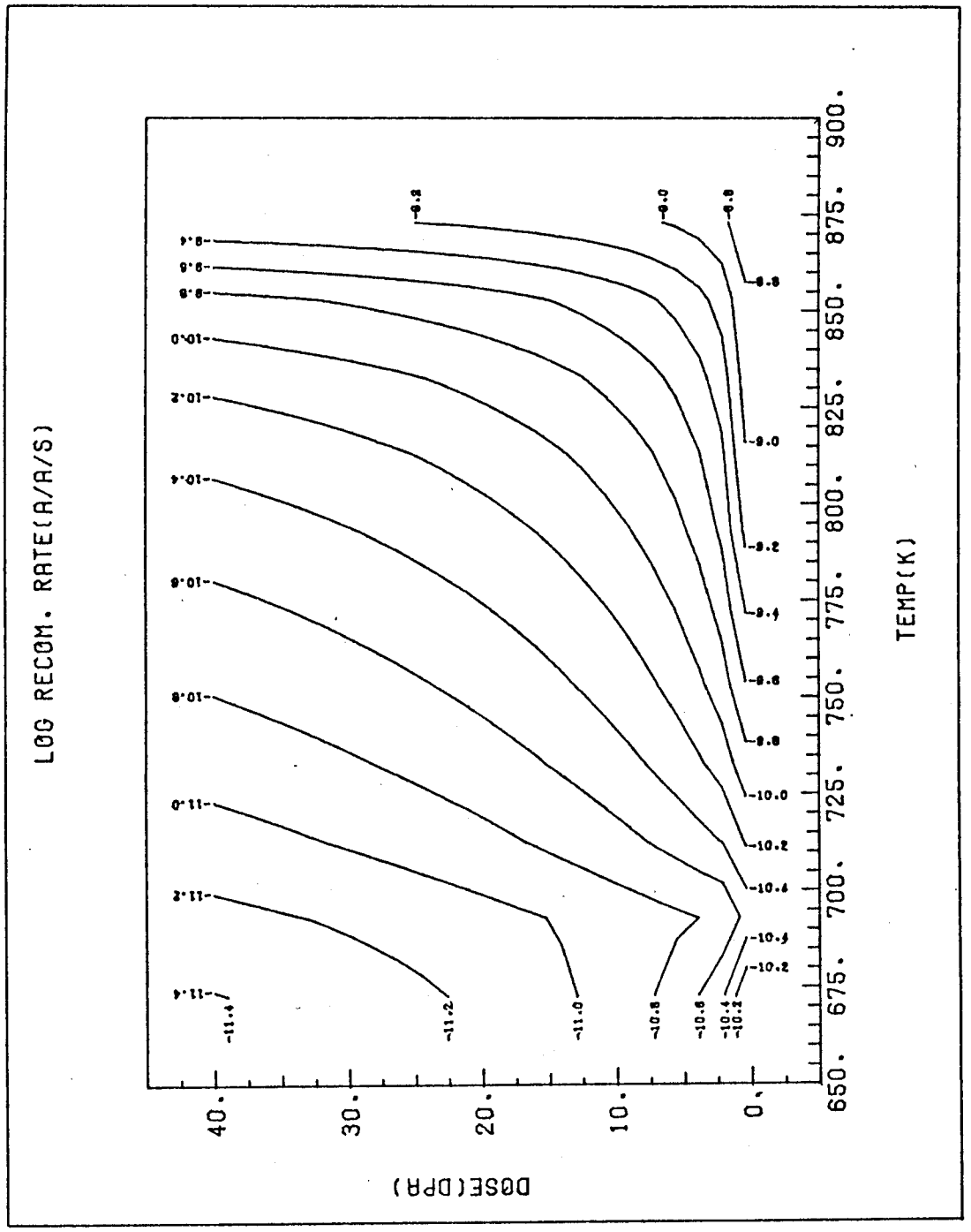

Fig. (77) Contour plot of point defect recombination rate (at/at/sec) as a function of dose and temperature for neutron irradiated ST stainless steel. The dose rate is 10^{-6} dpa/sec and the cascade efficiency is 0.001.

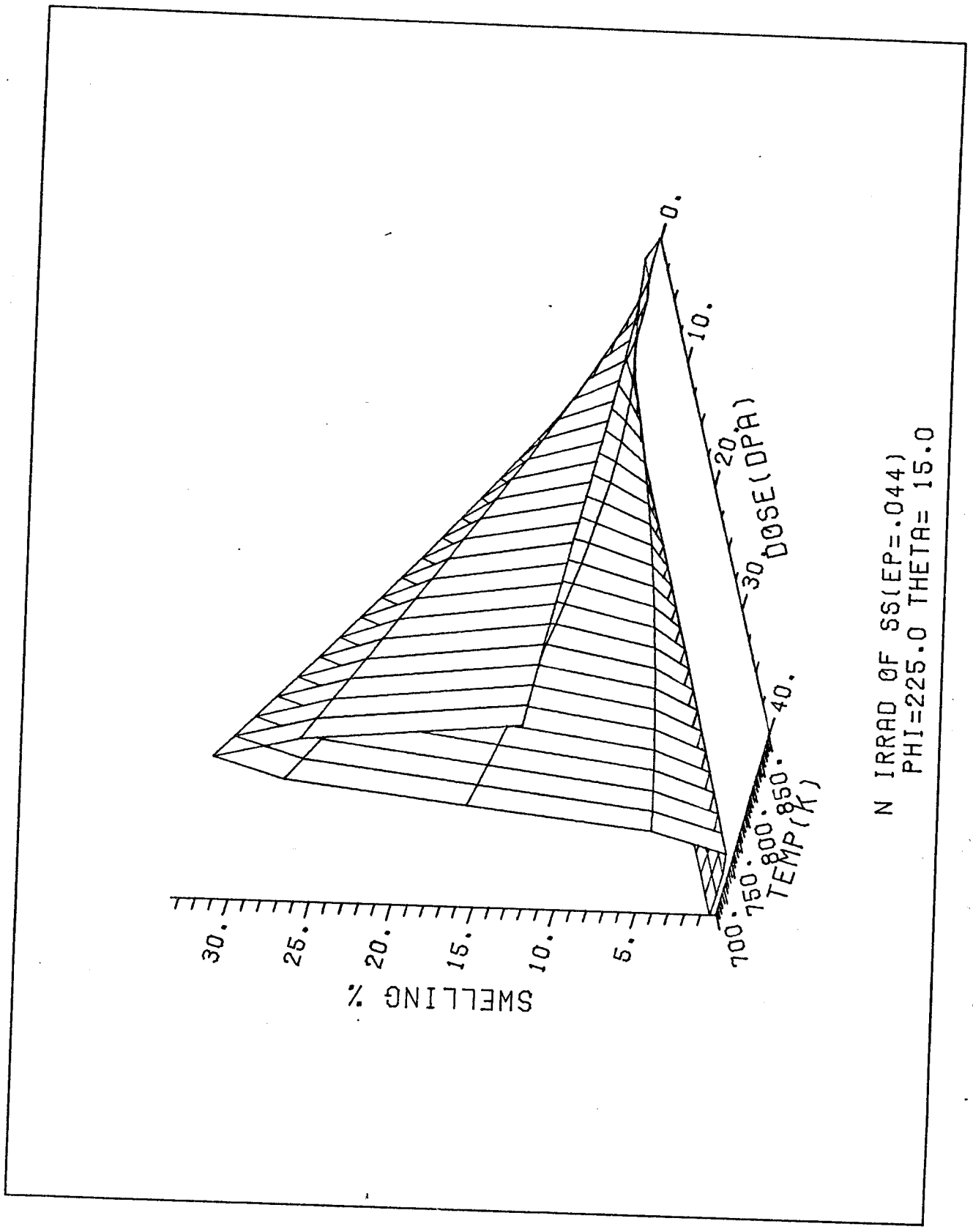

Fig. (78) 3-dimensional plot of percent swelling as a function of dose and temperature for neutron irradiated ST stainless steel. The dose rate is 10-6 dpa/sec and the cascade efficiency is 0.044.

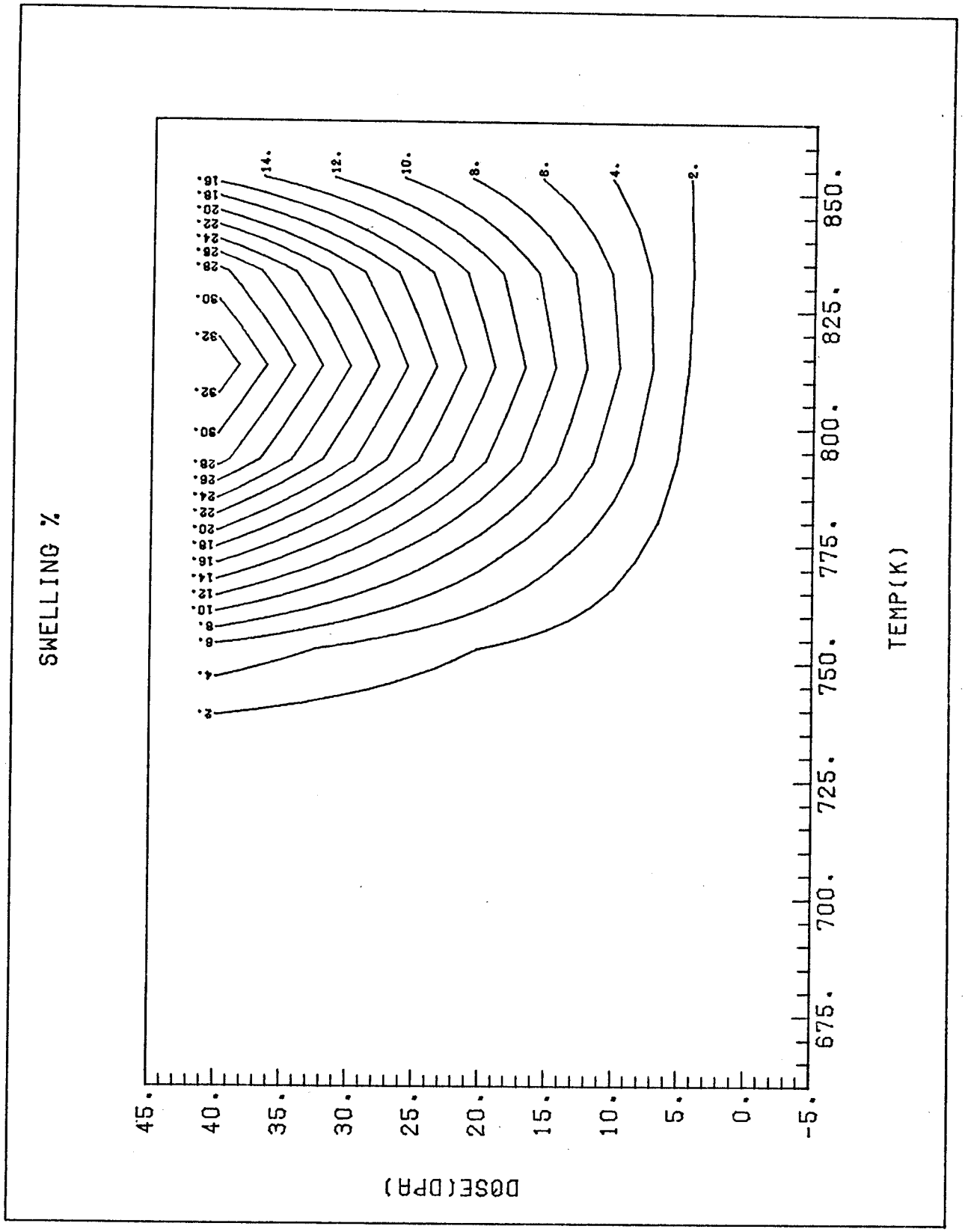

Fig. (79) Contour plot of percent swelling as a function of dose and temperature for neutron irradiated ST stainless steel. The dose rate is 10^{-6} dpa/sec and the cascade efficiency is 0.044.

The void vacancy thermal emission rate is shown in Figures (80) and (81) while the total vacancy thermal emission rate is shown in Figures (82) and (83). Again, it should be noticed that the void vacancy thermal emission is over 2/3 of the total emission rate. The total thermal vacancy emission rate is also considerable (30-40% of irradiation point defect production rate, at high temperatures and high doses). At even higher temperatures, the voids will be emitting more vacancies than produced and hence would shrink signifying the upper temperature limit on void swelling.

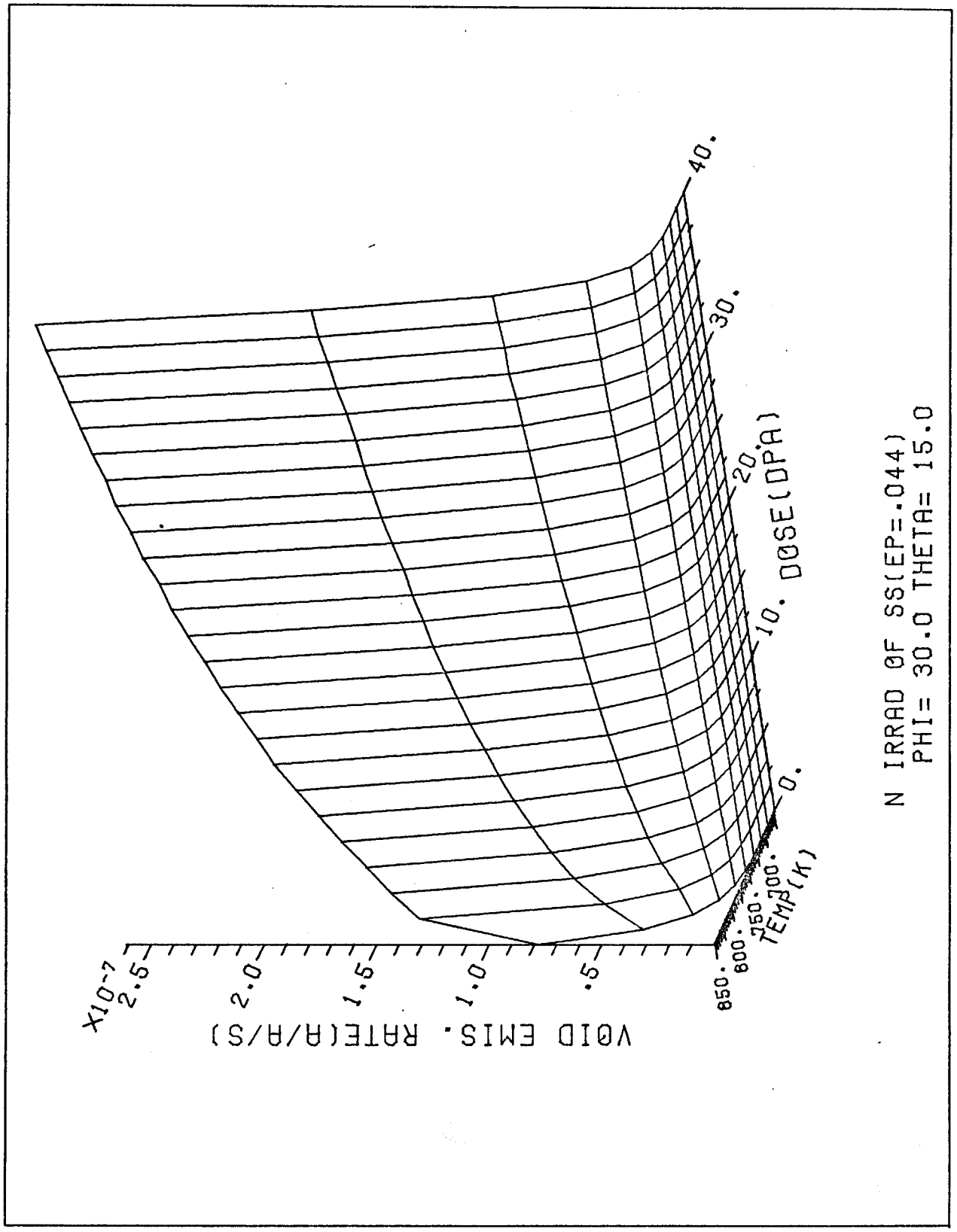

Fig. (80) 3-dimensional plot of void thermal vacancy emission rate (at/at/sec) as a function of dose and temperature for neutron irradiated ST stainless steel. The dose rate is 10^{-6} dpa/sec and the cascade efficiency is 0.044.

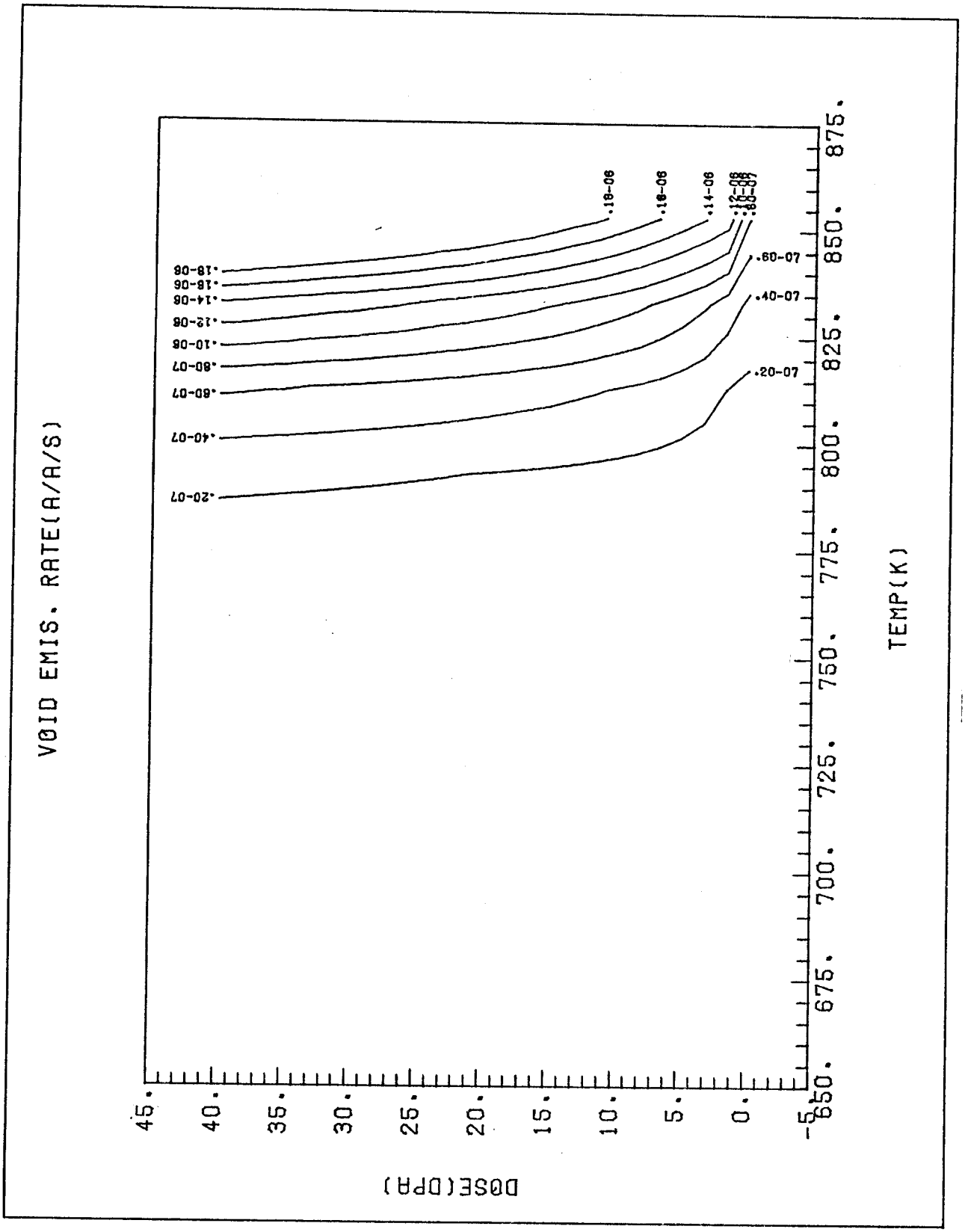

Fig. (81) Contour plot of void thermal vacancy emission rate (at/at/sec) as a function of dose and temperature for neutron irradiated ST stainless steel. The dose rate is 10-6 dpa/sec and the cascade efficiency is 0.044.

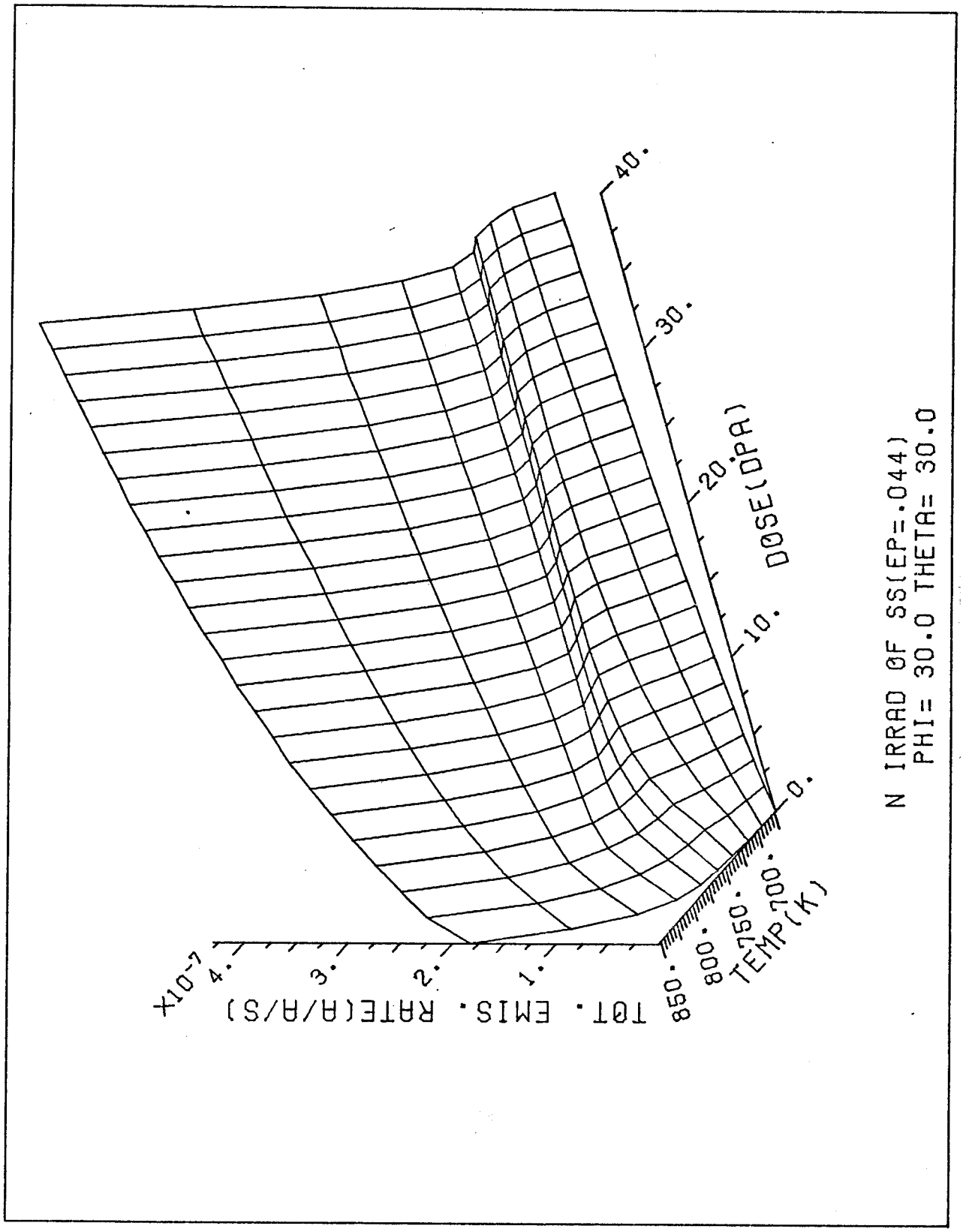

Fig. (82) 3-dimensional plot of total thermal vacancy emission rate as a function of dose and temperature for neutron irradiated ST stainless steel. The dose rate is 10^{-6} dpa/sec and the cascade efficiency is 0.044.

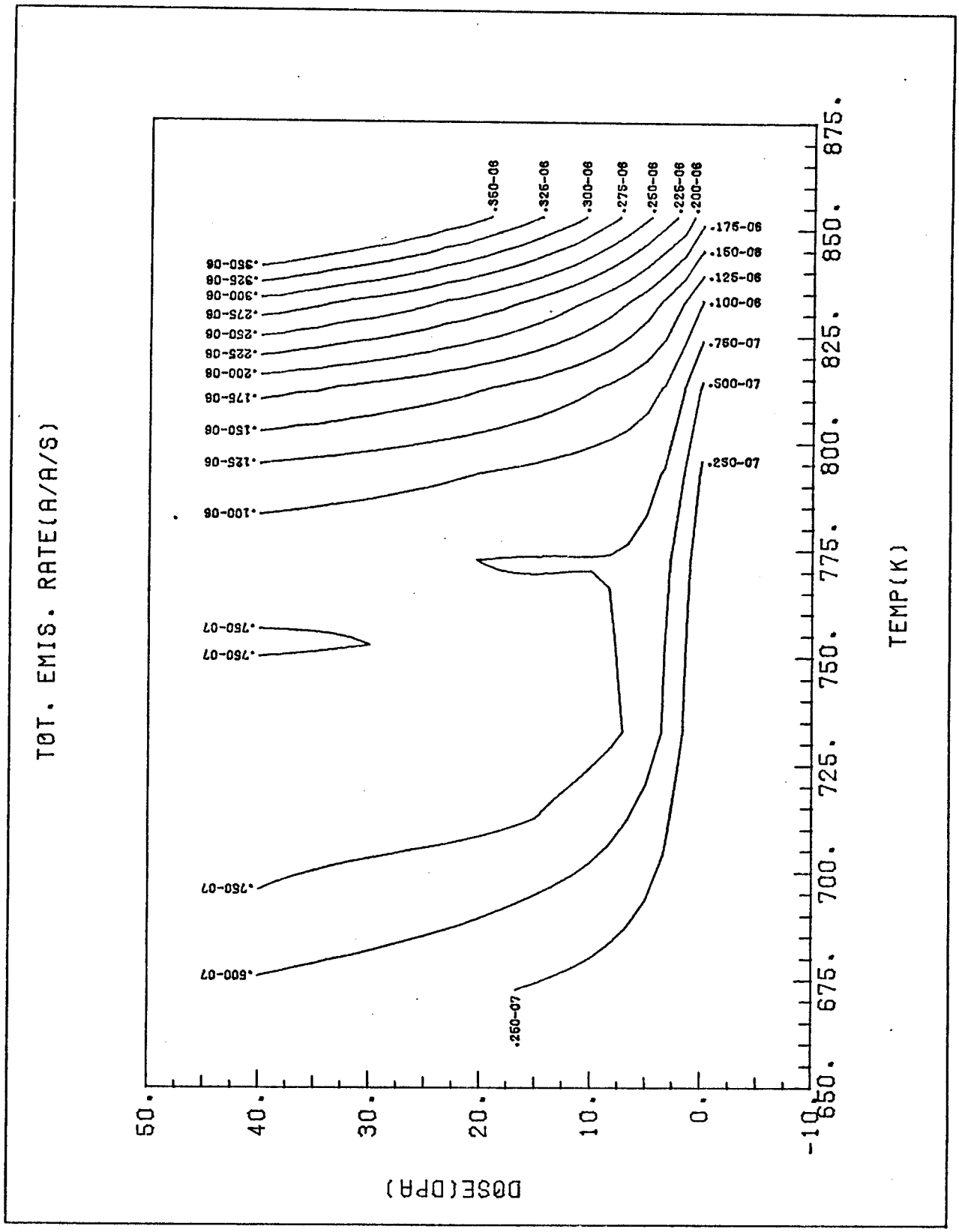

Fig. (83) Contour plot of total thermal vacancy emission rate as a function of dose and temperature for neutron irradiated ST stainless steel. The dose rate is 10^{-6} dpa/sec and the cascade efficiency is 0.044.

IV. Fixed Microstructure Calculations

The previous analysis has considered the details of point defect source and sink variations as a function of time and temperature. In this section we will study the displacement rate effects on swelling with a fixed microstructure that does not change as a function of temperature and irradiation time. The parameters used in these calculations are those of Brailsford and Bullough.[1]

Figure (84) shows point defect average concentrations as a function of temperature for different dose rates. As the temperature is increased, vacancy mobility increases and more vacancies are absorbed by present sinks. This causes a drop in vacancy concentration with temperature. Interstitial concentration, on the other hand, shows an increase as a function of temperature. This behavior is due to the dominance of recombination at lower temperatures which couples point defect concentrations. Thus, when vacancies disappear from the matrix, interstitials find a better chance to survive. At higher temperatures, recombination is unimportant as depicted in figures (85) and (86); and point defect concentrations vary independently as a function of time: vacancy concentration decreases due to a higher mobility and interstitial concentration saturates because of an almost constant mobility.

At even higher temperatures, the vacancy concentration becomes the thermal equilibrium value and the interstitial concentration becomes constant as a function of temperature. It is apparent that for smaller dpa rates the vacancy concentration approaches the thermal equilibrium value at a lower temperature giving rise to a precipitous decrease in swelling as shown in figure (87).

Figures (85) and (86) show that at low temperatures, point defects recombine faster than their removal by existing sinks. At higher temperatures, vacnacies are more mobile which give rise to a higher removal rate by sinks and a lower recombination rate. At even higher temperatures, the contribution of thermally emitted vacancies from the microstructure becomes appreciable. It is important to notice that as the point defect production rate goes up, the temperature range over which recombination rate dominantes becomes larger.

Figure (87) shows the relative swelling under neutron and ion irradiations for a fixed microstructure. The Brailsford and Bullough[1] model with a void surface energy of 0 ergs/cm^2 predicts a peak temperature shift of 190°C for 316 SS. The computer code TRANSWELL was used to calculate relative swelling for the same conditions of a fixed microstructure with a surface energy of 1000 ergs/cm^2. It predicts a peak temperature shift of 140°C and shows the sensitivity of the calculations to changes in the surface energy.

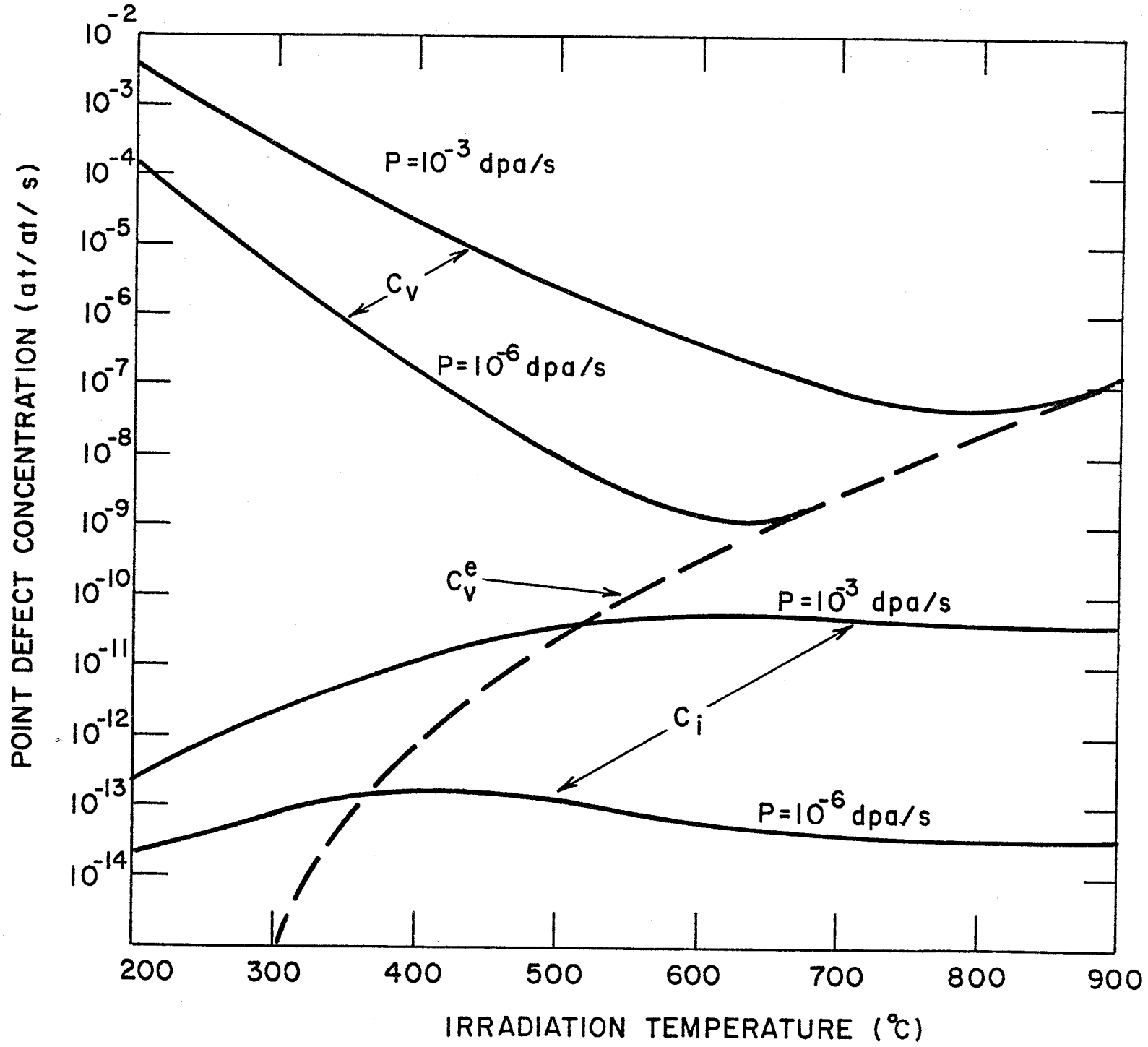
POINT DEFECT CONCENTRATION (at/at/s)
10^{-2}
10^{-3}
10^{-4}
10^{-5}
10^{-6}
10^{-7}
10^{-8}
10^{-9}
10^{-10}
10^{-11}
10^{-12}
10^{-13}
10^{-14}
$P=10^{-3}$ dpa/s
C_v
$P=10^{-6}$ dpa/s
C_v^e
$P=10^{-3}$ dpa/s
C_i
$P=10^{-6}$ dpa/s
200
300
400
500
600
700
800
900
IRRADIATION TEMPERATURE (°C)

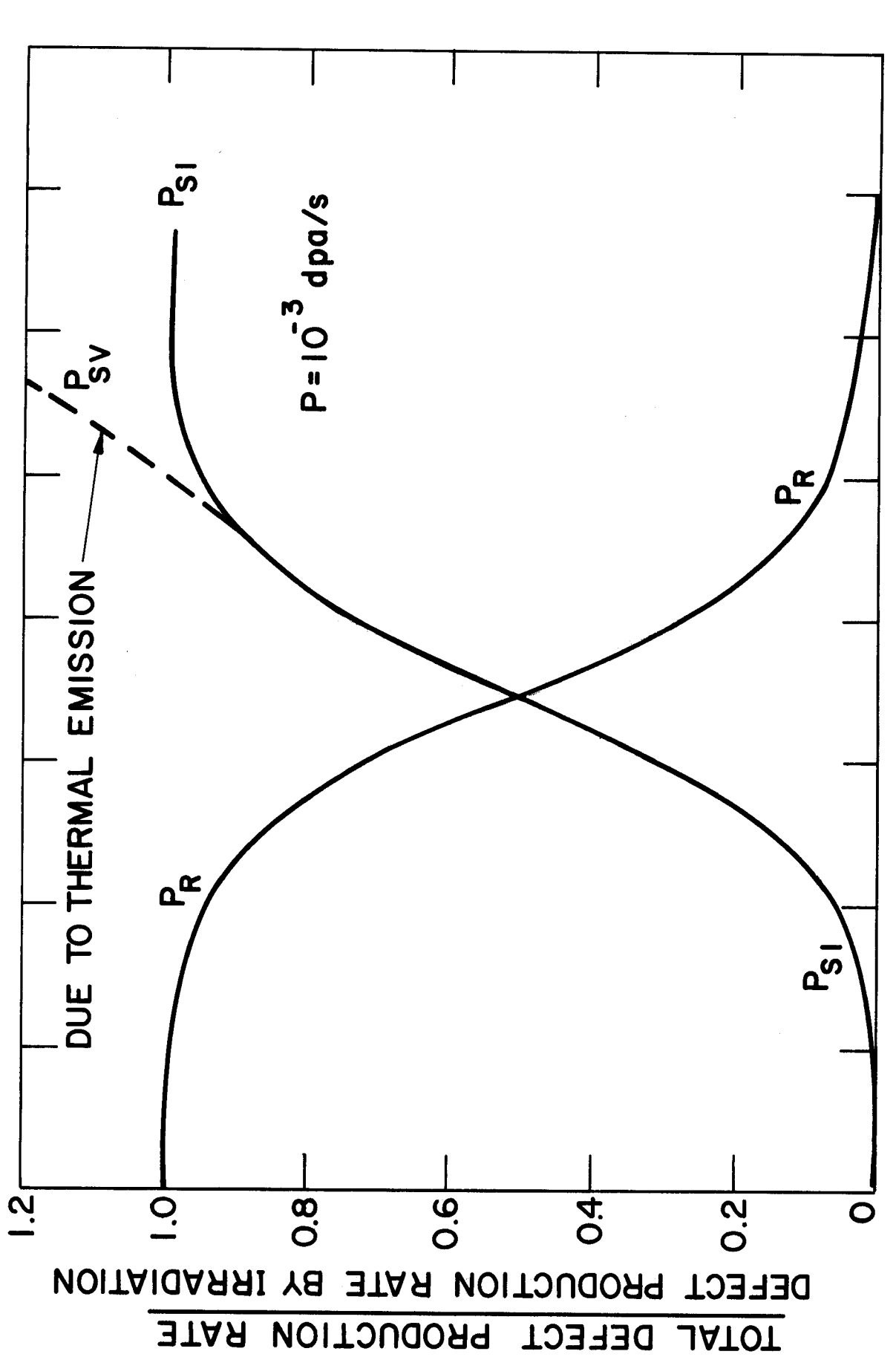

Figure (85) Relative Removal Rates of Point Defects as a Function of Temperture for Fixed Microstructure of 316 SS (Reactor Conditions)

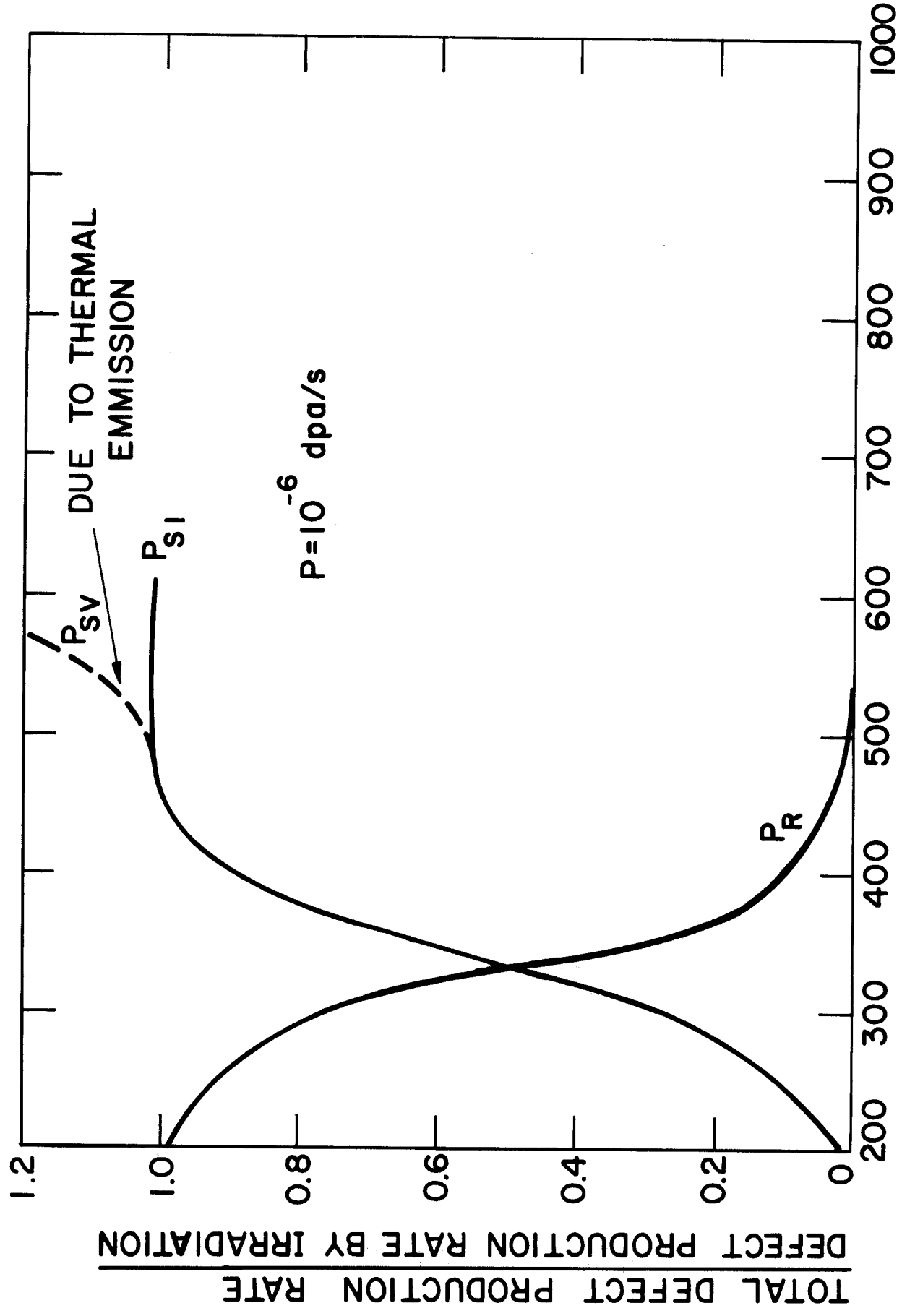

Figure (86) Relative Removal Rates of Point Defects as a Function of Temperature for Fixed Microstructure of 316 SS (Accelerator Conditions)

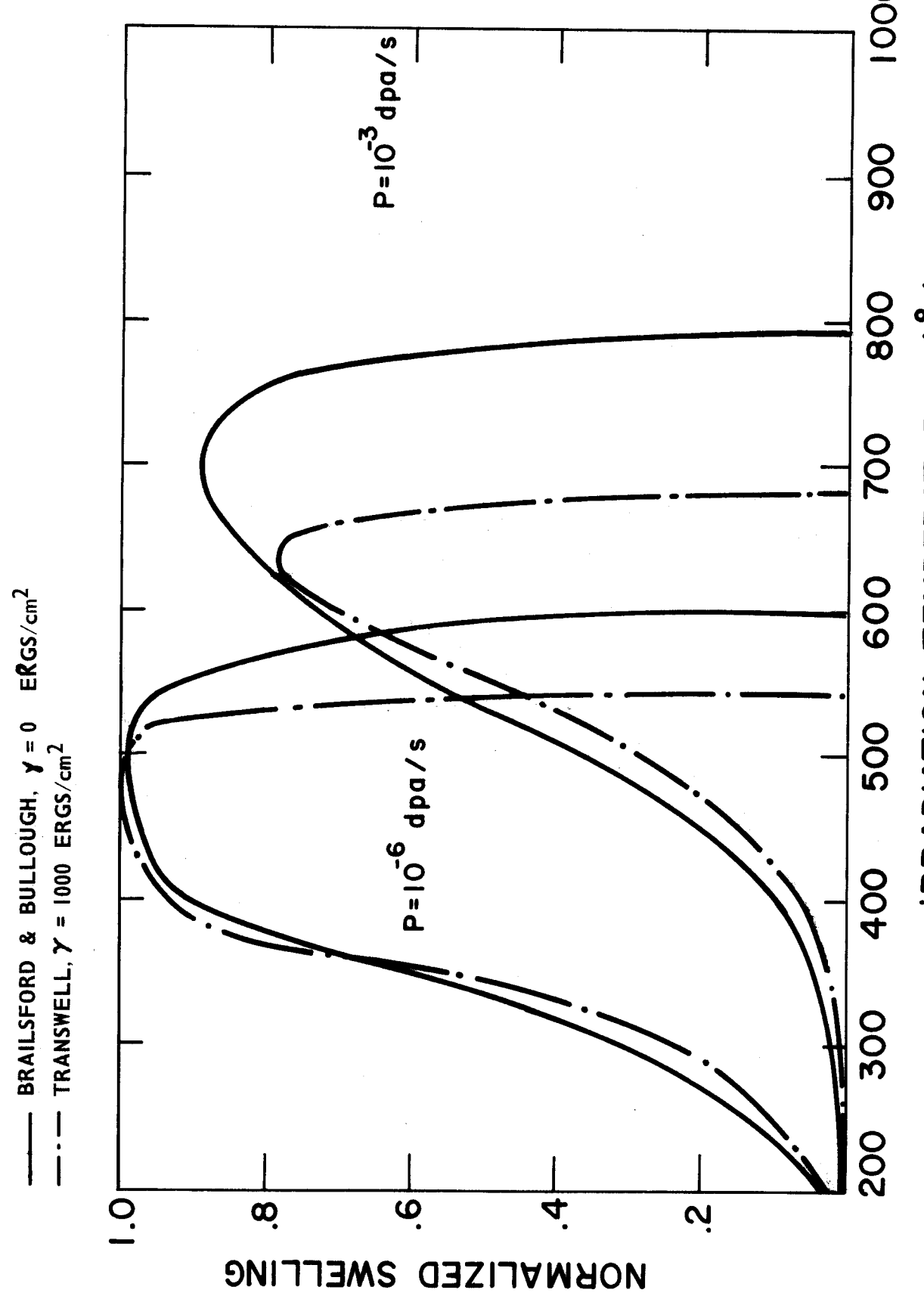

Figure (87) Relative Swelling of 316 SS for a Fixed Microstructure

Table (2)

Comparison Between Theoretical Predictions of the Peak Temperature Shift and Experimental Observations

Metal	Lower dpa rate	Higher dpa rate	Peak Temp. Shift, °C.	Investigator	Comments
316 SS	10^{-6}	10^{-3}	190	Brailsford and Bullough	Theoretical with fixed microstructure, γ = 0 ergs/cm^2.
316 SS	10^{-6}	10^{-3}	140	Ghoniem and Kulcinski	Theoretical with fixed microstructure, γ = 1000 ergs/cm^2.
316 SS	10^{-6}	10^{-3}	50	Ghoniem and Kulcinski	Theoretical with dose and temperature dependent microstructure, γ = 2000 ergs/cm^2.
316 SS	10^{-6}	10^{-2}	115	Bates, Straalsund, Johnston, Rosolowski, Turkalo and Lauritzen	Experimental, reactor and Ni ion irradiations.
Ni	10^{-6}	10^{-1}	110	Adda, Sprague, Westmoreland, Schmidt and Malmberg	Experimental, reactor and Ni ion irradiations.

V. Conclusions

A fully dynamic rate theory approach has been utilized to analyze in detail the dynamics of point defects as well as voids, interstitial and vacancy loops. The following major features emerge from this study:

1. The vacancy concentration exhibits a peak value at intermediate temperatures due to the competition between a drop in sink density and a vacancy mobility increase with temperature. This behavior has an appreciable effect on void nucleation rates calculated at intermediate temperatures since they are sensitive to vacancy supersaturation ratios.

2. The fraction of vacancies retained in vacancy loops has a great influence on void growth kinetics. However, this fraction is very sensitive to temperature and decreases sharply as the temperature increases.

3. Free point defect recombination rates are negligible compared to sink removal rates for neutron or ion irradiated metals at low temperature. Recombination of point defects becomes more dominant at vacancy loops. At high temperatures, the metal matrix becomes "cleaner" of sinks and free recombination between point defects is effective in point defect dynamics.

4. Vacancy thermal emission from existing microstructure can be neglected compared to point defect production rates for high dose rates (10^{-3} dpa/sec), but it is very important for low dose rates (10^{-6} dpa/s).

5. For ion or neutron irradiation vacancy loop line density is around 2 orders of magnitude higher than interstitial loop line density for temperatures approximately below the swelling peak. Therefore, it is a dominant sink of point defects that should be taken into consideration.

6. There exists a temperature and microstructure dependent free growth void radius. This is defined as the minimum radius at which a void can grow without the assistance of internal gas pressure. For

simplicity, we have taken a 10 Å void radius to be the critical size at 400 °C, determined the free growth void radius at the highest temperature, and linearly interpolated in between.

7. Table (2) shows a comparison between different theoretical models and experimental findings for the peak temperature shift in reactor and accelerator conditions. One can immediately see that:

(a) A fixed microstructure theoretical model is probably a crude approximation to metal swelling under irradiation and does not predict the correct shift for the peak temperature.

(b) A dynamic microstructure model that considers dose rate independent nucleation conditions predicts only 50°C for the peak temperature shift. We conclude that dose rate affects nucleation as much as it influences growth and it is responsible for the rest of the temperature shift.

8. There is a delicate balance in a metal's matrix between the vacancy flux (D_vC_v) and the interstitial flux (D_iC_i). For void growth under irradiation D_vC_v is greater than D_iC_i. The formation of vacancy loops influences this balance by reducing the free vacancy flux and for high collapse efficiencies the vacancy flux can be less than the interstitial flux. Should more interstitials than vacancies go to voids, void growth is inhibited and voids shrink instead of grow. Figure (88) explains this behavior and shows that for collision cascade efficiencies greater than 5% to 7.5%, void swelling is inhibited for steel over a wide range of dose rates and temperatures. This casts some light on metals of high collision cascade efficiencies (Au, Ti and Zr) and explains why they do not form voids and form vacancy loops instead. Alloying metals to increase the collision cascade efficiency can be a very useful potential to reduce or inhibit swelling of metals under irradiation.

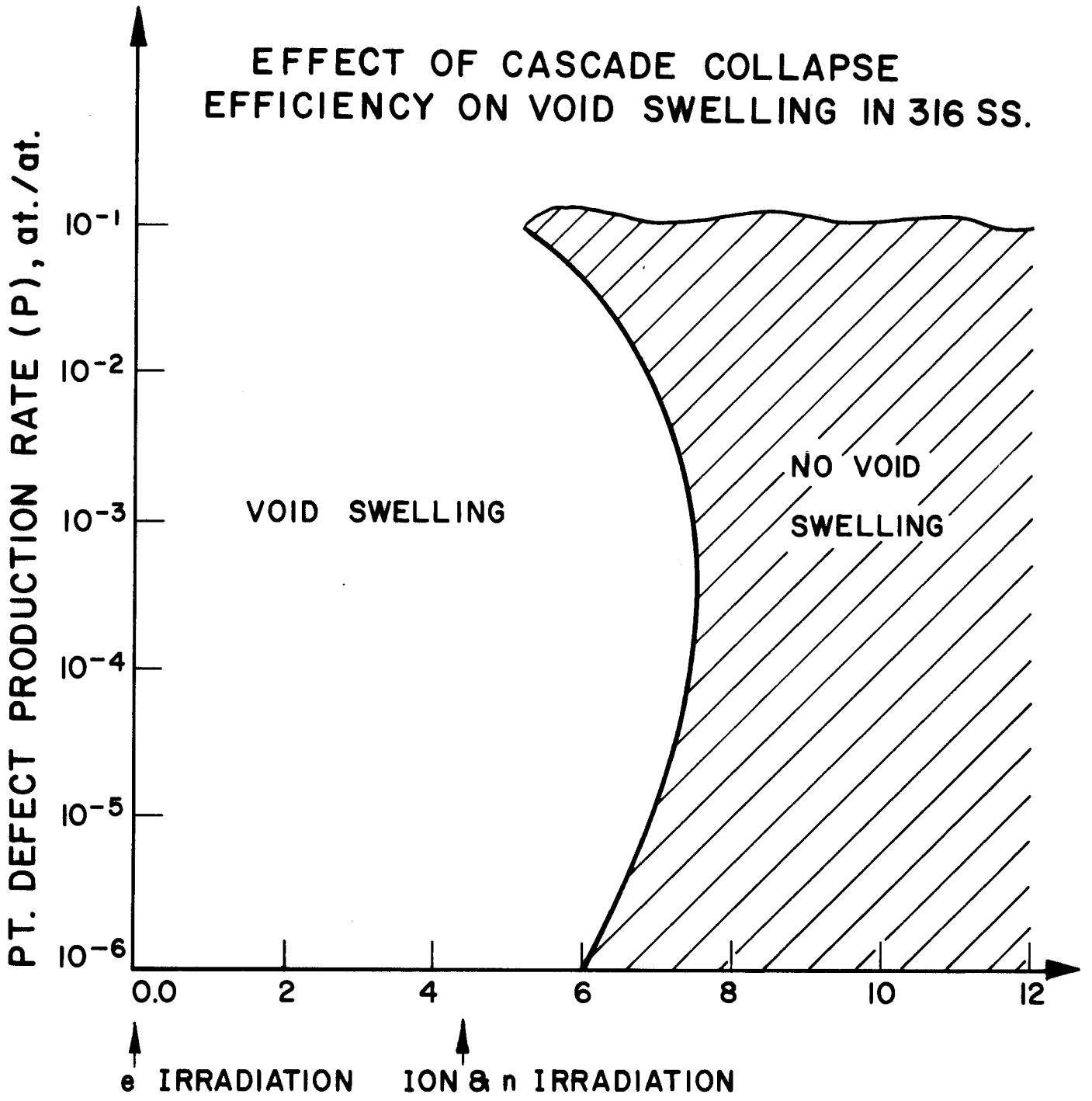
EFFECT OF CASCADE COLLAPSE
EFFICIENCY ON VOID SWELLING IN 316 SS.
PT. DEFECT PRODUCTION RATE (P), at./at.
10-1
10-2
10-3
10-4
10-5
10-6
VOID SWELLING
NO VOID
SWELLING
0.0
2
4
6
8
10
12
e IRRADIATION
ION & n IRRADIATION
CASCADE COLLAPSE EFFICIENCY (ϵ),%

Figure (88)

Acknowledgement

This work was prepared by the University of Wisconsin as an account of work sponsored by the Electric Power Research Institute, Incorporated (EPRI), and Wisconsin Electric Utilities Research Foundation (WEURF).

References

1. A. D. Brailsford and R. Bullough, J. Nucl. Mat. 44 (1972), 121.

2. N. Ghoniem and G. Kulcinski, Univ. of Wisconsin Fusion Design Memo, UWFDM-180 (1976).

3. W. G. Johnston, J. H. Rosolowski, A. M. Turhalo and T. Lauritzen, General Electric Technical Information Series, No. 73CRD217.

4. J. L. Straalsund, J. Nucl. Mat. 51 (1974), 302.

5. R. Bullough, B. L. Eyre and R. Krishan, Proc. R. Soc. Lond. A. 346, (1975).

6. N. Ghoniem and G. Kulcinski, Univ. of Wisconsin Fusion Design Memo, UWFDM-181 (1976).

7. N. Ghoniem and E. Anderson, Univ. of Wisconsin Fusion Design Memo, UWFDM-211 (1977).